DAVID WILLIAM MOORE

HEAT TRANSFER STUDIES IN UP-FLOW BOILING

Ph.D

MAY 1976

ACKNOWLEDGEMENTS

I wish to ackowledge the great help and encouragement I have received from the members of the Chemical Engineering Department at Aston University especially Dr J. D. Jenkins whose continuous guidance and help throughout was invaluable.

I would also like to thank Mr M. Gibson-Robinson and the members of the Computer Group whose advise and stimulating comments were of great assistance throughout.

For their great help with the practical work I wish to thank Mr H. Roberts and all of the technical staff especially the workshop staff under Mr G. Evans.

My thanks also to Mrs J. DeLuca for her patience and effort in transforming a sometimes illegible draft into its present form.

I must also thank the Science Research Council whose grant made this work possible.

Finally, my thanks to family and friends , especially Miss M. Tyler and Dr D. Wilkinson for their much needed encouragement throughout and to Dupli-Photo Service for printing this volume.

SUMMARY

Heat transfer during flow boiling in tubes is of continued interest to engineers for both practical and theoretical reasons and this work is part of a continuing research program into this area.

A summary of the relevent literature is presented and the relevent theoretical background is reviewed.

The experimental work was carried out using a vertical, single tube forced convection, heat transfer rig. The data were obtained in an electrically heated copper tube for water and a water-ethylene diacetate azeotrope. Thermocouple measurements of wall temperatures and measurements of the bulk pressure allowed point heat transfer coefficient values to be determined for a range of heat flux and flowrate values.

Various non-linear, least squares, optimisation methods were investigated for use with the data and a discussion of the problems encountered with each of the methods is given. The best of the methods tried was found to be that of Davis, Swann and Campey. This method was used to fit the water data to a number of models, including that of Chen and two other models developed from it. An analysis of the sources and degree of error in the experimental data is qiven as well as a discussion of the degree of correlation found with each of the models.

The water-ethylene diacetate data was found to be highly anomalous, but it was possible to fit the data to one of the models developed. The anomalous behaviour of the azeotrope data is discussed and a possible reason for it's behaviour put forward.

Suggestions are given for further work and a possible application for the anomalous behaviour of the water-ethylene diacetate system is proposed.

NOMENCLATURE

C_p	Specific heat (J/kg ^{o}C)
D	Diameter (m)
F	Chen parameter
F_L	ln(F)
g	Gravitational constant (m/s^2)
g_c	Gravitational conversion factor
h	Heat transfer coefficient (J/m^2 s ^{o}C)
h_{con}	Convective heat transfer coefficient (J/m^2 s ^{o}C)
h_{mic}	Microconvective heat transfer coefficient (J/m^2 s ^{o}C)
h_{film}	Film heat transfer coefficient (J/m^2 s ^{o}C)
j	Volumetric flux (m^3/m^2 s)
k	Thermal conductivity (J/m ^{o}C s)
Lv	Latent heat of vaporisation (J/kg)
p	Pressure (N/m^2)
P_b	Bulk pressure (N/m^2)
P_w	Saturated vapour pressure at wall temperature (N/m^2)
q $(=(\frac{Q}{A})$	Heat flux per unit area (J/m^2 s)
R	Universal gas constant
R_L	$\ln(Re_{tp})$
r	Radius of pit or orifice (m)
r*	Critical orifice radius (m)
S	Chen parameter
T	Temperature (^{o}C)
T_b	Bulk temperature (^{o}C)
T_{SAT}	Liquid saturation temperature (^{o}C)
V	Flow velocity (m/s)
V_m	Mean two-phase velocity (m/s)
XTT	lockhart-Martinelli parameter

x	Quality
z	Distance (m)
α	Void fraction
δ	Thermal boundary layer thickness (m)
ρ	Density (kg/m^3)
μ	Viscosity ($N\ s/m^2$)
ϕ_f^2	Two-phase fractional multiplier based upon pressure gradient for the liquid flowing alone
π	Heat flux per unit area ($J/m^2\ s$)
σ	Surface tension (N/m)
τ_w	Wall sheer stress

Subscripts

b	Model B
e	Effective
f	Fluid
g	Vapour
L	Liquid
tp	Two-phase
v	Vapour
w	Wall

CONTENTS

HEAT TRANSFER STUDIES IN UP-FLOW BOILING

I. Introduction and Basic Theory

The subject of convective boiling in vertical or horizontal channels is a very important one since the design of many items of chemical equipment or power plant depends upon a knowledge of flow dynamics and heat transfer processes occurring in flow boiling. However, despite the vast amount of literature on the subject of two-phase flow and heat transfer, the existing correlations used to predict two-phase behaviour are almost entirely empirical in nature. This is in part due to the inherently complex nature of two-phase flow and heat transfer and the very close interdependence between the two processes. The complexity of two-phase behaviour is essentially due to the heterogeneous nature of two-phase flow as opposed to the homogeneous nature of single phase flow.

The difficulty of analysing boiling heat transfer is also due to the fact that two-phase heat transfer is in general a non-equilibrium process since the continuous formation of vapour causes changes in the flow characteristics which in turn affect the local heat transfer. Because of these continuous changes in both the flow and heat transfer in flow boiling, equilibrium conditions never fully develop.

The situation is further complicated for multi-component systems where concentration differences leading to mass-transfer resistance between the two phases can greatly affect heat transfer coefficients. For this reason the present work is only concerned with single and pseudo-single component liquids.

From the above it is clear why, as yet, only empirical relationships have been developed for two-phase flow and heat transfer. It is obvious, however, that any empirical relationship for two-phase heat transfer should be based, as far as possible, upon whatever information is available as to the processes and mechanisms important in flow boiling. Also it would seem obvious that any useful model for two-phase heat transfer must reflect the complexity of two-phase phenomena. However until recently only equations which were linear or could be transformed into a linear form could be fitted to data using least mean square fitting procedures. This obviously greatly restricts the form of possible models for correlating boiling heat transfer data.

The most complex model employed to date is that developed by Chen (C3) which assumes two interdependent heat transfer mechanisms. This reflects what is known of flow boiling where at least two distinct heat transfer mechanisms have been observed. However the method of

optimisation used to fit this model to the data was an iterative method which would not necessarily arrive at the optimum parameter values. In order to fit data to non-linear models such as Chen's, it is best to use special non-linear least squares optimisation methods. These allow models even more complex than Chen's to be used to fit the data. However, they do require a large amount of computer time which may not always be feasible due to the cost of computer time.

This work is part of a general study of flow boiling and it was intended that this initial phase of the study would investigate the experimental and correlating techniques which could be used in the study of flow boiling. As the study progressed it became clear that the main theme of this preliminary study would be concerned with investigating the use of non-linear least squares optimisation methods to correlate flow boiling heat transfer data to a number of models including Chen's and models derived from it.

Since an empirical correlation can only be used with confidence for conditions covered by the data, it is obviously best to obtain data over a wide range of conditions and for a large number of experimental fluids. Unfortunately, however, the experimental rig used in this work could only be used with non-toxic, non-inflammable and non-corrosive liquids at, or very near to, atmospheric pressure. These restrictions effectively reduced the

possible experimental liquids to water and some water-based azeotropes and thus greatly narrowed the range of experimental data. Also due to the arrangement of the rig only one tube diameter was possible.

The narrow range of the experimental data imposed by the above restrictions greatly reduces the use of any correlation derived in this work. However the models themselves and the optimisation methods used to fit the experimental data to the models will be generally applicable to single component flow boiling heat transfer data.

All of the data in this work was for forced circulation as it had been found from previous experience when working with natural circulation that equilibrium took much longer to achieve and was much harder to maintain than with forced circulation loops. Also natural circulation loops are susceptible to rapid flow oscillations which would have greatly affected the data and would have made analysis, using a steady state model, impossible.

Electric heaters were used in preference to steam heating for a number of reasons. Firstly it is much easier to control, secondly it makes analysis of the data simpler since the heat flux is fixed, and finally it allows the heat flux to be held constant along the tube.

As already mentioned a knowledge of two-phase flow and of bubble nucleation is required for any understanding of flow boiling. A brief survey of both areas is given below together with a short introduction to pool boiling.

I.1 TWO-PHASE FLOW

I.1.1 Flow Patterns in Isothermal Two-Phase Flow

The description and isolation of flow patterns in two-phase flow tends to be rather imprecise because the differentiation between flow patterns has to be primarily based upon visual observations and is thus a subjective decision. However, five main flow patterns are generally recognised in vertical two-phase flow.

These are: (a) Bubbly flow

(b) Slug flow

(c) Churn flow

(d) Annular flow

(e) Mist flow

These flow regimes occur, in the order in which they are given, during flow boiling in a vertical tube and are illustrated in Diagram 1.1.

A number of generalised flow pattern maps have been derived for flow in tubes (B1, G2, H2) Such two-dimensional maps can only be used as a rough guide to the flow pattern likely to be encountered for a given set of conditions.

For each of the individual transitions various criteria have been proposed to enable the flow pattern in a given situation to be determined.

Figure 1.1 Flow Patterns in Vertical Two-Phase Flow

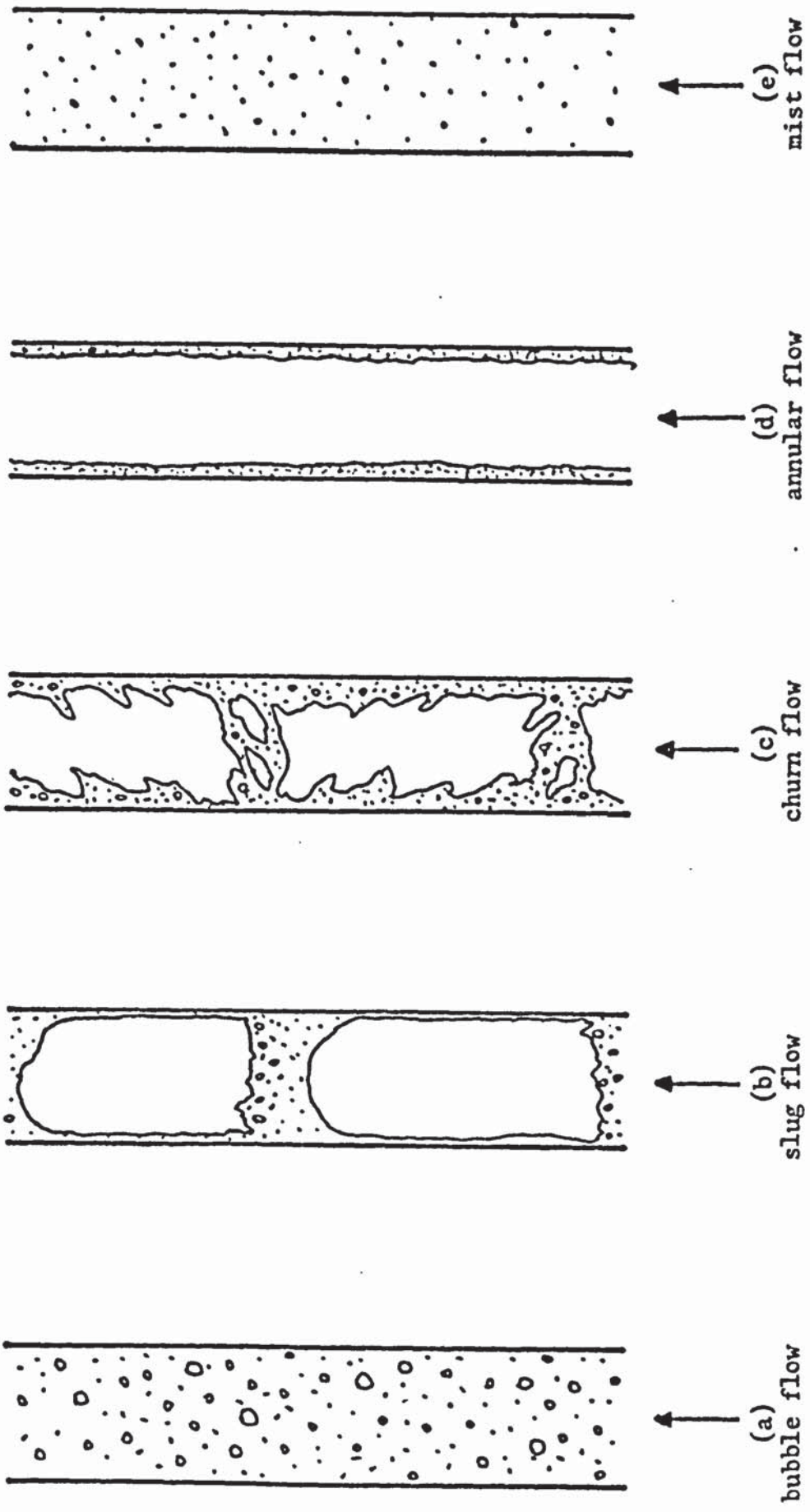

I.1.1 (1) Bubbly Flow - Slug Flow

Bubbly flow is two-phase flow consisting of a continuum of liquid with dispersed vapour bubbles present. As the number of bubbles increases, collision of bubbles and hence coalescence takes place. Radovcich and Moissis (R1) have shown that below a void fraction of about 0.1 the frequency of collisions and hence coalescence is relatively low. For void fractions above this the collision frequency increases until at a void fraction above 0.3 the rate of coalescence would be such that slug flow would be expected to occur. Such an analysis assumes that the bubbles are not stabilised by the presence of surface active agents such as detergents; at high voidages one would expect such a system to develop into a foam.

I.1.1 (2) Slug Flow - Churn Flow

In slug flow the vapour bubbles are of such a size that they occupy most of the cross-sectional area of the tube with only a thin liquid film on the tube wall. These slugs are separated by the liquid phase which normally contains smaller bubbles.

The transition to churn flow occurs when the liquid film on the tube wall becomes unstable (M2) and breaks down. Porteous (P2) showed that at the slug flow - churn flow transition the total volumetric flux was given by the equation

$$j = 0.105 \left(\frac{g D (\rho_f - \rho_g)}{\rho_f}\right)^{0.5} \qquad 1.1$$

for $\rho_f >> \rho_g$

$$\frac{j}{\sqrt{g D}} = 0.105 \qquad 1.2$$

or

$$Fr_{tp}^{0.5} = 0.105 \qquad 1.3$$

I.1.1 (3) Churn Flow - Annular Flow

Churn flow is characterised by its instability and 'churning' with the liquid mainly confined to the wall and the vapour concentrated in the centre of the tube. However in churn flow there are fildments of liquid which extend across the tube and the transition to annular flow can be considered to have taken place when the middle of the tube is occupied exclusively by vapour (H1).

Griffith (G5) found that the gas velocity at which liquid ceases to bridge the tube can be predicted by the equation

$$j_g' = 0.9 + 0.6\, j_f' \qquad 1.5$$

when $j_f' < 1.5$

where $$j_f' = j_f \left(\frac{g\, D\, (\rho_f - \rho_g)}{\rho_g}\right) \qquad 1.6$$

and $$j_g' = j_g \left(\frac{g\, D\, (\rho_f - \rho_g)}{\rho_g}\right) \qquad 1.7$$

I.1.2 Flow Patterns in Boiling Two-Phase Flow

All of the correlations given above were obtained in isothermal flow and thus can only be applied with great caution to boiling two-phase flow.

Some reasons for this are:-

(1) The above correlations were derived essentially from steady state flow experiments, i.e. the flow pattern was not changing rapidly up the tube. This is not the case in boiling flow where the quality and thus the flow pattern is changing rapidly.

(2) Vapour is produced at the wall in flow boiling and thus there is an ~~axial~~ radial fluid velocity which is not present in isothermal flow.

(3) The rapid change in quality in flow boiling causes the fluid to accelerate rapidly, an effect which is present only to a negligible extent in isothermal flow.

Sato et al.(S1) have shown experimentally that in boiling two-phase flow the flow pattern development does not follow the classical series of regimes. They found that at high flow rates the slug and churn flow regimes were suppressed and bubble flow developed directly into annular flow through a transition region. It would appear from their results that the transition to the annular regime is delayed in boiling two-phase flow, the delay being greatest at higher heat fluxes. However, these experiments were performed in a rectangular channel with heating only on two opposite faces, which does not allow direct comparison with boiling in a round tube.

I.1.3 Models for Two-Phase Flow

(1) Introduction

Pressure drop in two-phase flow can be analysed in terms of the three separate components causing the pressure drop.

$$\left(\frac{dp}{dz}\right) = \left(\frac{dp}{dz}\right)_F + \left(\frac{dp}{dz}\right)_a + \left(\frac{dp}{dz}\right)_z \qquad 1.8$$

where $\left(\frac{dp}{dz}\right)_a$ represents the pressure drop due to the acceleration of the two-phase mixture, $\left(\frac{dp}{dz}\right)_F$ represents the pressure drop due to friction on the wall and $(dp/dz)_z$ represents the pressure drop due to changes in elevation.

Using the conservation of momentums approach it may be shown that

$$-\left(\frac{dp}{dz}\right)_a = G^2 \frac{d}{dz}\left(\frac{x^2}{\rho_g a} + \frac{(1-x)^2}{(1-a)\rho_f} \right) \qquad 1.9$$

and (for a vertical tube)

$$-\left(\frac{dp}{dz}\right)_z = g\left(a\rho_g + (1-a)\rho_f \right) \qquad 1.10$$

In the above two pressure drop components a is the only unknown assuming the flow parameters and physical properties are known. To use the above equations to predict the two-phase pressure drop in a given situation it is necessary to estimate the void fraction, a and the frictional pressure drop component using some model for two-phase flow.

There are two main models for two-phase flow, the homogeneous model and the separated flow model.

I.1.3 (2) Homogeneous Model

In the homogeneous model it is assumed that

1) The liquid and vapour velocities are equal.
2) There is thermodynamic equilibrium between the phases.
3) There is a suitable single-phase friction factor that can be defined for two-phase flow.

These assumptions amount to the presumption that the flow of a vapour-liquid mixture can be represented as flow of a single-phase fluid with suitably defined physical properties. It would be expected that the model is most suitable for two-phase flows where one phase is uniformly dispersed in

in the other phase, i.e. bubble flow and mist flow, and that this model would be more accurate at high pressures where the properties of the two phases would be closer. This indeed is generally the case (C8).

However, since all of the present work was carried out at or near atmospheric pressure, and annular flow was the usual flow regime, this model is inapplicable to the present work. For this reason the homogeneous model is not discussed further. A full exposition of the homogeneous model can be found in Ref (C8).

I.1.3 (3) Separated Flow Model

The main assumptions implied in the separated flow model are:-

1) The vapour and liquid phases flow at different velocities which are constant across the area of the tube.

2) Thermodynamic equilibrium between the phases.

3) The two-phase multiplier, ϕ_f^2 , and the void fraction, α can be correlated in terms of the physical properties of the two phases and the flow parameters.

Lockhart and Martinelli (L2), who were the first to present this model, assumed that each phase could be either laminar or turbulent. Hence there are four possible pressure drop regimes. For this present work only turbulent-turbulent flow will be considered. The two-phase multiplier, ϕ_f^2 is defined as

$$\phi_f^2 = \left(\frac{dp}{dz}\,F\right)/\left(\frac{dp}{dz}\,F\right)_f \qquad 1.11$$

where $\left(\frac{dp}{dz}\,F\right)_{fg}$ is the calculated frictional pressure drop assuming the liquid flows alone, ϕ_f was assumed a function of XTT only, defined by;

$$XTT^2 = \left(\frac{dp}{dz}\,F\right)_f/\left(\frac{dp}{dz}\,F\right)_g \qquad 1.12$$

where $(\frac{dp}{dz}\,F)_g$ is the calculated frictional pressure drop assuming the vapour flows alone. The TT subscript on XTT refers to turbulent-turbulent flow.

Using the Blausius equation for turbulent flow

$$f = 0.079\,Re^{-\frac{1}{4}} \qquad 1.13$$

it can be shown that

$$XTT = (\frac{1-x}{x})^{0.875}\,(\frac{\rho_g}{\rho_f})^{0.5}\,(\frac{\mu_f}{\mu_g})^{0.125} \qquad 1.14$$

this is usually approximated to

$$XTT = (\frac{1-x}{x})^{0.9}\,(\frac{\rho_g}{\rho_f})^{0.5}\,(\frac{\mu_f}{\mu_g})^{0.1} \qquad 1.15$$

Lockhart and Martinelli presented graphs of ϕ_f^2 and a against XTT allowing two-phase pressure drops to be calculated. This method of calculating two-phase pressure drop was developed only for horizontal flow at or near atmospheric pressure and was extended by Martinelli and Nelson (M1) to vertical flow and higher pressure.

The Lockhart-Martinelli-Nelson correlation has been widely used and found generally satisfactory. However many investigators have found that there is a mass velocity effect in vertical flow (H1, H2, G2) that is not accounted for in this correlation. Various attempts have been made to allow for this mass velocity effect, notably by Chisholm (C5) and Baroczy (B2). The most interesting approach has been that used by Davis (D3) who used a Froude No. to account for this effect. Davis showed that the data

of Govier et al. (G3) and Isbin (I1) was better correlated if XTT was replaced by

$$XTT' = 0.19\ XTT\ \left(\frac{V_m^2}{D\ g}\right)^{0.185} \qquad 1.16$$

where V_m is the mean two-phase velocity. According to Davis the modification would be applicable only to vertical flow and was postulated to account for the effect of the different vapour and liquid velocities.

I.2 BUBBLE NUCLEATION

For a liquid to boil it is a necessary condition that the temperature of the liquid must be equal to or greater than the saturation temperature, T_{SAT}. However, the pressure inside a vapour bubble is higher than in liquid outside it due to the surface tension forces. The pressure difference is given by

$$p_g - p_f = \frac{2\sigma}{r} \qquad 1.17$$

This pressure difference means that for a vapour bubble to be stable, the liquid temperature must be higher than the saturation temperature.

From the Clausius-Clapyron relationship can be derived the superheat required for the growth of a vapour bubble

$$\Delta T_{SAT} = \frac{R\ T_{SAT}^2}{L_v\ M} \ln\left(1 + \frac{2\sigma}{p_f\ r}\right) \qquad 1.18$$

when $\frac{2\sigma}{p_f\ r} \ll 1$ then

$$\Delta T_{SAT} = \frac{R\ T_{SAT}^2}{L_v\ M}\ \frac{2\sigma}{p_f\ r} \qquad 1.19$$

This equation shows that the smaller the vapour bubble the higher the superheat required for its growth. Because of this some mechanism must exist to form vapour nuclei. Two main possible mechanisms have been described:

1) Homogeneous nucleation
2) Heterogeneous nucleation

I.2.1 Homogeneous Nucleation

In a hot liquid there is a small but finite probability that a group of molecules with vapour-like energies will come together to form a small bubble. The superheat required in a liquid for the rate of homogeneous nucleation to be significant can be found (S5). For water, at atmospheric pressure, the superheat required is about 220°F. This value of the superheat is greater than any obtained experimentally, thus it is clear that for water, at least, homogeneous nucleation is unimportant.

I.2.2 Heterogeneous Nucleation

If nucleation in a liquid is promoted by a solid surface this is considered as heterogeneous nucleation. The solid surface may be in the form of particles suspended in the liquid or the walls of the container in which the liquid is held.

The solid surface acts in two ways. The first is its effect in reducing the superheat required for homogeneous nucleation at the wall. This reduction in superheat is dependent upon the contact angle of the solid-liquid-vapour combination. For most systems this effect is of little importance.

The second and main way in which a solid surface aids nucleation is by the presence of pits and crevices in the solid surface. An idealised conical pit is shown in Fig. 1.2a with the various stages of growth of the bubble shown. A graph of the radius of curvature of a bubble growing in such a pit is given in Fig. 1.2b As can be seen the radius of curvature passes through a minimum position (see Fig. 1.2b) This critical radius can be seen to be equal to the radius of the pit orifice. This is true providing $0^{\circ} < \theta < 90^{\circ}$. This critical radius corresponds to a critical superheat required for nucleation at this site.

However, the growth of the vapour bubble in the pit requires an initial small vapour nucleus to develop from. This initial vapour nucleus can be gas present when the surface was dry and trapped in the pit when the surface was submerged. A further source for a pit from which a bubble has previously grown can be vapour left behind by a departing bubble. Also a bubble usually encompasses many pits and cavities before it detaches from the solid surface and vapour from this source can cause a previously liquid-filled cavity to become active (T2) . Equation 1.19 gives the superheat required for nucleation at an active site of known effective radius. However the equation is only strictly applicable to a situation where the temperature is constant throughout the liquid which is rarely the case in practical situations. The influence of thermal gradients upon nucleation has been investigated by Hsu (H4). Hsu postulated that bubble growth would take place when the

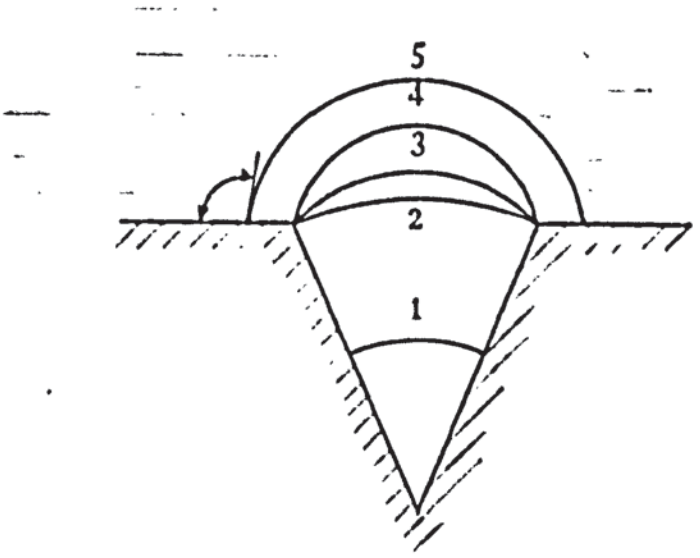

Fig. 1.2a Stages in Growth of Vapour Bubbles in Cavity

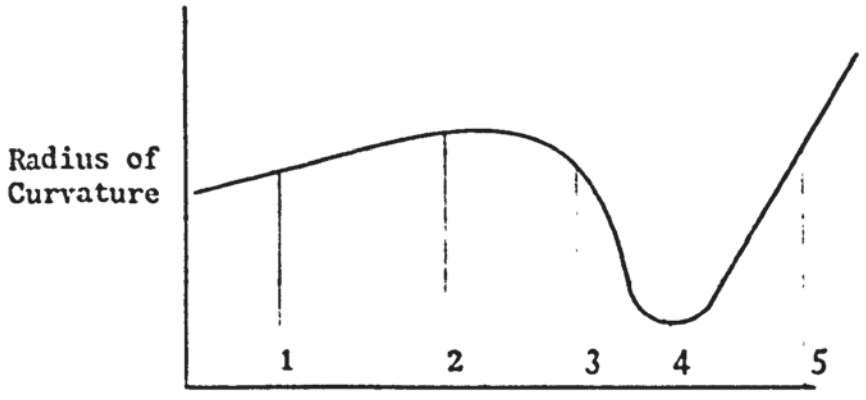

Fig. 1.2b Variation of Radius of Curvature of Bubble during Growth

temperature at the top of the bubble was equal to the equilibrium temperature for the bubble as given by equation 1.19. Assuming the bulk temperature of the liquid to be equal to the saturation temperature and allowing for distortion in the thermal boundary layer, Hsu was able to determine the range of diameters of active sites for a given wall temperature and fluid. Alternatively for a given size of active site the wall superheat could be determined.

However, the superheat required for water at atmospheric pressure as calculated from Hsu's equation is about $1^{o}C$, while in practice values in the range $10^{o}C$ - $15^{o}C$ are found. This discrepancy can be explained in terms of the sizes of active sites actually available for nucleation as Hsu's treatment assumed that active sites of all possible sizes were available.

I.3 POOL BOILING

Over the years a large amount of work has been carried out on nucleate pool boiling and a large number of correlations have been proposed. Many of the proposed correlations use a relationship of the form

$$Nu = C\, Re^{x}\, Pr^{y} \qquad 1.20$$

in an analogy with single-phase heat transfer. The different correlations result from the way the various parameters in the dimensionless numbers are defined (21)

The most widely used correlations of this type are the Rohsenow (R4) and the Foster-Zuber correlation (Z2)

The Rohsenow correlation

$$\left(\frac{Cp_f \Delta T_{SAT}}{L_v}\right) = C_{sf}\left(\frac{q}{\mu_f L_v}\left(\frac{\sigma}{g(\rho_f - \rho_g)}\right)^{\frac{1}{2}}\right)^{0.35}\left(\frac{C_p \mu_f}{k_f}\right)^{1.7} \quad 1.21$$

contains the parameter C_{sf} which has different values depending upon the solid surface-liquid combination This parameter is assumed to allow for the nucleating characteristics of the surface.

The Foster-Zuber correlation is

$$\frac{q}{g L_v}\left(\frac{\pi}{a_f}\right)^{\frac{1}{2}}\left(\frac{\rho_f r^3}{2\sigma}\right)^{\frac{1}{4}} = 0.0015\left(\frac{\rho_f}{\mu_f}\left(\frac{\Delta T_{SAT} k_f}{\rho_g L_v}\right)^2 \frac{\pi}{a_f}\right)^{\frac{5}{6}}\left(\frac{C_p \mu}{k}\right)_f^{0.33} \quad 1.22$$

where r is the equilibrium radius given by equation 1.18. It is probable that a correlation allowing for different solid surfaces, like the Rohsenow correlation, would show a smaller error than a general correlation like the Foster-Zuber correlation; for it has been shown that the surface preparation can have a very large effect upon the heat transfer coefficient (M1). However the use of the Rohsenow correlation requires knowledge of the appropriate value of C_{sf}. Unless the appropriate value can be found in the literature experimental work must be carried out to determine its value. This somewhat restricts the correlation's usefullness.

II LITERATURE SURVEY

II.1 FLOW BOILING HEAT TRANSFER REGIMES

Consider a uniformly heated vertical tube fed with sub-cooled liquid at its base and with vapour only leaving at the top. The different flow patterns, as described in section I.1.1, exist at the appropriate portions of the tube. In a similar way a number of heat transfer regions can be distinguished (c8).

First is the single convection heat transfer region where heat is transferred to the flowing liquid in a convective mode without any vapour formation. Eventually conditions at some point up the tube cause the formation of vapour bubbles from nucleation sites (see section 1.2). Initially the vapour is formed while the bulk temperature, T_b, is below the saturation temperature, T_{SAT}, and the vapour bubbles collapse as they move towards the centre of the tube. This region is called the 'sub-cooled nucleate boiling region'. When the bulk temperature, T_b, is no longer below the saturation temperature, T_{SAT}, the saturated nucleate boiling region is entered.

As the amount of vapour present increases the mechanism of heat transfer alters. Because of the vapour formed the flow accelerates progressively suppressing the formation of vapour bubbles at the wall. Heat is transferred by forced convection through the liquid film on the wall with evaporation occurring at the liquid film vapour core interface. The transition to this regime is closely proceeded by the Churn flow - Annular flow transition. This region is referred to as the two-phase forced convection region.

Fig. 2.1 Flow and Heat Transfer Regimes for Flow Boiling in a Vertical Tube

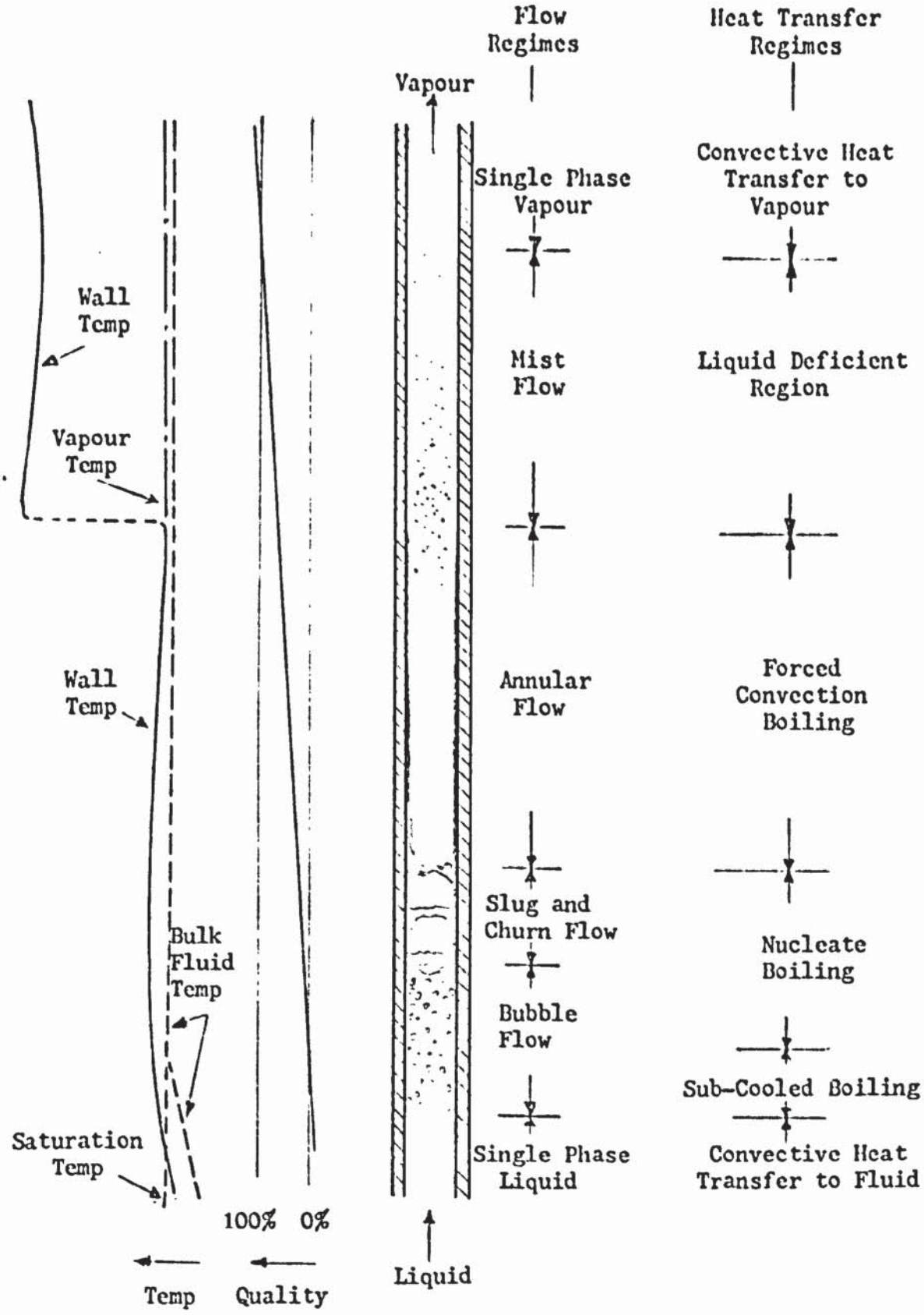

As the quality increases further liquid droplets are increasingly entrained in the vapour core, eventually the liquid film on the wall disappears completely. This is known as the 'dryout' or 'burnout' point. The region between the 'dryout' point and the complete vaporisation of entrained liquid droplets is called the liquid deficient region. Figure 2.1 shows the flow pattern and heat transfer regimes in a vertical pipe.

The work in this thesis is concerned only with the saturated nucleate boiling and two-phase forced convection regime and thus only work relevant to these regimes is considered in this survey of the literature.

Of paramount interest in this survey is the possibility or otherwise of using a single correlation to cover both the saturated nucleate boiling regime and the two-phase forced convection regime. Assuming this is possible it is also necessary to find the most suitable form of correlation to do this.

II.2 HEAT TRANSFER CORRELATIONS BASED ON XTT

Most workers in this area of heat transfer have based their correlations on the Lockhart-Martinelli parameter, XTT. (see section 1.1.3(2)). Many workers have developed equations which predict the ratio of the experimental two-phase heat transfer coefficient, h_{tp}, to the heat transfer coefficient for the liquid phase flowing alone, h_L.

Johnson and Abon-Sabe (J1) were the first to use this type of equation although the experimental work

was done on heat transfer to an air-water mixture in a steam-heated horizontal brass tube (2.21 cm I.D., 5.67 metres heated length) without any change in phase. They considered that the experimental two-phase heat transfer coefficient h_{tp} was made up of a liquid only coefficient, h_L, and a gas only coefficient, h_g, however, contribution of h_g was found to be negligible and the experimental data was successfully plotted as (h_{tp}/h_L) $(1 + 0.006\ (D\ G_g/\mu_g)^{\frac{1}{2}})$ against XTT; where D is the inside pipe diameter and G_g the air mass flow rate per unit area.

Fried (F1) used a similar approach to correlate his data for air-water mixtures passing through steam heated horizontal tubes. He found that a good correlation could be obtained by plotting (h_{tp}/h_L) against $(\Delta p/\Delta z)_{tp}/(\Delta p/\Delta z)_f$. He also found that h_{tp}/h_L could be plotted successfully against XTT but the data fell into separate bands for the two tube diameters used. This separation was postulated to be caused by a size effect or a difference in surface roughness.

Dengler and Addoms (D4) were the first to recognise that at least two different mechanisms of heat transfer could occur in flow boiling. Their results showed that the nucleate boiling mechanism was dominant when the rate of vaporisation was low but was progressively inhibited by the effect of forced convection which increased with increasing vaporisation. The experimental results were obtained for forced circulation boiling of water in a steam-heated 1 inch I.D., 20 feet long vertical copper tube.

Under conditions where forced convection heat transfer was presumed to be predominant the experimental results were correlated by

$$\frac{h_{tp}}{h_L} = 3.5 \left(\frac{1}{XTT}\right)^{0.5} \qquad 2.1$$

where

$$h_L = 0.023 \frac{k}{D} \left(\frac{G\,D}{\mu_f}\right)^{0.8} Pr_f^{\,0.4} \qquad 2.2$$

To correct for nucleate boiling the empirical multiplier

$$F_n = 0.067 \left((\Delta T - \Delta T_i) \left(\frac{dp}{dT_{SAT}} \frac{D}{\sigma}\right)_{T_w}\right)^{0.1} \qquad 2.3$$

was introduced. ΔT is $(T_w - T_b)$ where T_w is the wall temperature and T_b is the bulk temperature and ΔT_i the value of ΔT required for the initiation of boiling. $\frac{dp}{dT_{SAT}}$ is the gradient of the vapour pressure curve at T_{SAT}. The F_n factor, however, was only used when it was greater than unity.

They also found that the effect of the temperature difference was quite involved. At high levels of vaporisation the heat transfer coefficient appeared to be an inverse function of temperature difference considering the flowrate and quality as constant. Guerrieri and Talty (G6) used cyclohexane, methanol, benzene, pentane and heptane as test liquids under natural circulation conditions in oil heated brass tubes (1.905 cm I.D., 1.83 metres long and 2.54 cm I.D., 1.98 metres long). As with Dengler and Addoms they found that the heat transfer coefficient increased up the tube while the temperature difference $(T_w - T_b)$ decreased. Their data was correlated by

$$\frac{h_{tp}}{h_L} = 3.5 \left(\frac{1}{XTT}\right)^{0.45} \qquad 2.4$$

where

$$h_L = 0.023 \frac{k_f}{D} \left(\frac{G\,(1 - x)\,D}{\mu_f}\right)^{0.8} Pr_f^{\,0.4} \qquad 2.5$$

To allow for the nucleate boiling contribution to heat transfer an empirical parameter, the Nucleate Boiling Correction Factor (NBCF) was used where

$$NBCF = 0.187 \left(\frac{r^*}{\delta}\right)^{-5/9} \qquad 2.6$$

where r* is the radius of a thermodynamically stable bubble at the wall temperature, T_w, is given by equation 1.18 or 1.19, and δ is the laminar film thickness given by

$$\delta = \frac{10\,\mu_f}{\rho_f}\left(4\,\rho_f/\left(\frac{dp}{dz}\right)_{tp} D\right) \qquad 2.7$$

The values of $(dp/dz)_{tp}$ are predicted using the Lockhart-Martinelli correlation (L2). The Nucleate Boiling Correction Factor was only used when it was greater than unity. It was postulated that a value of NBCF less than unity corresponded to complete suppression of bubble nucleation at the wall.

Bennet et al. (B3) found an effect of heat flux upon the heat transfer coefficient for their experimental data for steam-water mixtures in internally heated vertical annuli. Their data was correlated by the dimensional equation

$$\frac{h_{tp}}{h_L}\left(\frac{Q}{A}\right)^{-0.11} = 0.64\left(\frac{1}{XTT}\right)^{0.7} \qquad 2.8$$

where h_L is given by equation 2.5 and $\left(\frac{Q}{A}\right)$ is in Btu/hr ft^2. The nucleate boiling data was separately correlated using Rohsenow's correlation. (see section 1.3) Schrock and Grossman (S^2, S3, S4) obtained their experimental data using water flowing under forced circulation through electrically heated vertical stainless steel tubes. (0.295 - 1.095 cm I.D., 38.2 - 101.6 cm heated length).

Data in the forced convection region was correlated by

$$\frac{h_{tp}}{h_L} = 2.5 \left(\frac{1}{XTT}\right)^{0.75} \qquad 2.9$$

where

$$h_L = 0.023 \frac{k}{D} \left(\frac{G\,D}{\mu_f}\right)^{0.8} Pr_L^{1/3} \qquad 2.10$$

To account for the nucleate boiling region the Boiling Number, Bo, was introduced where

$$Bo = \frac{q}{G\,Lv} \qquad 2.11$$

where Lv is the latent heat of vaporisation. The final correlation for all of the data was

$$\frac{h_{tp}}{h_L} = 0.739 \left(1.5 \left(\frac{1}{XTT}\right)^{2/3} + Bo \times 10^4\right) \qquad 2.12$$

Wright (W3) measured heat transfer coefficients in forced convection down flow boiling of water in electrically heated stainless steel tubes (1.2 cm I.D., 1.43 metres long and 1.83 cm, 1.73 metres long). Their data was correlated using equations similar in form to those used by Schrock and Grossman

$$\frac{h_{tp}}{h_L} = 2.721 \left(\frac{1}{XTT}\right)^{0.581} \qquad 2.13$$

for the forced convection region and for data where both heat transfer mechanisms are significant

$$\frac{h_{tp}}{h_L} = 1.39 \left(1.5 \left(\frac{1}{XTT}\right)^{2/3} + Bo \times 10^4\right) \qquad 2.14$$

where

$$h_L = 0.023 \frac{k}{D} \left(\frac{G(1-x)D}{\mu_f}\right)^{0.8} Pr_f^{1/3} \qquad 2.15$$

These forms of relationship were also used by Somerville (S6) to correlate his data for n-butanol in downflow in electrically heated tubes (1.19 cm I.D., 1.25 metres and 1.73 metres heated length).

All his data was correlated by

$$\frac{h_{tp}}{h_L} = 7.55 \left(\frac{1}{XTT}\right)^{0.328} \qquad 2.16$$

and by

$$\frac{h_{tp}}{h_L} = 2.45 \left(1.5 \left(\frac{1}{XTT}\right)^{2/3} + Bo \times 10^4\right) \qquad 2.17$$

where

$$h_L = 0.023 \frac{k}{D} \left(\frac{G(1-x)D}{\mu_f}\right)^{0.808} Pr_f^{1/3} \qquad 2.18$$

It should be noted that while Schrock and Grossman based the calculation of h_L on the total mass flowrate in the tube, Wright and Somerville evaluated h_L based upon the mass flowrate of liquid only. Pujol (P3) found that the differences caused by these two methods were small and for low values of the quality any differences were less than the scatter in the data.

Collier et al (C9) obtained a large amount of data for steam water mixtures in vertical, ~~electrically heated,~~ annuli with outside glass tubes (1.4 cm and 2.2 cm I.D., 73.6 cm and 122 cm heated length).* It was found that the equation which gave the best fit for their data in the forced convection region was

$$\frac{h_{tp}}{h_L} = 2.167 \left(\frac{1}{XTT}\right)^{0.699} \qquad 2.19$$

However the optimum values for the constants varied for each series of experiments. The value of the multiplier ranged from 2.065 to 3.732 and the value of the exponent from 0.491 to 0.749. h_L was calculated from

$$h_L = 0.023 \frac{k}{D} \left(\frac{G(1-x)\,D}{\mu_f}\right)^{0.8} Pr_f^{0.4} \qquad 2.20$$

A representative selection of their data was tested with the correlation of Schrock and Grossman (equation 2.12)

*(The inner cores with an electrically heated stainless steel tubes (O.D.s of 0.953 cm and 1.54 cm))

however their correlation was found to give errors of upto 100%. But the equation used by Schrock and Grossman for the forced convection region alone (equation 2.9) was found to be more representative of their data. However, using Wright's equation (2.14) the tested data fell within ± 35% of the predicted values.

Collier concluded that it was improbable that any single equation of the form of equation 2.17 could represent data accurately for both heat transfer mechanisms.

Pujol and Stenning (P3) investigated the effect of flow direction upon the boiling heat transfer coefficient using Refrigerant 113 in an electrically heated vertical stainless steel tube (1.58 cm I.D. and 5.8 metres heated length). In the forced convection region the heat transfer coefficient was found to be essentially the same for both upward and downward flow. Their data was correlated by

$$\frac{h_{tp}}{h_L} = 4.0 \left(\frac{1}{XTT}\right)^{0.37} \qquad 2.21$$

where

$$h_L = 0.023 \frac{k}{D} \left(\frac{G\,D}{\mu_f}\right)^{0.8} Pr_f^{\,0.4} \qquad 2.22$$

However for the nucleate boiling region the heat transfer coefficient was higher for upflow than downflow.

For upflow

$$\frac{h_{tp}}{h_L} = 0.9\left(4.45 \left(\frac{1}{XTT}\right)^{0.37} + Bo \times 10^4\right) \qquad 2.23$$

and for downflow

$$\frac{h_{tp}}{h_L} = 0.53\left(7.55 \left(\frac{1}{XTT}\right)^{0.37} + Bo \times 10^4\right) \qquad 2.24$$

All of the workers who used correlations of form of equation 2.24 found that this form of equation did not give as good results in the forced convection region as an equation of the form of equation 2.21, which does not include the boiling number Bo. However, the inclusion of Bo as in equation 2.24 did yield more accurate results in the nucleate boiling region.

One possible reason for this is that the contribution made to the heat transfer coefficient made by the Bo term is essentially constant over the length of the pipe (neglecting any change in h_L due to the change in x). This does not reflect the actual situation where the contribution made by the nucleate boiling mechanism varies over the length of the tube.

Wright obtained data for downflow using water and n-butanol in electrically heated vertical stainless steel tubes (1.185-1.825 cm I.D., 1.25-1.73 metres heated length). He found that the most successful expression which correlated his and other workers' data was (W2)

$$St = 0.9005\ Re_L^{-0.286}\ XTT^{-0.292}\ Bo^{0.191}\ Pr_f^{-0.233} \qquad 2.25$$

Using equation 2.20 for h_L, this equation can be rearranged to give

$$\frac{h_{tp}}{h_L} = 39.12\ \left(\frac{1}{XTT}\right)^{0.292}\ Re_L^{0.086}\ Pr_f^{0.367}\ Bo^{0.191} \qquad 2.26$$

The power on the Reynold's number is such that the effect of the Reynold's number is likely to be insignificant while the presence of the Boiling number as a multiplier implies that nucleate boiling mechanism is important in all conditions.

Calus et al. (C1) used copper and stainless steel, steam heated, vertical tubes (1.27 cm I.D. and 1.22 metres heated length) under natural circulation with water, iso-propanol, n-propanol and the two water-alcohol azeotropes. Their data was correlated by

$$\frac{h_{tp}}{h_L} = 0.065 \left(\frac{1}{XTT}\right) \left(\frac{T_{SAT}}{\Delta T_f}\right) \left(\frac{\sigma_{H_2O}}{\sigma}\right)^{0.9} \qquad 2.27$$

where

$$h_L = 0.023 \left(\frac{G(1-x)D}{\mu_f}\right)^{0.8} Pr_f^{0.4} \qquad 2.28$$

However, the correlation was derived for overall heat transfer coefficients and not point values which somewhat reduces its usefulness.

II.3 CORRELATIONS NOT BASED UPON XTT

All of the correlations so far discussed use XTT as a variable, however, some workers have developed correlations not based upon this variable.

Chawla (C2) correlated the data of a number of workers by introducing the parameter, E, the ratio of the mean liquid velocity to the mean vapour velocity. E is intended to represent those characteristics which distinguish a two-phase flow system from a single-phase one. E is determined from the relative roughness of the tube and the parameter

$$\left(\frac{1-x}{x}\right) (Re_L\, Fr_f)^{-1/6} \left(\frac{\rho_f}{\rho_g}\right)^{-0.9} \left(\frac{\mu_f}{\mu_g}\right)^{-0.5}$$

using a graph.

The heat transfer coefficients were then correlated by

$$Nu' = 0.0066 (Re_L Fr_L)^{0.475} \left(\frac{x}{1-x}\right) \left(\frac{\rho_f}{\rho_g}\right)^{0.3} \left(\frac{\mu_f}{\mu_g}\right)^{0.8} Re_L^{0.35} Pr_L^{0.42} \qquad 2.29$$

for $Re_L Fr_L < 109$ and

$$Nu' = 0.015 (Re_L Fr_L)^{0.3} \left(\frac{x}{1-x}\right) \left(\frac{\rho_f}{\rho_g}\right)^{0.3} \left(\frac{\mu_f}{\mu_g}\right)^{0.8} Re_L^{0.35} Pr_L^{0.42} \qquad 2.30$$

for $Re_L Fr_L > 109$, where

$$Nu' = \frac{h\,D}{k}\left(1 + \left(1 - \frac{(1-x)\rho_g}{x\,E\,\rho_f}\right)^{-\frac{1}{2}}\right) \qquad 2.31$$

Chawla's correlation, however, does not contain some of those variables normally associated with correlations which attempt to account for the nucleate boiling mechanism For example, the heat flux, Q (or what can be thought of as its reciprocal, ΔT), is not used as a variable. Thus it would seem unlikely that Chawla's correlation could be applicable over the whole range of boiling conditions.

Another correlation not using XTT as a parameter was developed by Penman and Tait (T1). Six different fluids were used under forced circulation in four different sized vertical tubes (0.762 cm-2.53 cm I.D., 173-189.5 ~~metres~~ heated length). The data was correlated by

$$\frac{h}{Cp_f}\left(\frac{D}{\rho_f\,\sigma\,g_c}\right)^{\frac{1}{2}} = 0.12\left(V_f\left(\frac{D\,\rho_g}{\sigma\,g_c}\right)^{\frac{1}{2}}\right)^{\frac{1}{2}} \qquad 2.32$$

The authors state that this correlation is applicable to the 'liquid film' region only. This presumably corresponds to the annular flow regime.

II.4 CHEN CORRELATION

The most widely used correlation for boiling heat transfer in tubes is the Chen correlation (C3). Chen compared the correlations of Dengler and Addoms, of Guerrieri and Talty, of Bennett et al, and of Schrock and Grossman, using a representative selection of 594 experimental data points. None of the correlations was successful in correlating all of the sets of data used.

Chen therefore proposed a new correlation to cover both the saturated nucleate boiling regime and the forced convection region.

Chen assumed that both heat transfer mechanisms operated over the entire range of conditions and that the contributions made by both mechanisms were additive. Thus

$$h_{tp} = h_{con} + h_{mic} \qquad 2.33$$

where h_{con} is macroconvective heat transfer coefficient and h_{mic} the microconvective heat transfer coefficient due to the nucleate boiling mechanism. It was assumed that h_{con} could be correlated by a Dittus-Boelter type equation

$$h_{con} = 0.023\ Re_{tp}^{0.8}\ Pr_{tp}^{0.4}\ \frac{k_{tp}}{D} \qquad 2.34$$

then assuming that the effective two-phase thermal conductivity and Prandl number can be represented by the fluid values and defining a parameter, F, by

$$F = \left(\frac{Re_{tp}}{Re_L}\right)^{0.8} \qquad 2.35$$

then

$$h_{con} = 0.023\ \frac{k}{D}\ \left(\frac{G(1-x)D}{f}\right)^{0.8}\ Pr_f^{0.4}\ F \qquad 2.36$$

Chen assumed that F was dependent upon flow conditions only and could be expressed as a function of XTT. Forster and Zubers equation for nucleate pool boiling (see section 1.2) was taken as the basis for the microconvective component. Using the effective values of the superheat and the superheat and the vapour pressure difference.

$$h_{mic} = 0.00122\ \left(\frac{k_f^{0.79}\ C_{2f}^{0.45}\ \rho_f^{0.49}}{\sigma^{0.5}\ \mu_f^{0.29}\ Lv^{0.24}\ \rho_g^{0.24}}\right) \Delta Te^{0.24}\ \Delta Pe^{0.75} \qquad 2.37$$

Chen then defined a suppression factor, S, as

$$S = (\Delta Te/\Delta T_{SAT})^{0.99} \qquad 2.38$$

Using the Clausius Clapeyron equation it can be shown that

$$S = (\Delta Te/\Delta T_{SAT})^{0.24} \quad (\Delta Pe/\Delta P_{SAT})^{0.75} \qquad 2.39$$

thus

$$h_{mic} = 0.00122 \left(\frac{k_f^{0.79} \; Cp_f^{0.45} \; \rho_f^{0.49}}{\sigma^{0.5} \; \mu_f^{0.29} \; Lv^{0.24} \; \rho_g^{0.24}}\right) \Delta T_{SAT}^{0.24} \Delta P_{SAT}^{0.75} \; S \qquad 2.40$$

Chen assumed that S was a function of the two-phase Reynolds Number Re_{tp} The functions for F and S were found empirically from experimental data using an iterative procedure (see section V.2.3). The empirical curves for F and S found by Chen are shown in Figs. 6.1 and 6.2. The correlation thus developed fitted the experimental data very well with an overall average error of 11%.

Hughmark has claimed (H5) that a constant value of S of 0.25 fitted his experimental data better than the S curve given by Chen. However a constant value of the suppression factor, S, implies that bubble nucleation is not affected by the flow velocity in the tube. This would seem unlikely.

Chen's correlation has been extended for use with boiling liquid metals (C8) and for subcooled boiling (C8) Thus it would seem that the approach used by Chen is valid for most flow boiling situations in channels.

II.5 Correlation Methods

All of the correlations discussed previously, apart from Chen's correlation, were fitted using linear correlation techniques. This approach was the

only possible one before the advent of large, very fast computers. However, the linear approach has the great disadvantage that only linear equations can be used as models. In this context a model can be considered as linear if it can be transformed into an equation of the form

$$y = a_1x_1 + a_2x_2 + \cdots\cdots\cdots a_nx_n \qquad 2.41$$

where $a_1 \cdots a_n$ are constants whose values are to be found, while $x_1 \cdots x_n$ are physical parameters.

Thus a correlating equation of the form of equation 2.1

$$\frac{h_{tp}}{h_L} = a\,(\frac{1}{XTT})^b \qquad 2.42$$

can be transformed into

$$\ln(\frac{h_{tp}}{h_L}) = \ln(a) + b\ \ln(\frac{1}{XTT}) \qquad 2.43$$

i.e.

$$y = a_o + a_1x \qquad 2.44$$

The same linear approach was used even for apparently non-linear type correlations such as Chawla's. Chen's correlation is the only exception, an iterative linear method being used (see section V.2.3). The presumption that flow boiling heat transfer can be adequately correlated using linear correlation techniques would seem somewhat optimistic especially as it is known that even single-phase forced convection heat transfer data can be correlated with significantly lower error using a non-linear model (E1).

Thus it is clear that non-linear optimisation techniques should lead to a much improved correlating equation.

III DEVELOPMENT OF THEORY

III.1 MODEL A

Since the Chen correlation has been found to be the most successful for correlating heat transfer data it was decided to use the Chen correlation as a starting point for developing a better correlating equation to fit the experimental data. The Chen correlation (see section 2.4) is given by the following equations:

$$F = f(1/XTT) \qquad 3.1$$

$$S = f(Re\ F^{1.25}) \qquad 3.2$$

$$h_{tp} = F\ h_{con} + S\ h_{mic} \qquad 3.3$$

In these equations h_{con} and h_{mic} are convective and microconvective heat transfer coefficients defined by equations 2.37 and 2.38 and F and S are defined by equations 2.36 and 2.39. To correlate the experimental data Chen plotted ln(F) against ln(1/XTT) and S against $\ln(Re\ F^{1.25})$ hence

$$\ln(F) = f(\ln(1/XTT)) \qquad 3.4$$

and $$S = f(\ln(Re\ F^{1.25})) \qquad 3.5$$

defining $$F_L = \ln(F) \qquad 3.6$$

then equations 3.1, 3.2 and 3.3 become

$$F_L = f(\ln(1/XTT)) \qquad 3.7$$

$$S = f(\ln(Re) + 1.25\ F_L) \qquad 3.8$$

and $$h_{tp} = e^{F_L}\ h_{con} + S\ h_{mic} \qquad 3.9$$

F was assumed by Chen to be dependent upon XTT only in an analogous manner to the friction factor in two phase flow. However, as discussed in section 1.1.3, Davis (D3) has shown that the friction factor can be more accurately

predicted if the Froude Number is also used as a correlating parameter. Davis defined a parameter, XTF,

$$XTF = 0.19 \; XTT \; Fr^{0.185} \qquad 3.10$$

where

$$Fr = \frac{V_m^2}{D g} \qquad 3.11$$

Davis used XTF instead of XTT in the Lockhart-Martinelli-Nelson model.

It would seem likely that the Froude Number could be used in an analogous way for flow boiling. Using a similar substitution as equation 3.10

$$F_L = f(\ln(1/XTT) + A \; \ln(Fr)) \qquad 3.12$$

where A is the exponent for the Fr. number, as yet unspecified.

In Chen's development of his correlation the exponent of F, 1.25, was derived from the value of the exponent of the Reynold's Number in the Dittus-Boelter equation, but it is by no means certain that the single-phase value of 0.8 is appropriate for heat transfer in flow boiling. Thus if the value of the exponent of F is to be determined from the experimental data the equation 3.8 becomes

$$S = f(\ln(Re) + B \; F_L) \qquad 3.13$$

where B is the exponent of F.

These two modifications to Chen's correlation should result in a more accurate model in so far as that with two extra constants a better fit to the experimental data should be possible.

The form of the F_L and S functions is discussed in section 3.3.

III.2 MODEL B

As mentioned in the previous section the value of hcon used in Chen's correlation and in Model A is that given by the Dittus-Boelter equation

$$h_{con} = 0.023\ Re^{0.8} Pr^{0.4} \qquad 3.14$$

This equation was originally derived for turbulent single-phase heat transfer in pipes. It would seem reasonable to suppose that a better model could be derived if a more applicable equation for h_{con} was used. It was suggested by Davis (D1) that a more suitable form of equation could be developed from a correlation proposed by Rosson and Myers (R6) for heat transfer coefficients during condensation in a horizontal pipe. Rossen and Myers used the Von Karman analogy between heat transfer and momentum transfer and obtained the equation

$$h = \frac{\rho C_p}{Pr} \left(\frac{\tau_w}{\rho}\right)^{\frac{1}{2}} / \left(5 + 5\,\frac{Pr_t}{Pr}\ \ln\left(1 + 5\frac{Pr}{Pr_t}\right)\right) \qquad 3.15$$

where τ_w is the sheer stress at the wall and Pr_t is the turbulent Prandtl Number defined as the ratio of the eddy diffusivity of momentum to the eddy diffusivity of heat. This equation is for the heat transfer coefficient for a vapour condensing on a liquid film on the inside of a horizontal pipe.

Rosson and Myers assumed that the sheer stress at the wall was approximately equal to the average sheer stress in the film and used the Lockhart-Martinelli Model to determine its value. The Lockhart-Martinelli model used the parameter ϕ_f. ϕ_f is defined as (see 1.1.3(2))

$$\phi_f^2 = \left(\frac{dp}{dz}\ F\right) / \left(\frac{dp}{dz}\right)_f \qquad 3.16$$

$$\text{then} \quad \phi_f^2 = \frac{f_L\ V_m^2}{f_{Ls}\ V_L^2} \qquad 3.17$$

where f_L is the friction factor for two-phase flow, V_m is the mean two-phase velocity, f_{Ls} is the friction factor for the liquid flowing alone and V_L the mean velocity of the liquid if it was flowing alone. However f_L can be replaced using the equation

$$f_L = \frac{2\tau_w}{\rho_L V_L^2} \qquad 3.18$$

For a liquid Reynolds Number below 2100

$$f_{Ls} = 16/Re \qquad 3.19$$

Then from equation 3.17, 3.18 and 3.19

$$\tau_w = 8 \phi_f^2 \rho_L V_L^2/Re \qquad 3.20$$

This equation for τ_w can be substituted into equation 3.15 giving

$$h = \frac{\rho C_p}{Pr} \left(\frac{8 \phi_f^2 V_L^2}{Re}\right)^{\frac{1}{2}} / \left(5 + 5 \frac{Pr_t}{Pr} \ln\left(5\frac{Pr}{Pr_t} + 1\right)\right) \qquad 3.21$$

rearranging gives

$$h = \frac{\phi_f k}{D} (8 Re)^{\frac{1}{2}} / \left(5 + 5 \frac{Pr_t}{Pr} \ln\left(5 \frac{Pr}{Pr_t} + 1\right)\right) \qquad 3.22$$

This is the equation developed by Rossen and Myers who then assumed that the eddy diffusivity of momentum was equal to the eddy diffusivity of heat and thus $Pr_t = 1.0$ giving

$$h = \frac{\phi_f k}{D} (8 Re)^{\frac{1}{2}} / (5 + 5(\ln(5 Pr + 1))/Pr) \qquad 3.23$$

However for correlating boiling heat transfer data suggested that a value of 0.5 for Pr_t should be used.

In the above derivation it was assumed that f_{Ls} can be calculated using equation 3.19 which is for laminar flow only. If the Blausius equation

$$f_{Ls} = 0.079 Re^{-0.25} \qquad 3.24$$

is used then equation 3.22 becomes

$$h = \frac{\phi_f k}{D} (0.079 Re^{1.75})^{\frac{1}{2}} / \left(5 + 5\frac{Pr_t}{Pr} \ln\left(5\frac{Pr}{Pr_t} + 1\right)\right) \qquad 3.25$$

However Davis (D1) has recommended that equation 3.22 be used in preference to equation 3.25. Equation 3.22 can be rearranged to give

$$h = \phi_f \frac{k}{D} (0.32\ Re)^{\frac{1}{2}} / (1 + \frac{Pr_t}{Pr} \ln(5 \frac{Pr}{Pr_t} + 1)) \qquad 3.26$$

ϕ_f, the two-phase multiplier, can be predicted using the Lockhart-Martinelli-Nelson model for two-phase flow but it can also be considered in an exactly analogous manner to F in the development of Model A, since ϕ_f was postulated to be a function of 1/XTT only in a similar manner to F. Then replacing ϕ_f by e^{F_b} and defining h_{film} by

$$h_{film} = \frac{k}{D} (0.32\ Re)^{\frac{1}{2}} / (1 + \frac{Pr_t}{Pr} \ln(5 \frac{Pr}{Pr_t} + 1)) \qquad 3.27$$

a correlation analogous to Model A can be formed

$$h_b = e^{F_b}\ h_{film} + S_b\ h_{mic} \qquad 3.28$$

where the subscript b refers to Model B and where

$$F_b = f(\ln(1/XTT) + A_b \ln(Fr)) \qquad 3.29$$

and $$S_b = f(\ln(Re) + B_b\ Fb) \qquad 3.30$$

The value of Pr_t in equation 3.27 can be assumed to be 0.5 or Pr_t can be a constant whose optimum value is to be found using any of the optimisation methods given in Chapter V.

III.3 The Correlating Functions for F and S

To fit the F and S functions, it was decided to use polynomials in the independent variable. Various other possible correlating functions were considered but were rejected as unsuitable for various reasons.

The main advantages of the use of polynomial functions are:-

1) A polynomial function will fit any continuous function over the range of interest to any specified accuracy if sufficient terms are used.

2) The computing of the value of the dependent variable from a polynomial function is faster than for any of the possible alternative functions. This is important in non-linear sum of squares optimisation where most of the computing time is used in the sum of squares error evaluations.

3) It is comparatively easy to add additional terms.

In non-linear optimisation (see Chapter V) the rate of optimisation is highly dependent upon the number of constants whose values are to be optimised. Hence it is important to use the lowest order polynomial compatible with accuracy. Further discussion of this point is left until Chapter IV.

IV. APPARATUS and OPERATION

IV.1 DESCRIPTION OF APPARATUS

IV.1.1 Introduction

The experimental work was carried out in a forced circulation, single tube evaporator (shown in Fig. 4.1) A schematic flow diagram of the rig is shown in Fig. 4.2 The rig was constructed of standard Q.V.F. glassware except where otherwise stated, with the pipework connecting items on the rig being mainly of 2.5 cm (1") or 3.8 cm ($1\frac{1}{2}$") diameter glass sections. The gaskets between the individual sections were all standard asbestos or P.T.F.E. gaskets as supplied by Q.V.F.

Glassfibre and asbestos insulation was used where appropriate to reduce heat losses. The parts of the rig that were insulated are shown in Fig. 4.2.

For the purpose of description the rig can be divided into three sections:-

(1) Reboiler section

(2) Liquid supply and measurement section

(3) Experimental section

IV.1.2 Reboiler Section

The purpose of this section is to initially heat up and degas the experimental liquid and then to maintain it at its atmospheric boiling point. This was achieved by recirculating the liquid held in the 45.8 cm (18") diameter glass reservoir (12) through a 15.2 cm (6") diameter steam boiler (11) with a Stuart-Turner No. 22 centrifugal pump (9)

Figure 4.1. Photograph of Experimental Rig

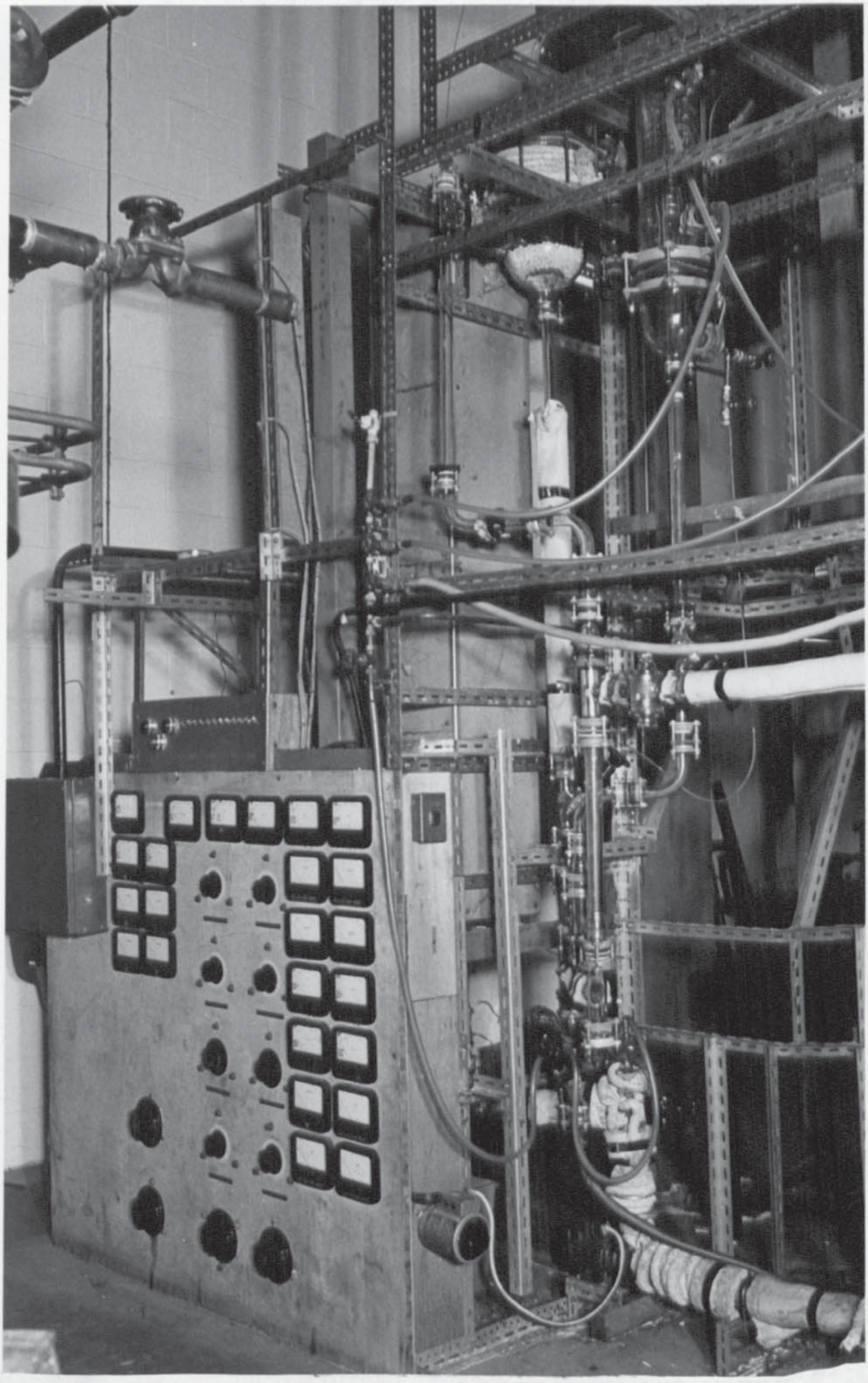

Figure 4.2. Schematic Flow Diagram of Rig

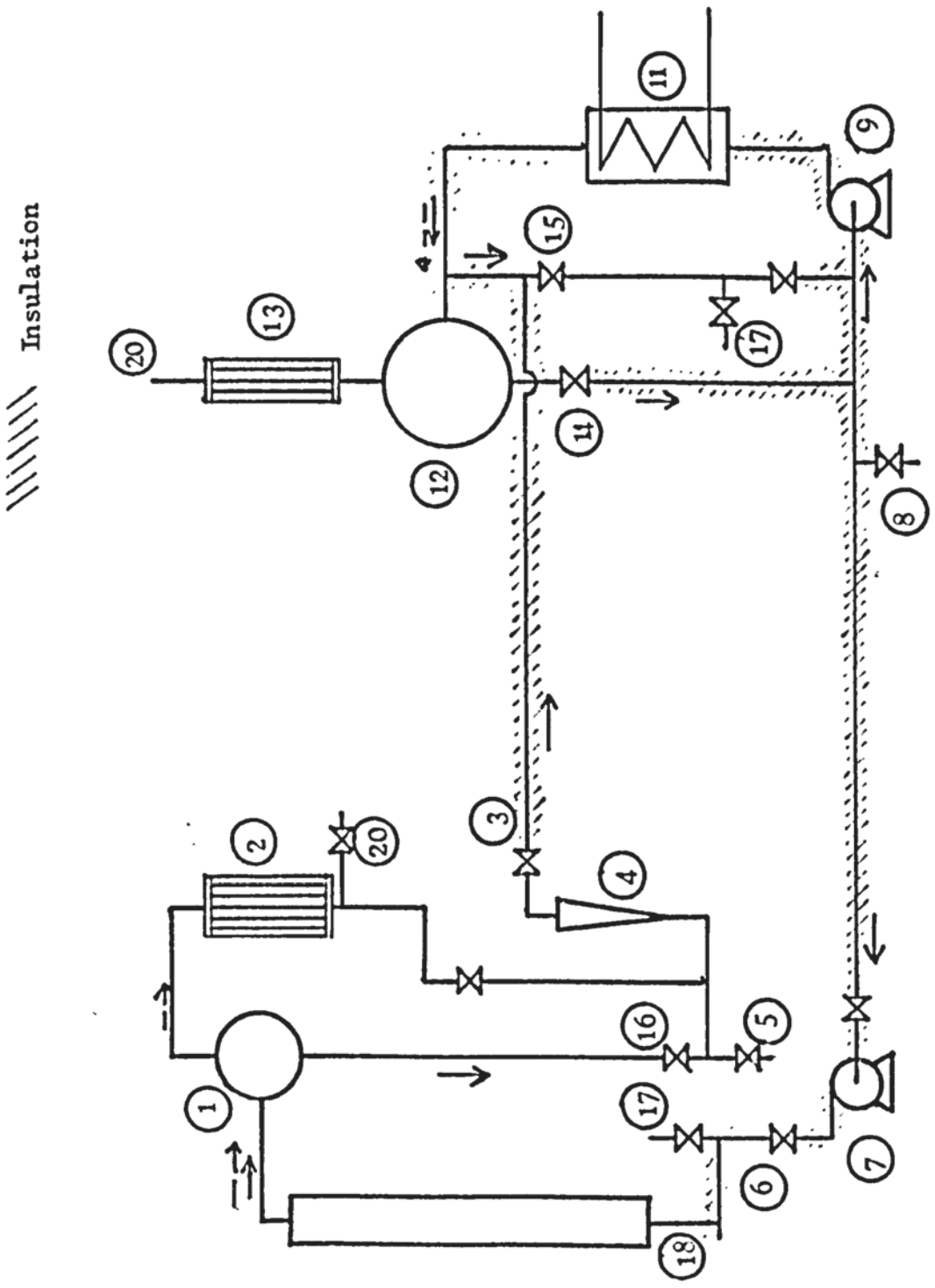

Any vapour produced in the boiler was returned to the reservoir from the 3.8 cm (1½") diameter water-cooled condenser (13). The top of the condenser was vented to the atmosphere. The rate of circulation through the boiler was controlled by altering the pump speed with a 'Variac' variable transformer.

There was also a secondary recycle through valve (15) into which was fed the liquid returning from the flow measurement section. Experience had shown that in the absence of this recycle the pump (9) was prone to 'slugging'.

The steam for the boiler (11) was drawn from the laboratory steam main at approximately 7 bars (90 P.S.I.G.) and after passing through two pressure reducers was fed to the boiler at approximately 2 bars (15 P.S.I.G.)

IV.1.3 Supply Flow Measurement Section

The purpose of this section was threefold:-

(1) To supply the experimental liquid to the experimental section.

(2) To condense the vapour produced in the experimental section.

(3) To measure the liquid flow rate.

The liquid was pumped into the experimental section by the pump (7), a Stuart-Turner No. 12 centrifugal pump. The speed of the pump could be controlled by means of a 'Variac', however, the liquid flow rate was normally varied by use of the valve (6).

The 30.5 cm (12") long glass pipe section (18) leading to the base of the experimental tube had the same bore as the experimental tube itself (1.59 cm) and was intended as

a calming section. Before, this calming section was a mercury in glass thermometer accurate to 0.1°C protruding into the liquid to measure the liquid inlet temperature.

The vapour-liquid mixture leaving the experimental tube discharged into a 30.5 cm (12") diameter vapour-liquid separator (1). Several layers of 1.2 cm diameter glass balls were placed in the bottom of the separator in order to prevent a vortex forming in the liquid outlet and to reduce vapour entrainment in the liquid phase. The vapour fraction from the separator was fed into the top of a 15.3 cm (6") diameter water-cooled condenser (2) via a 5 cm (2") diameter glass pipe. The condensate from the base of the condenser flowed through a valve and joined the liquid fraction from the separator. The combined streams then passed through a 'Rotameter' flow meter, (4) a valve (3) and thence returned to the reboiler section.

By use of the valves (3) and (16), the liquid level in the separator was maintained about 5 cm (2") above its base. This was found to be the most suitable level in order to obtain the most stable reading with the Rotameter. The Rotameter had previously been calibrated for water at 97°C and at 18°C (see Appendix II).

IV.1.4 Experimental Section

(1) General arrangement

The experimental section consisted essentially of a thick-walled copper tube heated by 12 concentric electrical heater sections 15.3 cm (6") long. The wall temperature

Figure 4.3. Photograph of Upper End of Experimental Tube

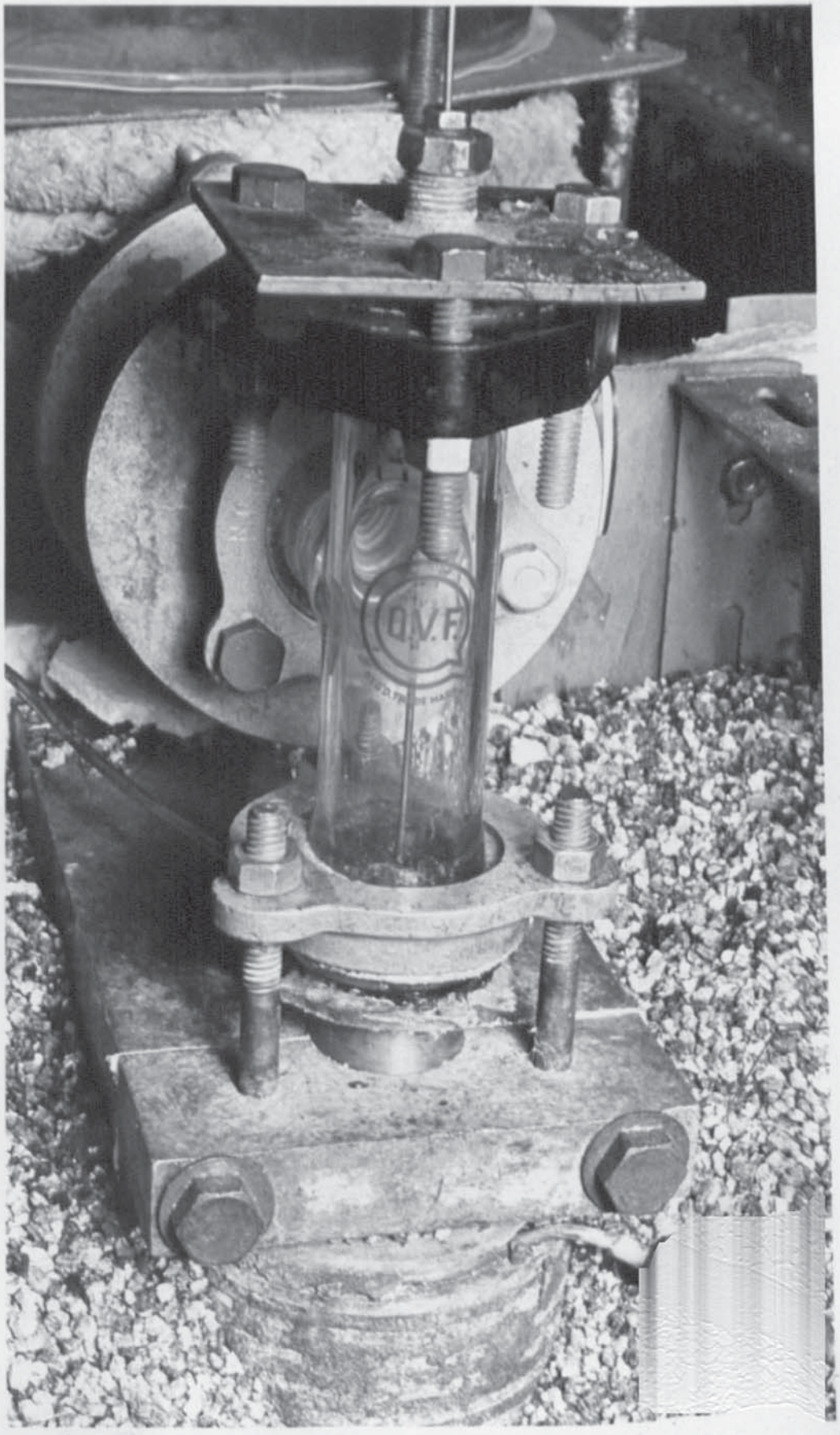

Figure 4.4. Photograph of Lower End of Experimental Tube

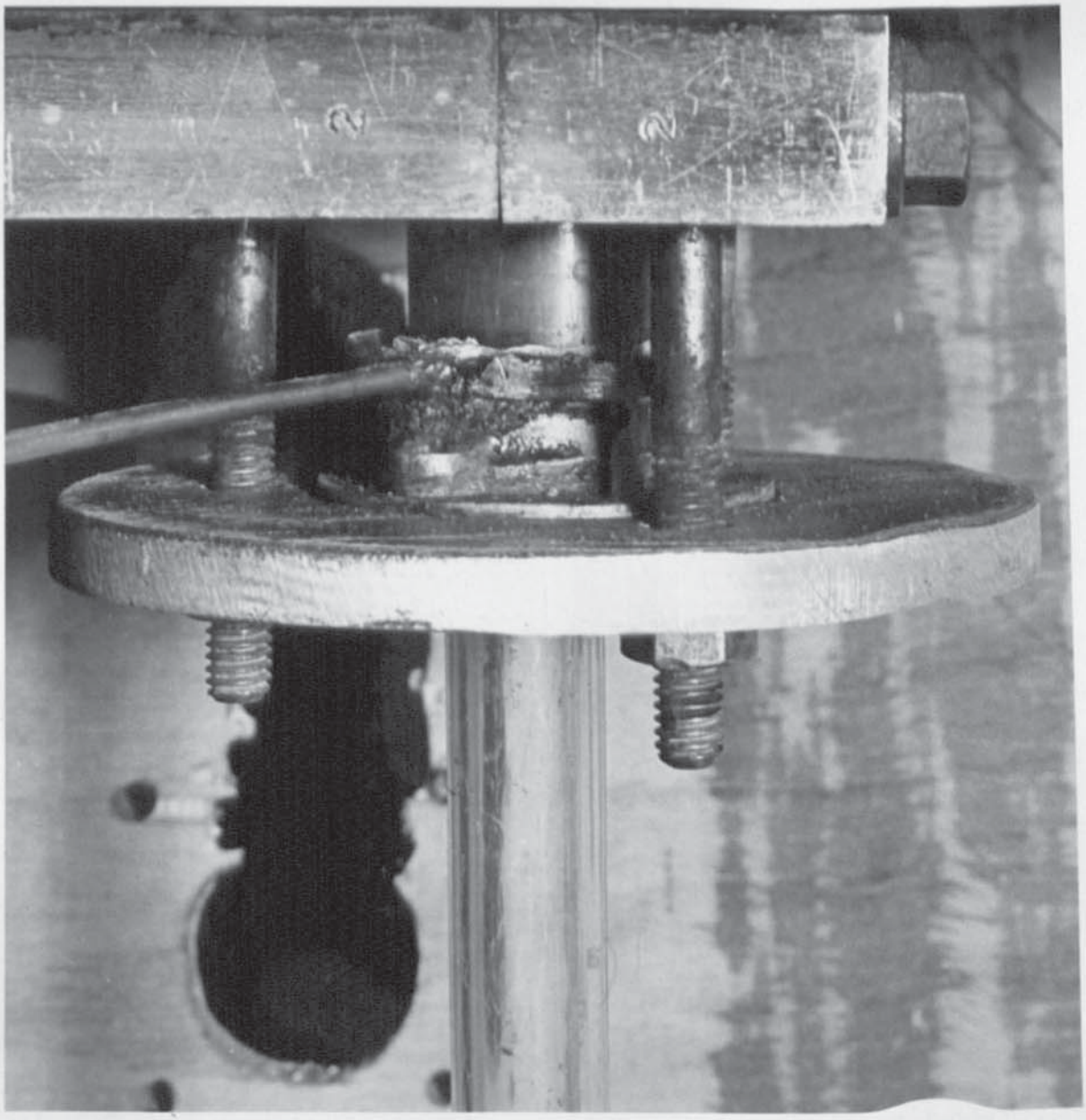

at each increment was measured using thermocouples inserted into the wall of the copper tube, while the bulk temperature of the two-phase mixture was determined using a pressure measuring probe which could be moved along the centre line of the tube. The overall length of the tube was 202 cm (79.5") with a heated length of 182.9 cm (72") with an outside diameter of 3.167 cm (1.247") and an I.D. of 1.58 cm ($\frac{5}{8}$")

The copper tube was clamped at both ends; the upper clamp, however, was supported by metal springs and was thus free to move vertically to allow for expansion when the tube was heated. The column of heater sections was supported by the base of the box surrounding the experimental section. This base was a 2.5 cm (1") thick square of 'Sindanyo', a hard asbestos based insulating material. The box was approximately 30.5 cm (12") square with 0.635 cm ($\frac{1}{4}$") thick plywood sides supported by a metal frame. The space in the box around the heaters was filled with 'Vermiculite', a granular high temperature insulation. Diagrams 4.3 and 4.4 show details of the upper and lower end of the tube.

IV.1.4 (2) Experimental tube and thermocouples

In order to achieve the maximum possible accuracy in the measurement of the wall temperature, $\bar{T}_w$, it is necessary that the following precautions be taken:-

(a) The end of the thermocouple is as close as possible to the inner wall of the tube.

(b) The thermocouple has the least possible effect upon the temperature it is measuring.

These two aims are best achieved by using the smallest sized thermocouple possible and by having the thermocouple inserted into the tube wall at an angle and not radially. Diagram 4.5 shows the details of the arrangement chosen. The thermocouple holes were 7.62 cm (3") apart and in a vertical line with the bottom thermocouple 3.81 ($1\frac{1}{2}$") above the start of the heated section of the experimental tube. Thus there were two thermocouples in each heater section making a total of 24 thermocouples in all.

As it is very difficult to drill deep holes into copper with a diameter of less than about 1.5 mm (1/16") it was decided to use 1.58 mm (1/16") diameter holes. Into each hole was inserted a section of 1.58 mm O.D. copper needle tubing with an internal diameter of 0.51 mm. Before insertion each section was covered with carbon grease in order to ease insertion and also to reduce thermal resistance between the main experimental tube and the copper needle tube.

The thermocouple lead wires were led through a groove cut in the heater blocks and then out through a groove cut in the base of each heater block (see section IV.1.6). From here the wires were taken out of the box surrounding the tube, between sections of the plywood sides and thence to electrical connecting blocks.

For the early experimental runs (up to run 60) two different types of thermocouple were used in alternate positions up the tube. One was a single wire copper-constantan thermocouple and the other a metal sheathed manufactured thermocouple.

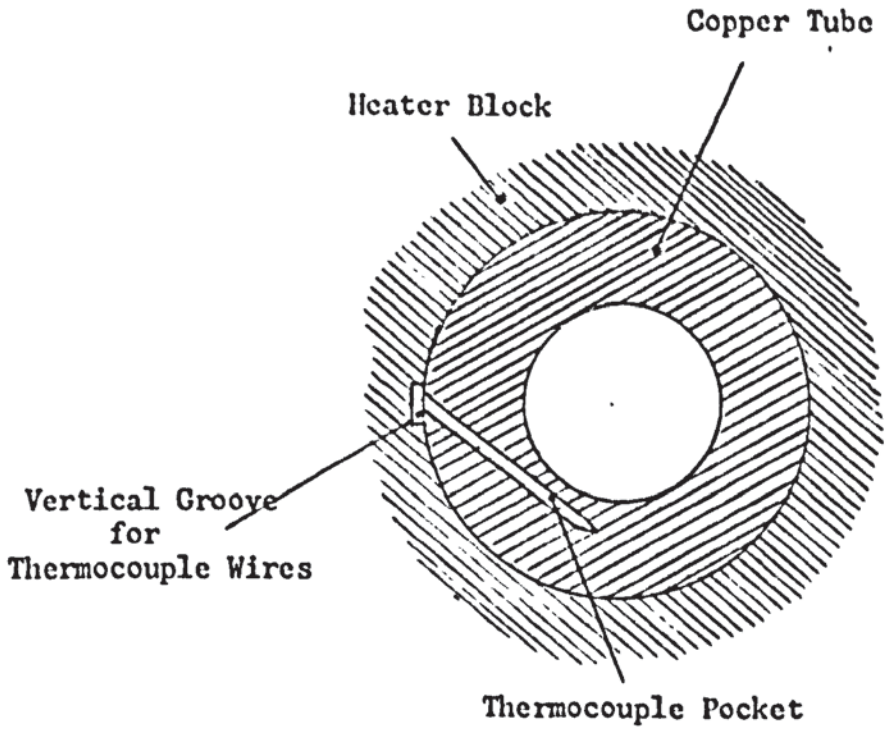

Figure 4.5(a) Horizontal Section through Experimental Section

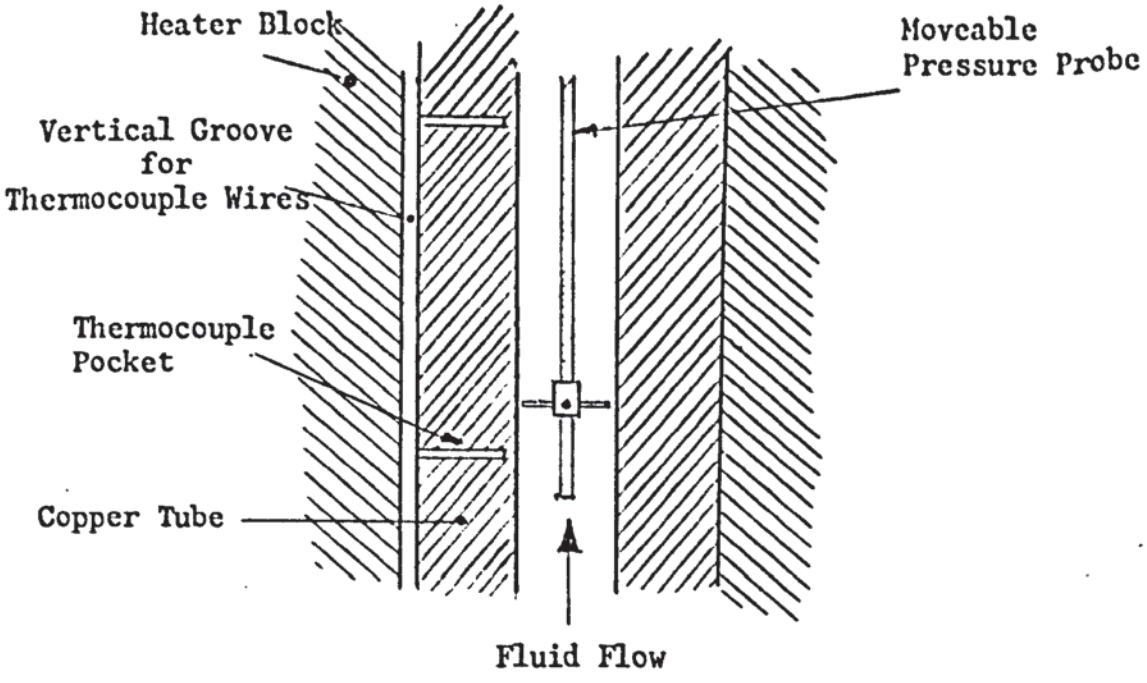

Figure 4.5(b) Vertical Section through Experimental Section

1) Copper-constantan thermocouple.

The design of this type of thermocouple is shown in Fig. 4.6(b). The method of manufacture is as follows:- The 0.38 mm diameter constantan wire was coated in 'Araldite' epoxy resin for the final 2.5 mm of the wire. When this has hardened the final 1 mm of the wire was stripped of Araldite using a small needle file. The wire was then carefully pushed through a section of needle tubing, cut to the correct length, until the bare end of the wire was clear of tubing. The resistance between the wire and the tubing was measured. This being satisfactory (> 100 megohms) the wire was pulled back into the needle tubing until the end of the wire was level with the end of the tubing. The end millimetre of the tubing was squeezed in a vice until it firmly gripped the constantan wire. The end of the tubing was then rounded off and the assembly was now ready to be inserted into the thermocouple hole. The bare thermocouple lead wire was insulated using small bore P.T.F.E. tubing. The copper experimental tube itself was used as the other 'wire' thus all of the copper-constantan thermocouples had a common positive terminal.

These thermocouples were found to be quite satisfactory with regard to accuracy of measurement, however, the P.T.F.E. insulation was prone to breakdown, especially where the wire passed between the heaters. For this reason and their general fragility the use of these thermocouples was discontinued after run 60 and chromel-alumel thermocouples, as described below, used throughout.

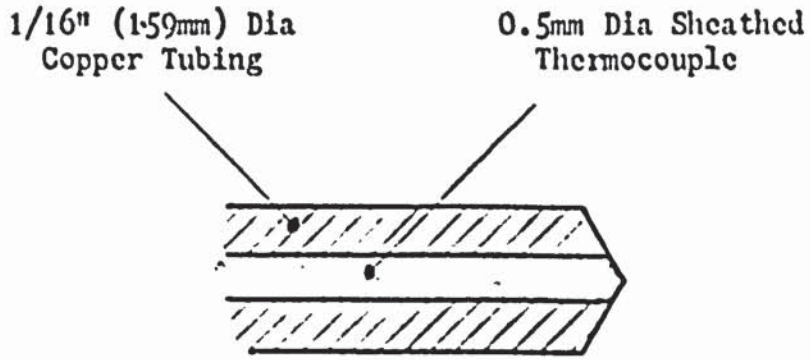

Figure 4.6(a) Section through Chromel/Alumel Thermocouple

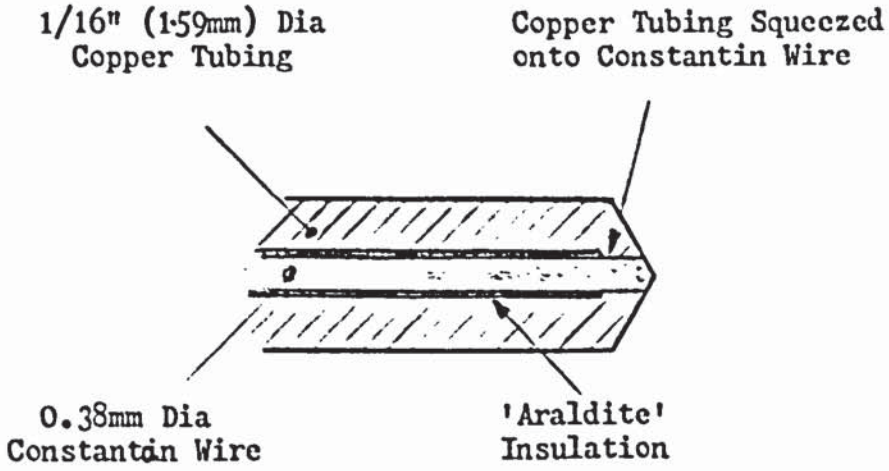

Figure 4.6(b) Section through Copper/Constantin Thermocouple

2) Chromel-Alumel thermocouples.

The chromel-alumel thermocouples were of the bonded junction type and as supplied by Pyrotenax Ltd with mineral insulation and stainless steel sheathing, type TO5 HT7/NC-NA. The outside diameter of the thermocouples was 0.5 mm and thus a good fit in the copper needle tubing.

IV.1.5 E.M.F. Measurement

All the thermocouple leads were connected to a 50-point two-pole selector box. The output from this was connected to the output from a reference junction, a chromel-alumel thermocouple in an ice-filled vacuum flask. The resulting e.m.f. was measured with a digital voltmeter (D.V.M.). A D.V.M. was used in preference to a potentiometer because of the much greater speed with which readings can be taken.

The D.V.M. used was a type DM2-1 made by Computing Techniques Ltd, reading 1.999 V to -1.999 V, with provision for an internal, high input impedence operational amplifier. The amplifier chosen for use was a very low thermal coefficient type.

The amplification chosen was 250 giving an F.S.D. equivalent to 195°C with the last figure on the D.V.M. equivalent to approximately 0.1°C. However it was found that amplifying by 250 in one stage led to instability. To overcome this another similar amplifier was used as a pre-amplifier thus giving amplification in two stages. This arrangement was found to be much more satisfactory and was used throughout the work.

The impedence of the circuit used was given in the specifications of the instrument as $10^{11}\ \Omega$, however it

Figure 4.7(a). Photograph of Assembled Heating Section

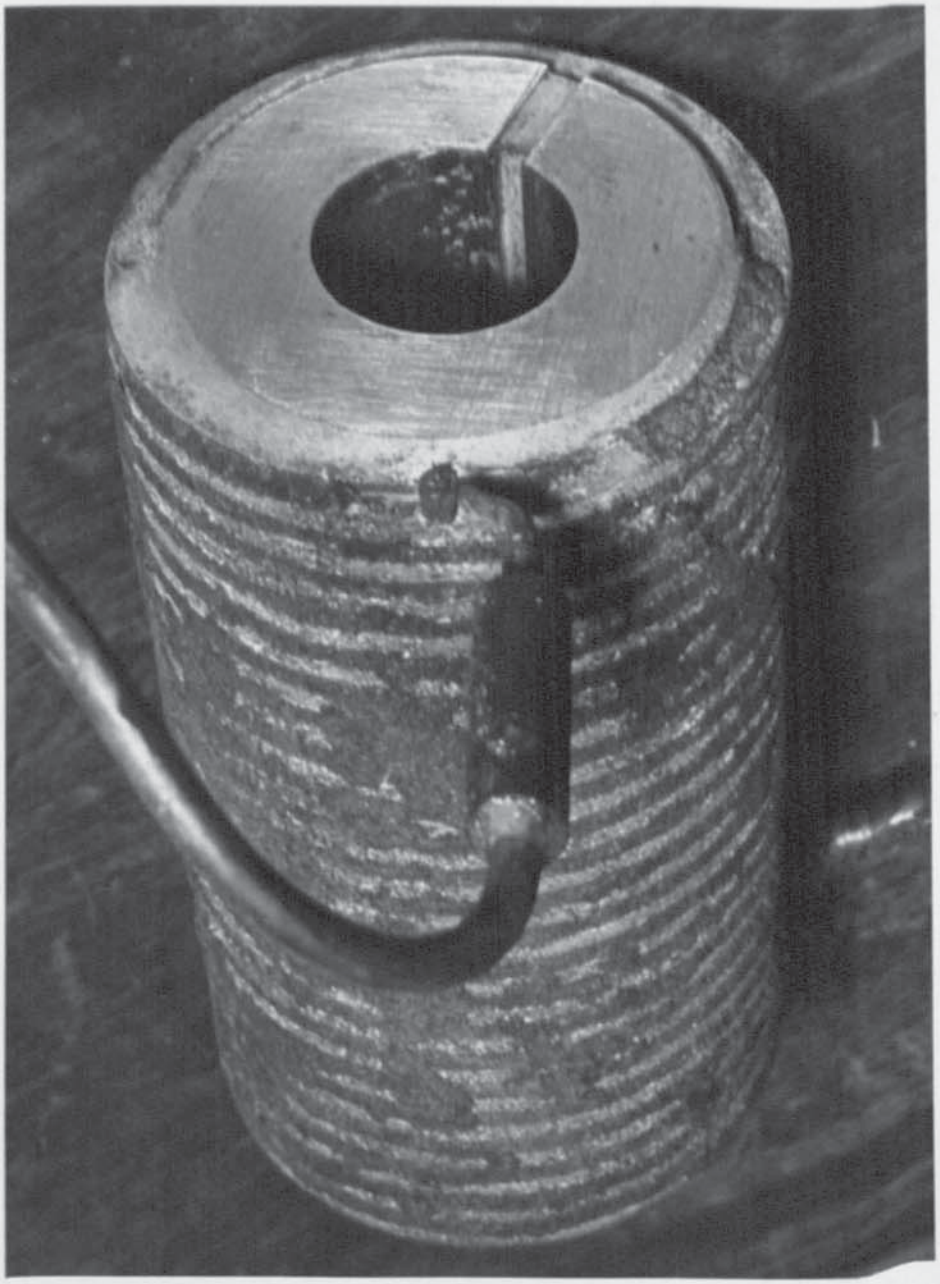

Figure 4.7(b). Photograph of Heater Block

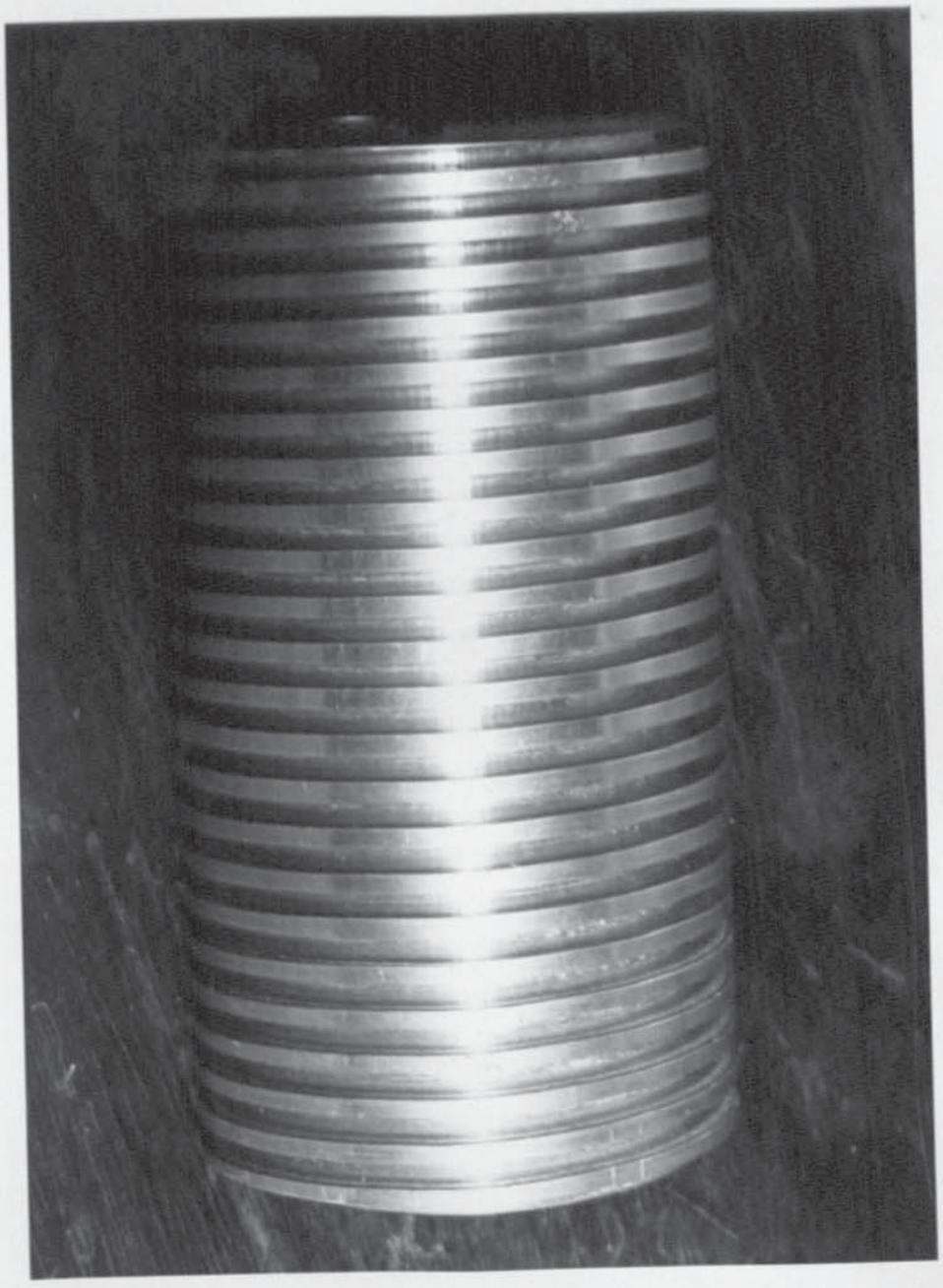

was found that the impedence of the thermocouples affected the reading given. For this reason each thermocouple had to be individually calibrated before each day's runs. Further details of the method of calibration is given in Appendix I.

IV.1.6 Heaters

Fig. 4.7(a) shows a fully assembled heating section and Fig. 4.7(b) shows a heating block before the fitting of the electric element. The heating blocks were thick-walled aluminium tubes 8.26 cm diameter by 15.2 cm (6") long. On the outside of the tubes was cut a 3.175 mm ($\frac{1}{8}$") spiral groove with a 6.35 mm ($\frac{1}{4}$") pitch. The base of the groove was semi-circular and had a diameter of 6.533 cm. This value was chosen so that the heating element would just fill the 24 turns on each block.

The tube had a bore of 3.175 cm ($1\frac{1}{4}$") diameter with a groove, 4.7 mm wide by 1.5 mm deep, cut along the inside wall and another was cut radially in one end of the block so as to meet the internal groove. These grooves were for the thermocouple wires and can be clearly seen in Fig.4.7(a)

The electric elements used in the heaters were mineral-insulated, stainless steel sheathed, heating cable supplied by Pyrotenax Ltd, ref. HSQ1M-4000. The heating part of the cables were 5 metres long with an outside diameter of 3.175 mm ($\frac{1}{8}$"). At each end of the heating element was a high temperature gland and 2 metres of copper sheathed lead-in cable.

The heating element was wound as tightly as possible in the spiral groove, being held in place at each end by a grub screw fitted through the end-most fin. The rest of the groove was then filled with iron cement in order to aid conduction from the outside of the element which would otherwise have been in contact with air only. It was hoped that by thus reducing the maximum sheath temperature the possibility of an element burning out would be minimised.

Each heater section was fitted by sliding it down the tube after the insertion of the thermocouples in its section. The copper tube was first given a thin layer of carbon grease in order to reduce thermal resistance between the heaters and the tube and to ease assembly.

The heater lead-in cables were taken through the sides of the insulation box between sections of the plywood sides and thence to heavy duty connecting blocks. Each heating section was controlled by a 12 amp Variac and fitted with an ammeter and voltmeter to measure the power input. These were calibrated in situ and it was estimated that the maximum error in reading each was 2%, thus giving a maximum error in the calculated wattage of 4%.

The resistance of the heating elements was found to be between 22.2 Ω and 23.2 Ω ; assuming a supply voltage of 240 volts, the maximum wattage per heater would be 2500 watts. In practice the maximum used was 2200 watts.

IV.1.7 Pressure Measurements

For the purposes of this work it was necessary to find the bulk temperature and pressure at each increment up the tube. However, once bulk boiling has commenced the bulk

temperature can be determined from the pressure and vice versa. This being so, only one need be determined experimentally.

Determining the temperature using a thermocouple would have been more convenient as essentialy the same electrical equipment used for measuring the wall temperature would have been used. However, for water at 100°C, a change in temperature of 0.1°C is equivalent to a pressure change of 2.8 mm Hg and while it was comparatively easy to measure pressure to an accuracy of 2.8 mm Hg it would have been much more difficult to measure the bulk temperature to 0.1°C. For this reason it was decided to measure the pressure at each increment with a probe instead of the temperature using a thermocouple.

Details of the probe are shown in Fig. 4.8. The probe was made from a 2 metre length of thin-walled, stainless steel, needle tubing of 1.59 mm (1/16") outside diameter. The stainless steel spider was made separately and then slid along the tubing to the required position where it was held in place using epoxy resin adhesive. In addition, the tubing on both sides of the spider was slightly flattened thus preventing any movement in the spider even if the adhesive failed. The end of the tubing was blocked using epoxy resin adhesive and two small opposing holes drilled just above the blockage. This was to eliminate the velocity component from the pressure measurements.

The tubing passed through a gland fitted to the glass 'tee piece' at the top of the experimental tube (see Fig. 4.3)

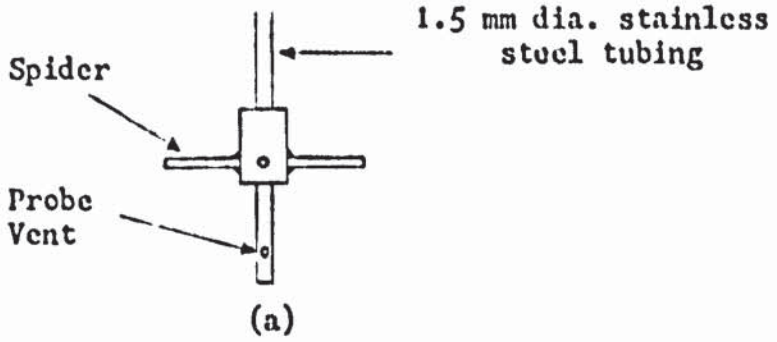

(a)

VERTICAL VIEW OF PROBE

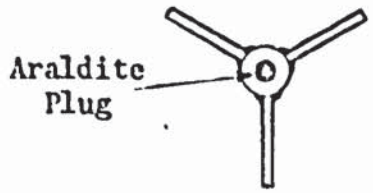

(b)

BOTTOM VIEW OF PROBE

Fig. 4.8 DETAILS OF PRESSURE PROBE

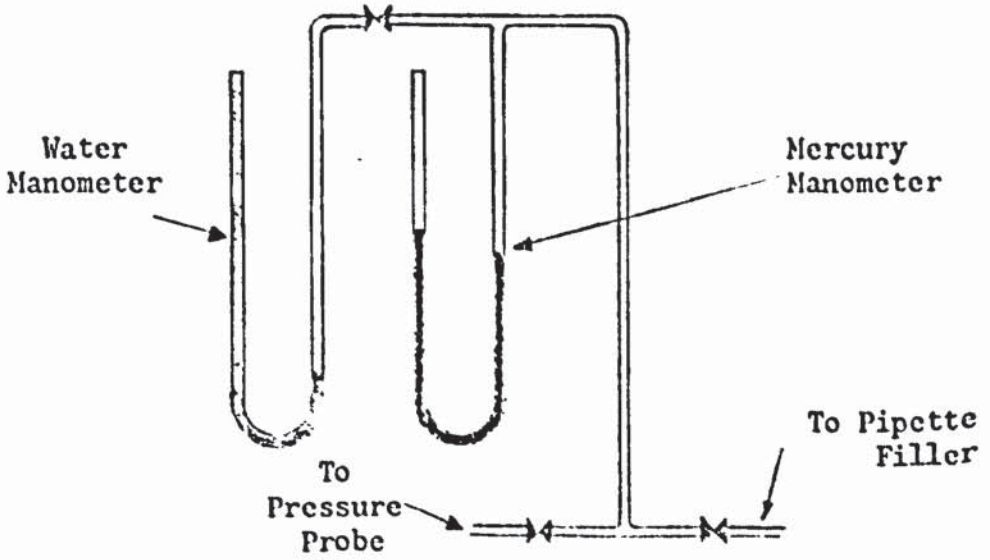

Fig. 4.9 DIAGRAM OF ARRANGEMENT USED TO MEASURE PROBE PRESSURE

This allowed the probe to be moved to any required position in the tube. The position of the end of the probe was determined by measuring the length of tube protruding above the gland.

Fig. 4.9 shows the arrangement used to determine the pressure at each increment. The pressure line was pressurised to above the expected value using the pipette filler, the excess pressure venting through the probe until the mercury manometer settled down to the required value. Readings were taken starting at the bottom and moving up the tube. This meant that pressure readings decreased each time and thus the pressurisation procedure only had to be performed once per run and also less air was vented into the experimental tube.

There were also pressure tappings at the top and bottom of the experimental tube, but as the readings obtained from these were not used in the work presented here, no details are given herein.

IV. 2 Method of Operation

(1) Start-Up

With valves (6) and (3) (see Fig. 4.2) closed, the reboiler section was filled with experimental fluid, until the level was about 5 cm from the top of the reservoir. This amounted to about 45-50 litres of fluid.

After making sure that valves (14) and (15) were open, the recycle pump (9) was started and steam supply to the boiler commenced. Once the liquid flowing from the boiler was seen to boil, the cooling water supply to the condenser (13) was turned on. The fluid was then left circulating for at least 2 hours to degas.

Meanwhile, cold tap water was fed, via valve (17), through the experimental section and then through valve (16) and out through the drain valve (5). While this was reaching equilibrium the thermocouple reference chamber was refilled with ice and the D.V.M. switched on to warm up. The zero and amplification of the D.V.M. were then checked using an accurate potentiometer box and reset if necessary.

Once the inlet water temperature and the wall thermocouple readings had reached equilibrium (usually after about an hour) measurements of all of the thermocouple e.m.f.s were taken and the inlet water temperature noted.

These calibration measurements having been taken the water supply was turned off and valves (17) and (5) closed after the water had been drained away. Valve (6) was then opened and the supply pump (7) switched on. Once the fluid level was high enough, valve (3) was opened and the hot fluid flowing through the experimental section continuously recycled. As before, when the inlet water temperature and the wall thermocouple readings had reached equilibrium, measurements of the wall thermocouple readings and the water inlet temperature were taken.

The calibration readings having been taken (seeAppendix I) the heaters were switched on and adjusted approximately to the wattage to be used for the subsequent experimental runs and the cooling water supply to the condenser (2) turned on. Once degassing was complete the rig was ready for experimental runs to be undertaken.

The start-up procedure outlined above was used for both single-phase and boiling experiments with only minor

modifications for the single-phase experiments. For the single-phase runs it was not necessary to degas the fluid in the reboiler section as it was not used as the experimental liquid but only to calibrate the thermocouples. When the calibration readings had been taken the steam supply was turned off and the hot water in the reboiler section drained away through valve (8).

(2) Single-Phase Experiments

Before any work with boiling fluid was commenced some single-phase runs with cold water were performed in order to test the equipment and to calibrate the rig for heat losses from the experimental section.

Cold water from the mains was fed through valve (17) with valve (6) closed. After passing through the experimental section and the Rotameter it was run to waste through valves (3) and (8). A thermometer accurate to 0.1°C was inserted into the fluid outlet from the experimental tube, through a rubber bung fitted to the glass 'tee' and the top of the experimental section.

It was found that the heat loss from the experimental section varied between 1.5% and -0.5%. Since these were less than the expected error in the determination it was decided to assume that heat losses from the experimental section were negligible.

(3) Boiling Experiments

When the rig was found to be approaching equilibrium after start-up, the wattage of each heater was adjusted to the required value and using valve (6) the flow rate was set.

As mentioned previously, the level of liquid in the downcomer pipe was held about 5 cm above the base of the vapour liquid separator using valves (3) and (16).

When equilibrium was reached the readings were taken. Equilibrium was assumed to have been reached when the wall temperatures, flow rate and the power inputs were unchanged for a period of not less than five minutes. The readings were generally done in the following order: power inputs, fluid inlet temperature, thermocouple readings, flow rate and finally the probe pressure measurements.

This order was chosen so as to minimise any effect of the air vented into the boiling fluid when taking pressure measurements. However, as expected, the presence of the probe was found to affect the pressure drop over the experimental tube. This effect was minimised by positioning the end of the probe just above the last increment in the tube when pressure measurements were not being taken. It was found that by doing this, the pressure at the bottom of the tube was increased by no more than 6 mm Hg when the probe was lowered to the first increment. Indeed, since only readings of that part of the tube where bulk boiling occurs were used, the error in any of the data due to this effect is estimated at no more than 4 mm Hg and this only at high power inputs.

It was found that each run took about 40 minutes; 10 minutes for the readings to be taken and about 30 minutes to reach equilibrium. Thus the experimental fluid was being degassed for about 30 minutes between each run to eliminate any dissolved air resulting from pressure measurements on the previous run.

With each experimental fluid the runs were carried out starting at the lowest heat flux and varying the flow rate to about 10 different values, then the heat flux was increased and the flow rate varied again. This procedure was continued until the highest heat flux was reached.

At first, runs were carried out during the day with the rig shut down overnight, however, it was found that this resulted in a high failure rate of thermocouples. This was deduced to be due to the differing amount of expansion in the copper experimental tube and the column of aluminium heating blocks. At the top of the experimental tube this was estimated to be about 6 mm. It was assumed that flexing of the thermocouples caused by this movement eventually resulted in the thermocouple sheath breaking. To overcome this problem the remaining runs (101-154) were carried out without switching the heaters off. This appeared to prevent any further thermocouple failures.

It was found that the mains voltage varied during the day. This meant that wattage of each heater had to be continually checked and re-adjusted. During certain times of the day the voltage variations were especially large and rapid, such that any experimental readings were impossible. This problem was overcome by operating overnight when only very slow variations of the supply voltage were noted.

(4) Shut Down Procedure

When the readings of the last run of the day's experimental programme had been completed the electrical heaters were turned off and the flow rate of the liquid

feed increased to near the maximum. When the thermocouple readings showed that the wall temperatures had reached equilibrium with the liquid, a set of thermocouple calibration readings were taken (see 4.2 (1). Equilibrium was normally reached in 45-60 minutes depending upon the heat flux used for the last run. These calibration values were compared with those taken before the experimental runs. Experimental readings from those thermocouples whose calibration had changed significantly were subsequently ignored. Normally, however, the difference in the calibrations was less than 0.2°C.

Once the calibration readings had been taken the steam supply to the reboiler was shut off and after about 15 minutes, when the liquid in the reboiler section had ceased boiling, the rig was shut down and, if required, emptied.

V. DATA PREPARATION AND ANALYSIS

V.1 DATA PREPARATION

To present the experimental and derived data in a form suitable for analysis various computer programs were written in Basic-16 (H3) for running on the departmental digital computer, a Honeywell 316 computer system.

The first program, Program I, was one to present the data in a form such that selection of data for further analysis was possible. The data from each run was punched up on paper tape for input to the computer. The data derived from the use of Program I was for each run first output on a teletype. From this output a plot of the bulk temperature and wall temperature, both experimental and as predicted using the Chen correlation, was made. Using these graphs the selection of data to be used for further analysis was made. The criteria used to decide whether an item of data was to be used were as follows:-

(1) Only data from increments where bulk boiling had occurred were used. The somewhat arbitary dividing time of 0.5% vapourisation was chosen. This was the lower limit Chen had found for the applicability of his correlation.

(2) Experimental data points which were obviously grossly in error were not used in the subsequent analysis. This criterion was easy to apply since it was found that, in general, the experimental points formed a fairly smooth curve when plotted, except for a few points which fell a

long way from the rest of the data and were obviously incorrect and could be discarded. Generally points discarded under this criterion were consistent from run to run thus implying a systematic error as opposed to a random error.

Figs. 6.8 - 6.16 show some typical graphs of experimental data, showing those points used in subsequent analysis. When the data to be used subsequently had been selected, the raw data were run again using Program II which output the selected data onto paper tape in a format suitable for further processing.

Both of these programs are discussed further in Appendix IV .

It was intended that the data fitting and correlation would be performed on the Aston University ICL 1905E computer system, however, the paper tape code of the Honeywell 316 was incompatible with that of the ICL 1905E. This difficulty was overcome by using a machine code program on the Honeywell 316 to convert the paper tape output to a form compatible with the ICL 1905E.

This final paper tape output was then loaded into the ICL 1905E and stored upon permanent magnetic tape files. This data, however, was stored in a comparatively bulky and inconvenient form, with each data value requiring two lines. In order to compact the data and store it in a more convenient form a small program was written and run. These files were then used in all of the correlating programs.

PAGE NUMBERING AS ORIGINAL

Later a much faster CDC 7600 computer at the University of Manchester Regional Computer Centre (UMRCC) was used. This required the data files to be transferred to the file store at UMRCC.

V.2 DATA ANALYSIS AND CORRELATION

V.2.1 Outline of Problem

We assume that the heat transfer coefficients can be correlated by an equation of the form

$$h = f(x_1, x_2, \ldots x_k, v_1, v_2, \ldots v_m) \qquad 5.1$$

where $x_1 .. x_k$ are correlating constants and $v_1 ... v_m$ are physical values, e.g. bulk temperature, physical properties. Then defining;

$$S = \Sigma_1^n (h - h_x)^2 \qquad 5.2$$

where h_x are experimental heat transfer coefficients and n the number of experimental points.

Then the optimum values for $(x_1 .... x_k)$ are those giving the minimum value of S. The root mean square error, Sr is a function of the value of S, given by

$$Sr = (S/n)^{\frac{1}{2}} \qquad 5.3$$

V.2.2 Introduction

Because none of the models described in Chapter III are linear, nor can they be transformed into linear equations, non-linear least squares optimisation methods must be used to determine the optimum values for the correlating constants.

However, for the Chen correlation an iterative linear method can be used due to the particular form of the correlation. This method is fully explained in section V.2.3 below.

More general methods for non-linear least squares optimisation proceed by varying the correlating constants from 'base' values until a set of correlating constants giving a lower sum of squares error is found. These new values then become a new base point and the procedure repeated. The various non-linear least squares optimisation methods differ in the procedure used to derive the search points.

Non-linear least square optimisation methods can be divided into those using derivatives and those not. According to Jones (J2), the best method using derivatives is the Spiral Algorithim (J2). The method is described in section V.2.4. However when the Spiral Algorithim was used to fit the experimental data it was found not to be entirely satisfactory. For this reason methods not requiring derivatives were investigated. A program using Rosenbrock's method (R5) was available in the department (G1) and this program was modified for use with the various models described in Chapter III. This program is described in section V.2.5. Later this program was further modified so as to use the method of Davis, Swann and Campey

V.2.3 Iterative Linear Method

This method is applicable only to Chen's model as defined by equations 3.7, 3.8 and 3.9.

$$h_{tp} = e^{F_L} h_{con} + S\, h_{mic} \qquad 5.1$$

$$F_L = f(\ln(1/XTT)) \qquad 5.2$$

$$S = f(\ln(Re) + 1.25\, F_L) \qquad 5.3$$

The following procedure is used. An initial estimate of the polynomial function F in equation 5.2 is made. Using the values of F thus derived from the experimental data the equivalent values for S can be found. From equation 5.1

$$S = (h_{tp} - e^{F_L} h_{con})/ h_{mic} \qquad 5.4$$

These values of S thus derived can then be correlated with the values of $(\ln(Re) + 1.25 F_L)$ derived from the experimental data and by the use of the assumed polynomial equation for F_L

Using the correlation for S thus derived a similar procedure for F_L can be carried out. From equation 5.1

$$F_L = \ln(h_{tp} - S h_{mic})/h_{con}) \qquad 5.5$$

These values of F_L can then be fitted to the values of $\ln(1/XTT)$ derived from experimental data. This iterative procedure is repeated until the coefficients in the polynomials for F_L and S reach stable values. Fifth order polynomials were used for the F_L and S functions. A fourth order polynomial fitted to Chen's F graph was used as the initial function for F_L

The procedure outlined above is similar to that used by Chen, however, it was found that unlike in Chen's work, the sum of squares error increased with each iteration. Various reasons can be proposed to account for this:-

(1) The polynomial least squares procedure used in this method minimises the sum of squares error on the F_L and S functions. However, since F_L is an exponent in the final equation the polynomial found when fitting F_L is not

necessarily the optimum polynomial for minimising the sum of squares error of the total correlation (L1). This difficulty can be at least partially overcome by using weights on each data point in the polynomial fitting procedure(L1). However this would have greatly complicated the program written to implement this method and would have negated the method's advantages, which are its speed, simplicity and ease of programming.

(2) The range of the experimental data points may not have been wide enough to give stable solutions and thus the iterative solutions found were unstable and hence each iteration diverged instead of converging upon the optimum.

Chen (C3) gives few details of the iterative procedure used to obtain his correlation hence it is difficult to determine whether the possible reasons for non-convergence given above would apply to the exact method used by Chen.

However, since Chen used data from more than one system and over a much wider range of parameter values it is unlikely that the second possible reason would apply to Chen's work.

A listing and brief description of the program used is given in Appendix IV .

V.2.4 Spiral Algorithm

The spiral algorithm is a non-linear optimisation procedure developed by Jones (J1), who claimed it to be the best optimisation procedure using derivatives for non-linear problems. The program used was based upon

a program written by Coleby (C7). The program was found to be good for initial optimisation from a bad starting point, however, once the initial fast reduction in the sum of squares had been achieved the rate of progress rapidly fell off until progress virtually ceased. It is possible that the failure of the spiral algorithm near the optimum was due to the very steep sum of squares 'valley' which was presumed to exist in region of the optimum. References (J1) and (C7) describe in detail the theory and use of the spiral algorithm and thus further details of the procedure are not presented in this thesis.

V.2.5 Rosenbrock's Method

Rosenbrock's method is one of the most widely used non-linear least squares optimisation procedures and together with Davis, Swann and Campey's method have the advantage over the spiral algorithm of being very easily modified to handle different models. Only the subroutine for evaluating the sum of squares need be altered. This allows many different models to be investigated without tedious program modifications.

Rosenbrock's method (R5) uses n mutually orthogonal direction vectors, where n is the number of parameters to be optimised. For the first stage the co-ordinate vectors are used. Starting from an initial 'base' point the search commences by making a step along each vector in turn, the step d_i being associated with the i^{th} vector. If a step gives a sum of squares error no greater than the base

value this point is termed a success and becomes the new base point. If a step gives a sum of squares error that is larger than the base value, then this step is termed a failure. With a success the step length di is increased by a factor α while for a failure the step length is multiplied by β

When a step has been considered along all n vectors the process is repeated until a success has been followed by a failure along each vector. At this point a new set of orthogonal vectors are derived, the first vector being in the direction of total progress made during the stage.

The re-orthogonalisation procedure used by Rosenbrock breaks down if the progress made along any of the vectors is zero or very small compared to the total progress made. For this reason the procedure used by Davis, Swann and Campey (D2), which does not have this drawback, was used. α and β were given the values 3 and -0.5 as recommended by Rosenbrock.

Experience showed Rosenbrock's method to be reasonably satisfactory, but it was found to be prone to breaking down due to numerical overflow caused by the vector step lengths becoming too small. This problem could be partially overcome by ignoring those vectors whose step lengths fell below a specified limit. However, this led to other problems especially that of slow convergence. It was for this reason that the program was modified so as to use Davis, Swann and Campey's method.

V.2.6 Davis, Swann and Campey's Method

This is a modification of Rosenbrock's method incorporating a multivariate search along each vector (D2).

Taking each vector in turn a search was performed along the vector to find the optimum point. As with Rosenbrock's method a success generates a point further along the vector, however, in this method α is equal to 2, with β equal to -0.5, as in Rosenbrock's method. When a success is followed by a failure along the vector a point midway between the last two points is investigated. This procedure gives four equally spaced points along the vector. Taking the best point and the two adjacent points a quadratic interpolation is performed. A sum of squares evaluation is performed on this interpolated point and the best point found on the vector is used as the base point for further optimisation. When each vector has been thus investigated a vector re-orthogonalisation is performed as in Rosenbrock's method and the procedure repeated until the optimum point has been reached.

The method of Davis, Swann and Campey was found to be the best of those used, however, it was not without its problems. Convergence was found to be fairly slow, but it is unlikely that any other method would have been significantly faster. Convergence was found to proceed in a stepwise manner with periods of rapid convergence alternating with periods of negligible progress. This is probably due to the method requiring a large number of sum of squares evaluations to re-orientate itself along the sum of squares valley after each period of rapid progress.

As with Rosenbrock's method problems were encountered when the step length along any of the vectors became very small and the same modifications as used on Rosenbrock's method were used to circumvent this problem.

Initially, convergence was assumed to have occurred when the step lengths on all of the vectors had fallen below a specified limit. Normally when this occurred the value of the sum of squares error was seen to have changed very little over the final few iterations and thus the assumption of convergence appeared reasonable. However, it was found that a further, often considerable, reduction in the sum of squares could be achieved if the final parameter values found were used as the initial starting points for a further attempt at optimisation using the same program. It is possible that this was due to the procedure used in the program of initially optimising along the co-ordinate vectors. This may have had the effect of 'tightening up' the parameter values, leading to a period of comparatively rapid optimisation. It was also found that by slightly perturbing one or more of the parameter values before re-optimisation further improved the rate of convergence.

A listing of the final form of the program used is given in Appendix IV .

V.2.7 General Comments

The main difficulty with all non-linear optimisation procedures is the difficulty of determining whether the global optimum has been reached (L1). For problems involving complicated expressions, such as in this work,

it is possible that more than one local minimum may exist. However it is normally impossible to confirm the existence, or otherwise, of more than one local minimum except by determining the contours of the sum of squares surface over the total parameter range. Such a procedure is normally unrealistic due to the immense amount of computer time it requires. In practice, the optimisation is normally performed from more than one starting point. This procedure, while not infallible, will normally show whether the global minimum has been reached. However, for problems such as in this work, with a very large amount of experimental data even such a procedure as this is unrealistic due to the very large amount of expensive computer time necessary. Even with a very fast computer such as the CDC 7600 up to 500 seconds were required to complete an optimisation. A further indication of whether the global minimum value of the sum of squares has been reached is if the sum of squares error is approximately equal to the expected experimental error in the data. But it is normally impossible to have a measure of the experimental error without first having an equation correlating the experimental results. Thus, it must often be a matter of personal judgement as to whether the best possible correlation for the experimental data has been determined.

VI. RESULTS and DISCUSSION

VI.1 Introduction

It was originally intended to fit both the water data and the azeotrope data simultaneously, however, the azeotrope data was found to be highly anomalous and so it became impossible to fit both sets of data to any single correlation. From tests carried out it was concluded that the ethylene diacetate azeotrope had been subject to partial hydrolysis which greatly affected the experimental results. For this reason both sets of data had to be correlated separately; the water data results are discussed in section VI.3 and the azeotropnic data in section VI.4.

Before the results are considered in detail it is necessary to give some attention to the accuracy of the data in order to consider properly the significance of the root mean error associated with each correlation. An analysis of the sources of error in the experimental data and their effect upon the accuracy of the data appears in section VI.2 below.

It is important to realise the true significance of the root mean square percentage error associated with each correlation. Since the data points were selected so as to exclude those data points with a high error the overall percentage errors in themselves have little significance as absolute values. Their main importance is in their use to compare the correlations.

Figs. 6.5 to 6.13 show the measured wall temperatures, wall temperatures predicted from Chen's correlation and wall temperatures predicted from five of the correlations derived in this work for nine of the experimental runs. The nine runs presented were selected so as to cover the full range of heat flux and flowrate values.

It was found, however, that the wall temperatures predicted from the derived correlations were, in general, so close that it was found impossible to draw separate curves for the five correlations. For this reason the five correlations have been represented by one line although this does not imply that the five correlations are always coincident.

No pattern could be perceived in the slight divergences that occurred between the curves for each of the correlations nor in the magnitude and distribution of the errors.

VI.2 Accuracy of the Data

That there are a large number of sources of error in the experimental data is due to the large number of variables which affect the experimental heat transfer coefficients. Each experimental variable which must be measured has its associated error and thus to obtain an estimate of the magnitude of the experimental error associated with each data point it is necessary to consider each experimental variable in turn.

For the purposes of this discussion three different heat transfer coefficients must be recognised at each data point. The measured heat transfer coefficient is the first and the second is the actual but unknown heat transfer coefficient. The third heat transfer coefficient is called the predicted heat transfer coefficient. It is assumed that a correlation of the same form as Chen's correlation is used but that this hypothetical correlation would fit the data exactly if there was no experimental error; i.e. the correlation is perfect. However, this predicted heat transfer coefficient was measured values of the experimental variables and errors in these measurements will lead to errors in this 'predicted' heat transfer coefficient.

VI.2.1 Inlet Temperature

As mentioned in section IV.1.3 the maximum error expected in the measurement in the inlet temperature is $0.1^{o}C$. In the boiling section of the experimental tube the bulk temperature is derived from the bulk pressure and thus is unaffected by errors in the inlet temperature. However the inlet temperature is used in the calculation of the quality in the boiling section. It can easily be shown that a $0.1^{o}C$ error in the inlet temperature measurement leads to an error of 0.0002 in the predicted quality. As only points with a quality greater than 0.005 were used, this gives a maximum error of 4% in

the quality which corresponds to an error of approximately 4% in the predicted heat transfer coefficient. However for most of the data points the error is likely to be much smaller than this.

VI.2.2 Bulk Pressure

The maximum error in the bulk pressure measurement over the boiling section is likely to be about 2.5 mm Hg which is equivalent to an error of 0.1°C in the bulk temperature. As with the inlet temperature discussed above this error leads to an error in the predicted heat transfer coefficient of upto 4% due to the error caused in the predicted quality. However there are a number of other ways in which an error in the bulk pressure affects the predicted heat transfer coefficient. First errors in the bulk pressure and temperature lead to errors in the predicted physical properties, but the effect of this on the predicted heat transfer coefficient is likely to be small, less than 1%. Secondly, the terms $(P_w - P_b)$ and $(T_w - T_b)$ are parameters in the nucleate boiling term in the Chen correlation, however, the effect of bulk pressure errors upon these terms will be small, usually less than 0.5%.

An error in the predicted bulk temperature will affect the measured coefficient. The maximum error caused by a bulk temperature error of 0.1°C will be about 3%.

VI.2.3 Wall Temperature

Errors in the wall temperature measurements are by far the most important source of error in both the measured and predicted heat transfer coefficients. In the data used for fitting the maximum error in the wall temperature measurements was of the order of 1.5°C to 2.0°C depending upon the heat flux. This corresponds to errors in the measured heat transfer coefficients of upto 20%.

Errors in the wall temperature measurements also affect the predicted heat transfer coefficients due to their effect on the terms (P_w-P_b) and (T_w-T_b). Errors in the predicted heat transfer coefficient due to wall temperature errors will be of upto 15% in the nucleate boiling region but much less in the two-phase forced convection region where the nucleate boiling term is much smaller.

The errors in the predicted and measured heat transfer coefficients are opposite in sign and thus the difference between the measured and predicted heat transfer coefficients could be upto 35%. However data points with errors as high as this would almost certainly have not been used for fitting the correlations. (See section V.1).

VI.2.4 Flowrate

The maximum error in the measured flowrate is unlikely to be more than 2%. An error in the flowrate

would cause an error in the predicted quality approximately equal to the error in the flowrate. This would cause a maximum error in the predicted heat transfer coefficient of upto 2%. An error in the measured flowrate also results in errors in the predicted Re and Fr numbers causing an error in the predicted heat transfer coefficient of upto 1.5%. Thus the total maximum error in the predicted heat transfer coefficient due to error in the measured flowrate is about 3.5%

VI.2.5 Heat Flux

The maximum error in the setting of the heat flux was estimated to be about 4%. This would correspond to an error of 4% in the measured heat transfer coefficient. Errors in the heat flux only directly affect the predicted heat transfer insofar as they affect the wall temperature. This effect is likely to be small.

The error in the total heat flow will be smaller than the 4% error on each heater since errors on each of the heaters will tend to cancel each other out. The maximum overall error in the assumed heat flow is likely to be of the order of 1.5%. Due to its effect upon the quality this error will cause a corresponding error in the predicted heat transfer coefficient.

VI.2.6 Physical Properties

For water whose physical properties are accurately known over the range of experimental conditions, the equations used to predict the physical properties are

probably all accurate to at least 1% and thus the maximum error in the predicted heat transfer coefficient is probably no more than 0.5%. For the azeotrope physical properties errors of upto 5% could be expected for those physical properties whose values were not derived from experimental data. The physical property correlations derived from experimental data are probably accurate to.2%.

However, it appeared that the EDA in the azeotrope was subject to partial hydrolysis. If this was so then the errors in the physical property values are likely to be substantially higher. This is discussed further in VI.4.

VI.2.7 Overall Errors

When all of the possible sources of error are considered it is clear that the maximum likely errors in both the measured and predicted heat transfer coefficients are very high. However it must be remembered that data points which appeared to have a high error were not used. (see section V.1) Thus it would be expected that the maximum error in the data used would be less than that expected from the foregoing analysis, and this was found to be so. Indeed the maximum difference found between the measured heat transfer coefficient and the predicted heat transfer coefficient using any of the derived models was of the order of 25%.

VI.3 WATER DATA

The water data used in fitting the various correlations consisted of 520 selected points covering the range of conditions given below:-

Flowrate 0.07 to 0.325 kg/s (352 to 1633 kg/m^2s)

Heat flux 0.955×10^5 to 2.89×10^5 w/m^2

Quality 0.5 to 12.7%

An initial attempt was made to fit the data to Chen's model using the iterative procedure used by Chen outlined in section V.2.3 However the method was found not to work when used with the data presented in this thesis. The possible reasons for the failure of this method have already been discussed in section V.2.3 The water data was subsequently fitted using the Davis, Swann and Campey optimisation program discussed in section V.2.6 The data was fitted four different models; a five parameter model, Chen's model and two models developed in Chapter III.

VI.3.1 Five Parameter Model

In order to test the optimisation program and to give an error datum for the other correlations, the selected data was fitted to a simple five parameter model derived from the Chen model but assuming S constant over the range of the data. F_L was fitted as a fourth order polynomial in terms of $\ln(\frac{1}{XTT})$. The optimum fit found was

$$F_L = 1.195 + 0.5568 \ln(\tfrac{1}{XTT}) + 0.07817 (\ln(\tfrac{1}{XTT}))^2 - 0.009097 (\ln(\tfrac{1}{XTT}))^3 \quad 6.1$$

and $S = 0.0131$ 6.2

These equations are used in conjunction with equations

$$h_{con} = 0.023 \frac{kf}{D} \left(\frac{G\ (1-x)\ D}{\mu_f}\right)^{0.8} Pr^{0.4} \qquad 6.3$$

$$h_{mic} = 0.00122 \left(\frac{k_f^{0.79}\ Cp_f^{0.45}\ \rho_f^{0.49}}{\sigma^{0.3}\ \mu_f^{0.29}\ Lv^{0.24}\ \rho_g^{0.24}}\right) \Delta T_{SAT}^{0.24}\ \Delta P_{SAT}^{0.75} \qquad 6.4$$

$$h_{tp} = h_{con}\ e^{F_L} + h_{mic}\ S \qquad 6.5$$

The root mean square percentage error was 13.26%.

Fig. 6.1 shows the F_L curves for Chen's correlation together with those found for each of the other correlations based on Chen's model. Similarly Fig. 6.2 shows the S curves for Chen's correlation and for the other correlations based upon Chen's model. This correlation is discussed further in conjunction with the other correlations found for the water data.

VI.3.2 Chen's Model

Chen's model was presented in section II.3 and was optimised on the selected water data using the Davis, Swann and Campey optimisation method described in section III.3.

The optimum functions found for F_L and S were:

$$F_L = 1.3577 + 0.5814 \ln\left(\frac{1}{XTT}\right) + 0.05896 \left(\ln\left(\frac{1}{XTT}\right)\right)^2 - 0.001799 \left(\ln\left(\frac{1}{XTT}\right)\right)^3 \qquad 6.6$$

$$S = 14.642 - 2.4199\ R_L + 0.1391\ R_L^2 - 0.003356\ R_L^3 \qquad 6.7$$

$$\text{where } R_L = \ln(Re_{tp}) = \ln\left(\frac{G\ (1-x)\ D}{\mu_f}\right) + 1.25\ F_L \qquad 6.8$$

These equations are used in conjunction with equations 6.3, 6.4 and 6.5. This fit has a root mean square percentage error of 11.10%. As previously mentioned the F_L and S curves are shown in Fig. 6.1 and 6.2 respectively.

Figure 6.1 Graphs of ln(F) v/s ln $(\frac{1}{XTT})$

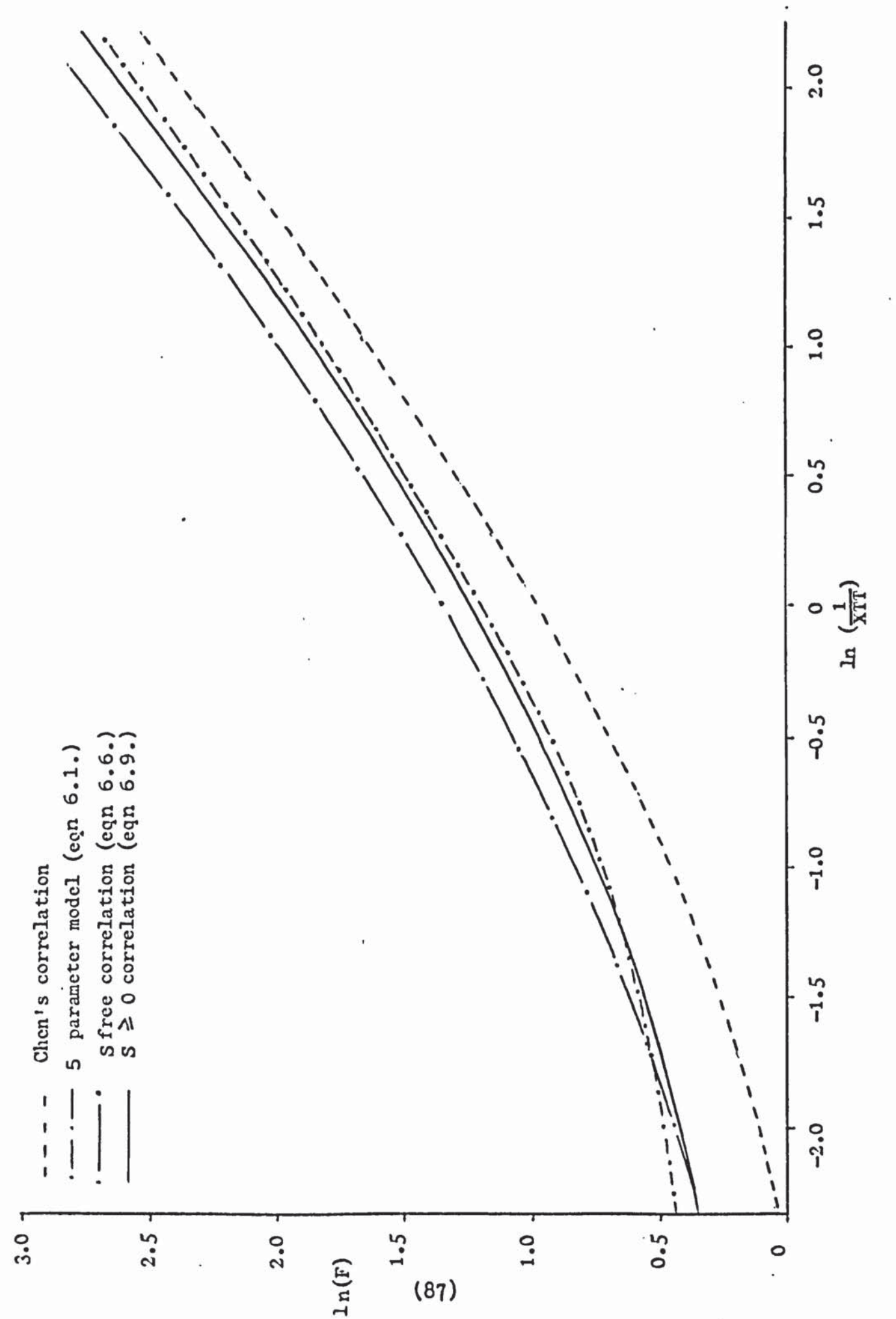

Figure 6.2 Graphs of S v/s $\ln(Re_{tp})$

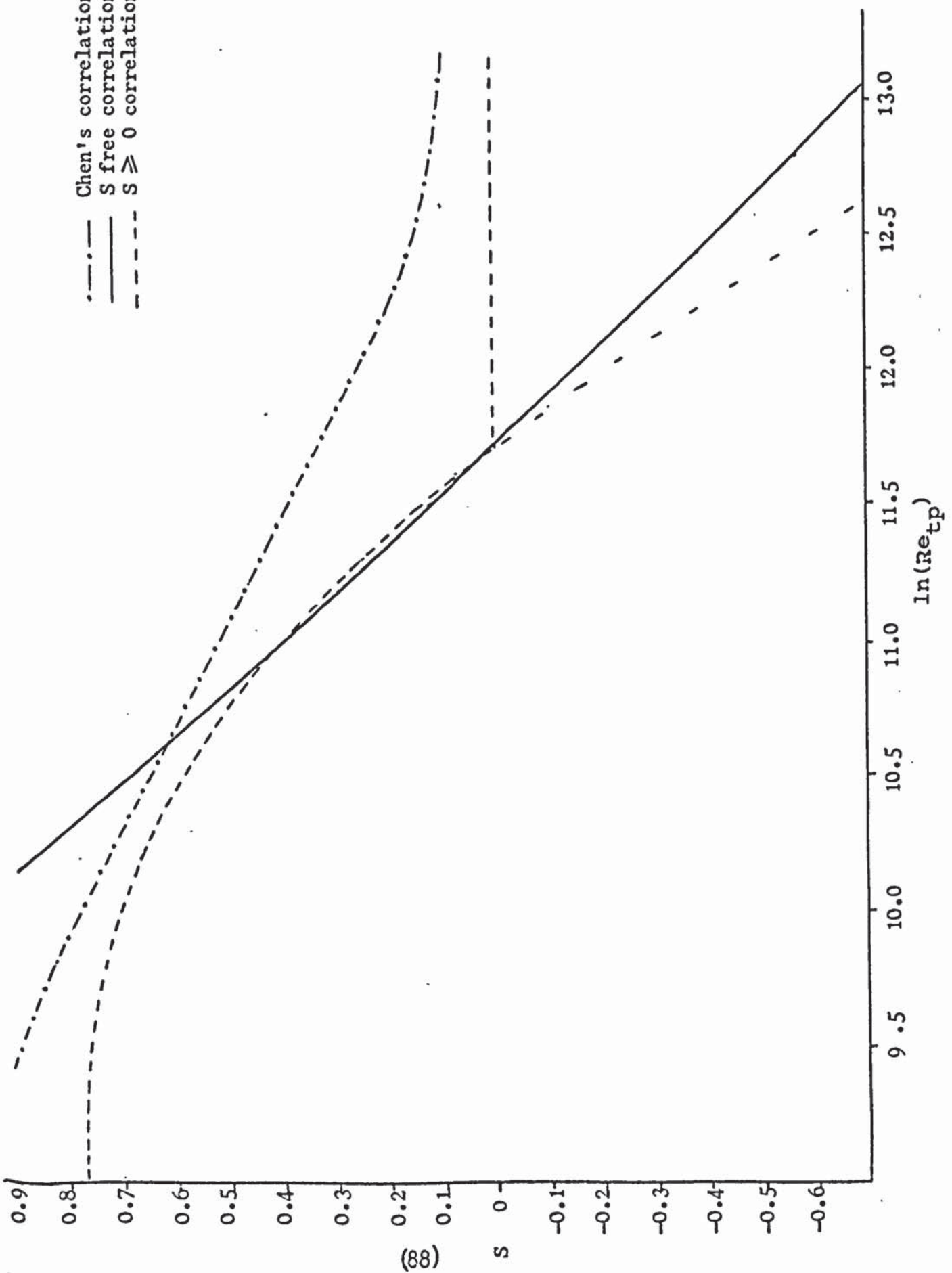

Both the F_L and S curves differ significantly from the curves found by Chen. The F_L curve has a similar shape to that found by Chen but it is offset upward. This follows the trend of the experimental data where the measured heat transfer coefficients were approximately 25-30% higher than those predicted from Chen's correlation. This difference between the experimental and predicted heat transfer coefficients was at first thought to be due to either an error in one of the many calibrations or a systematic error in the calculation procedure. However exhaustive checking of the calibrations and calculation procedures failed to reveal any such error and it was thus presumed that the discrepancy was real. The offset between the F_L curve found by Chen and the F_L curve found for this correlation is roughly constant at a value of 0.34. This corresponds to an increase in F_L of about 40%. This increase in F_L is partly compensated for by a decrease in the value of the S function found for this correlation over the range of experimental data, compared with that given by Chen.

It can be seen from Fig. 6.2 that the value of the S function falls below zero for a large part of the range of the experimental data. It is difficult to see how a negative value of S can be reconciled with the Chen model since a negative S value implies that the nucleate boiling heat transfer mechanism causes heat to flow from the bulk liquid to the wall, against the temperature gradient which is a thermodynamic impossibility. But if the correlation is seen merely as a mathematical form fitted

to the data then no difficulty arises. However, acceptance of such an approach certainly reduces the usefulness of the model as a description of the mechanism important during flow boiling.

Another possible approach is to regard the nucleate boiling term as a correction applied to the convection term. The relevance of this approach is clear when one considers that the nucleate boiling term never accounts for more than 20% of the total heat transfer coefficient and for the majority of the data points less than 10%. Using this approach it becomes easier to see how the S function can become negative. Only a slight upward movement of the F_L curve would cause the S function to greatly decrease in value and become negative. This could be caused merely by the approximation involved in using a cubic equation to represent the F_L and S curves. It is possible however that an additional factor could be the narrow range of experimental data available. This is discussed further in section V.2.3.

The fact that the nucleate boiling term is normally much smaller than the convective term and is greatly affected by small changes in the F_L function does not imply that it is of negligible significance. When the correlation above, based on the Chen model, is compared with Five Parameter correlation presented earlier it is seen that the use of a variable S value significantly lowers the root mean square percentage error from 13.26% to 11.1%.

In order to further investigation the phenomena of negative S values a second optimisation was performed while fixing the minimum value of the S function at zero. The optimum F_L and S functions found were

$$F_L = 1.2422+0.5592*\ln(\frac{1}{XTT})+0.06554*(\ln(\frac{1}{XTT})^2+0.00529*(\ln(\frac{1}{XTT}))^3 \quad 6.9$$

$$S = -5.747+1.002\ln(Re_{tp})+0.01065*(\ln(Re_{tp}))^2-0.00463*(\ln(Re_{tp}))^3 \quad 6.10$$

where $S \geqslant 0$ 6.11

These functions are used in conjunction with equations 6.3, 6.4, 6.5 and 6.8 with a root mean square percentage error of 11.73%.

From fig. 6.1 and 6.2 it can be seen that preventing S from becoming negative causes the F_L curve to fall in value over the whole range of $\ln(\frac{1}{XTT})$ values. It is significant that the difference between the two F_L curves increases at high $\ln(\frac{1}{XTT})$ values since high values of $(\frac{1}{XTT})$ are generally associated with high values of Re_{tp}. It is a high Re_{tp} value that the difference in value between the two S functions is greatest. The difference between the errors associated with each of the two correlations is not large (0.63%) and must be due entirely to the constant upon the minimum value of S. As mentioned earlier there is no noticable pattern in the differences in the wall temperature values predicted by the two correlations.

VI.3.3 Correlations based on Model A

Model A was derived in section III.1 and the data was fitted to this model using the optimisation methods previously described. The optimum fit was found to be given by the correlation defined by the equations

$$XF = \ln\left(\frac{1}{X_{TT}}\right) + 0.0604 \ln(Fr) \qquad 6.12$$

$$F_L = 1.0786 + 0.5313\ XF + 0.04839\ XF^2 - 0.001644\ XF^3 \qquad 6.13$$

$$R_L = \ln(Re_{tp}) = \ln(Re) + 1.429\ F_L \qquad 6.14$$

$$S = -6.955 + 1.7653\ R_L - 0.10713\ R_L^2 + 0.000681\ R_L^3 \qquad 6.15$$

These equations are used in conjunction with equations 6.3, 6.4 and 6.5. This fit has a root mean square percentage error of 11.02%. Plots of the F_L and S functions are given in Figs. 6.3 and 6.4 respectively. Fig. 6.6 and 6.7. show the F_L and S curves for the correlation based upon model B and discussed in section 6.3.4.

It should be noted that none of the curves on Figs. 6.3 and 6.4 are directly comparable with each other or with the curves on Fig. 6.1 and 6.2. This is because the XF and Re_{tp} are defined differently for these correlations and are thus not equivalent.

From Fig. 6.4 it can be seen that, as with the correlations based on Chen's model (see section VI.3.2) the function for S, 6.15, is negative over a large proportion of the data points. The discussion of the meaning of negative S values given in the previous section, VI.3.2, is equally applicable to this correlation.

Figure 6.3 Graphs of F_L v/s XF

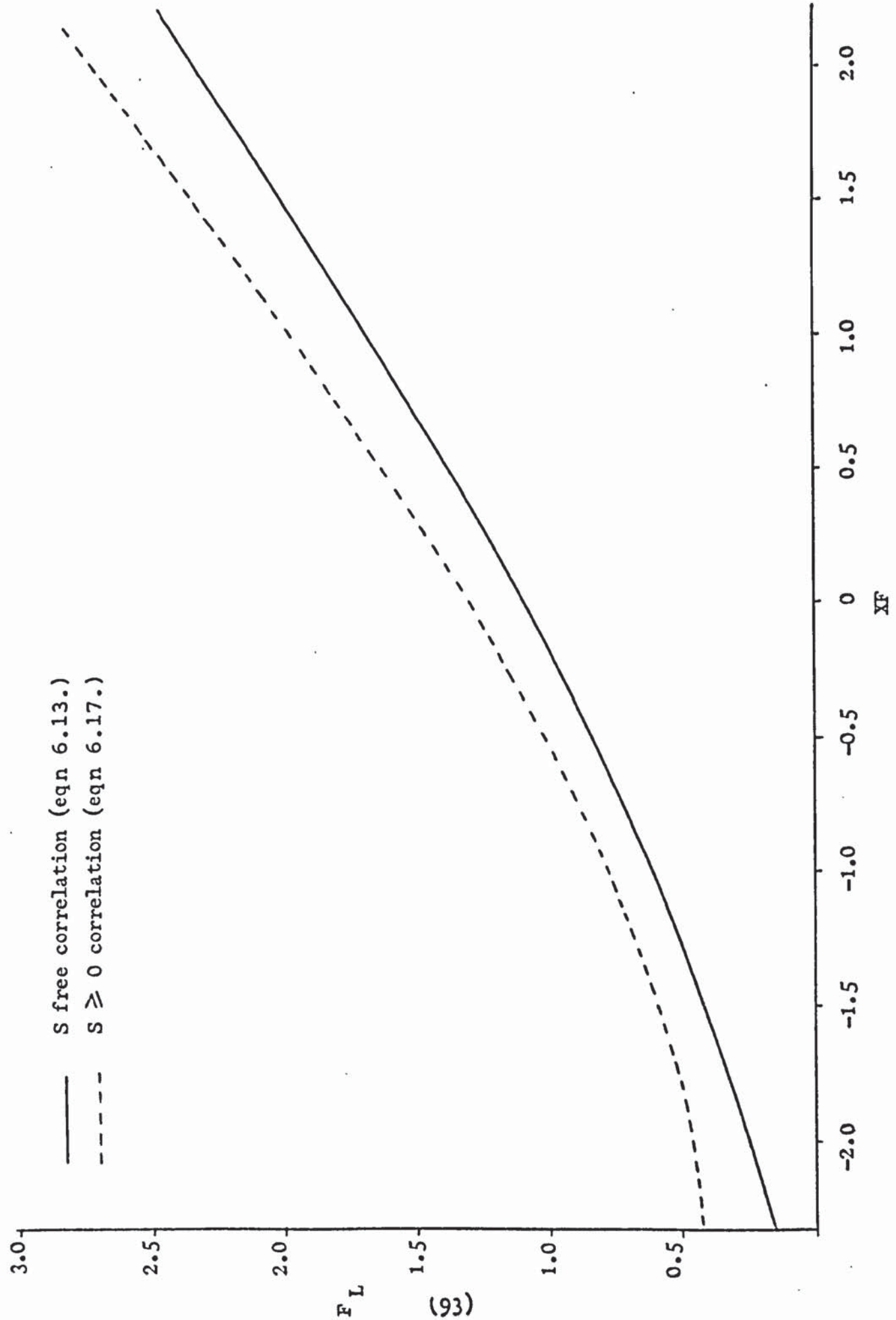

Figure 6.4 Graphs of $S_{v/s}^{R}{}_{L}$ for Correlations based upon Model A

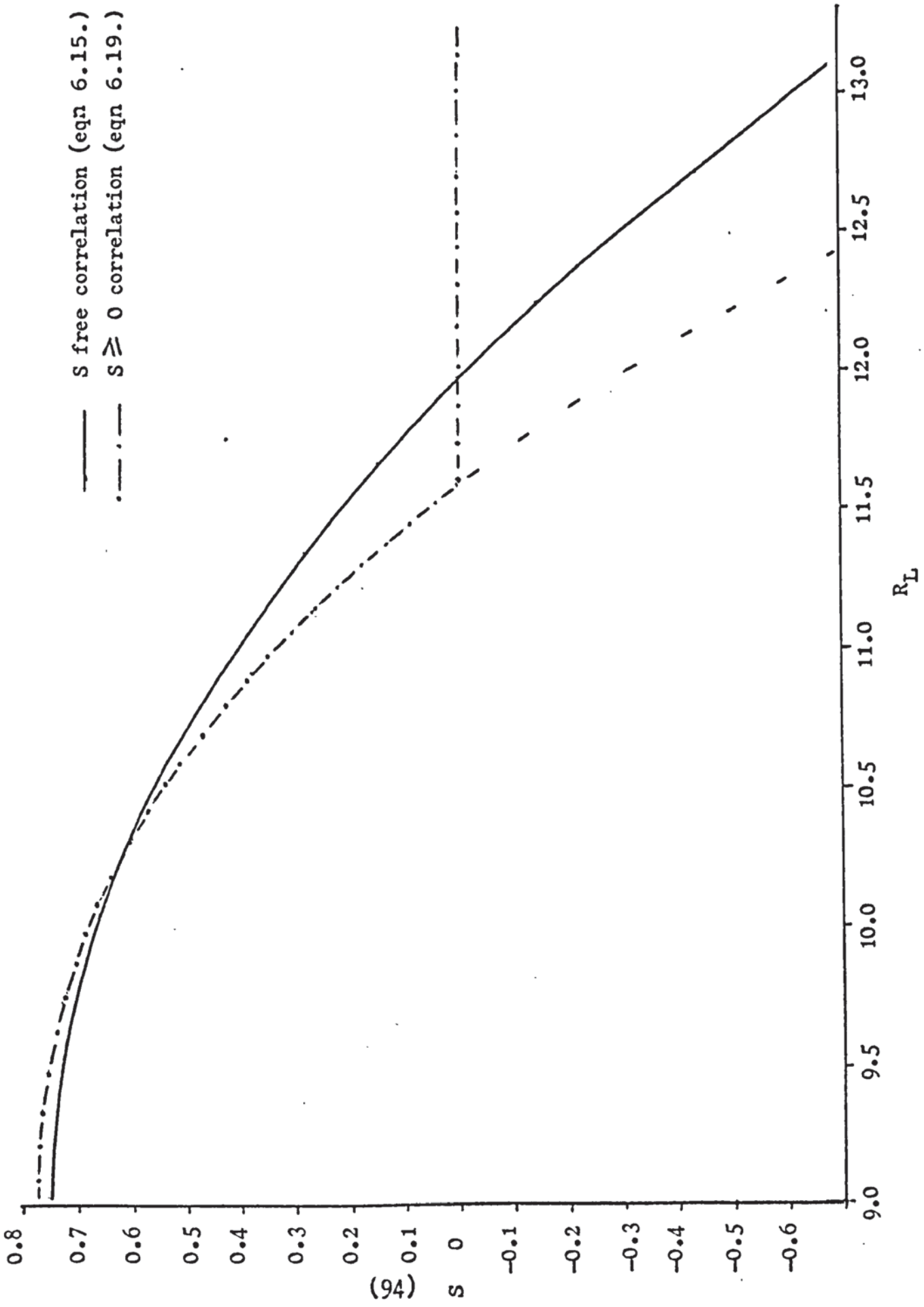

As with the Chen model a correlation was derived where S was prevented from becoming negative. The optimum fit found was

$$XF = \ln\left(\frac{1}{XTT}\right) - 0.0197 * \ln(Fr) \qquad 6.16$$

$$F_L = 1.3387+0.5987*XF+0.06676*XF^2- 0.007897*XF^3 \qquad 6.17$$

$$R_L = \ln(Re_{tp}) = \ln(Re) + 1.0895 * F_L \qquad 6.18$$

$$S = -5.639+1.0007*R_L + 0.01128*R_L^2- 0.004808*R_L^3 \qquad 6.19$$

$$S > 0.0 \qquad 6.20$$

with a root mean percentage error of 11.71%.

When the above two correlations are compared with the equivalent correlations using the Chen model in section VI.3.2 it is surprising to find that there is very little improvement in the error associated with each correlation. It would seem that the addition of the Froude number is a further variable and the optimisation of the exponent on F do not greatly improve the accuracy of the correlations. It is probable that these two additional variables only become important when correlating data from a wider range of data than was available in the present work. This is an important point which is worth examining in some detail. The concept is easily seen when the simple example in Fig 6.5 is considered.

The solid line is the graph of a cubic equation representing some physical relationship while the points represent experimental data. If only the points represented by crosses are available then any line between the dotted straight lines will represent the data with reasonable accuracy even though none of them represent the true relationship at all well over the whole range. Also there will be little improvement

Figure 6.5 Graph of $y = f(x)$

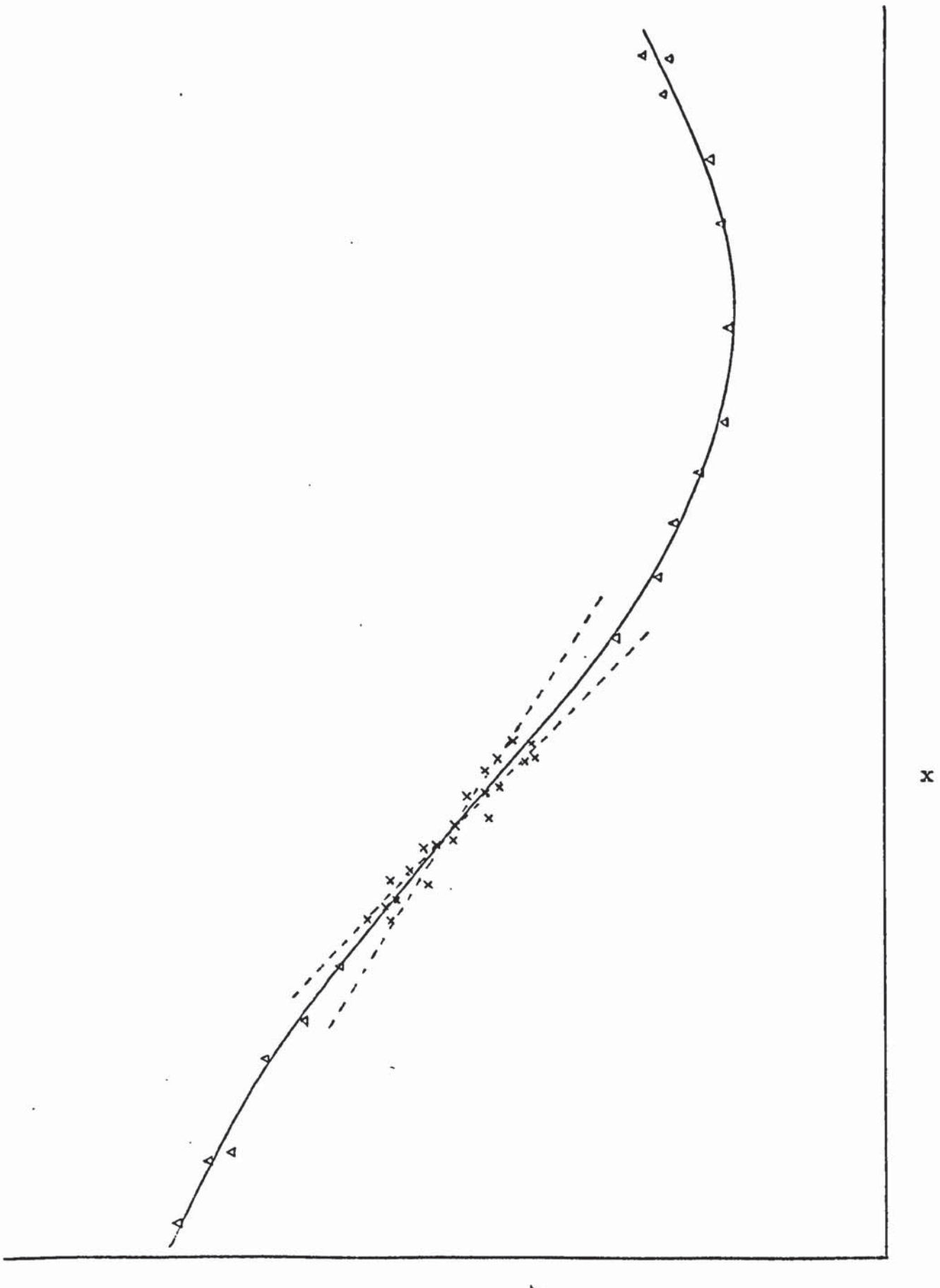

in accuracy of fitting this data if a quadratic or cubic equation and if a cubic equation was used there is little change of deriving the correct cubic equation from such a narrow range of experimental data.

If another form of correlation, such as exponential with a similar number of optimising parameters, is used a similar effect would undoubtedly be found.

Thus there will be a wide range of values for the correlating parameters which would give equations fitting the data with roughly the same accuracy. This results in the situation where a slight change in the data or in the model will lead to very large changes in the 'optimum' fit on the data. In order to obtain a reasonable approximation to the actual relationship a wider range of additional data is necessary, such as is represented by the circle data points in Fig. 6.5.

The same situation as described above probably arises in the present work. The range of data is fairly narrow and thus the Froude Number and the variable exponent in F are superfluous. However it is very likely that with a wider range of data these variables become more important.

VI.3.4 Correlations based on Model B

Model B was derived in section 3.2 and the water data was fitted to this model using the Davis, Swann and Campey optimisation method previously discussed in section IV.2.6 The optimum fit was found to give by the correlation defined by the equations

$$XF = \ln\left(\frac{1}{XTT}\right) + 0.5659 \quad \ln(Fr) \qquad 6.21$$

$$F_b = 1.3386 + 0.0199 \times XF + 0.0344\ XF^2 - 0.001422\ XF^3 \qquad 6.22$$

$$R_L = \ln(Re_L) + 1.7893\ F_b \qquad 6.23$$

$$S_b = 8.6371 - 1.3533\ R_L + 0.0885\ R_L^2 - 0.00262\ R_L^3 \qquad 6.24$$

where $S_b \geqslant 0$ 6.25

The above equations are used in conjunction with the equations:

$$h_{film} = \frac{kf}{D}\ (0.32\ Re_L)^{\frac{1}{2}}/(1 + 0.5\ \ln(10\ Pr\ + 1.0)/Pr) \qquad 6.26$$

for 3.27

and $h_b = h_{film} e^{Fb} + h_{mic}\ Sb$ 6.27

together with equation 6.4 for h_{mic}

This correlation had a root mean percentage error of 11.837%. The graph of F_b v/s XF is shown in Fig. 6.6 while Fig. 6.7 shows the graph of S_b v/s R_L.

Fig. 6.6 shows F_b over a much wider range of XF values than any of the previous plots. This is because the large value of the exponent in the Froude number results in a much wider range of experimental XF values. For the same reason S_b is given over a wider range of values of R_L in Fig. 6.7.

The much larger value of the exponent on the Froude

Figure 6.6 Graph of F_b v/s XF for correlation based upon Model B (eqn.6.22)

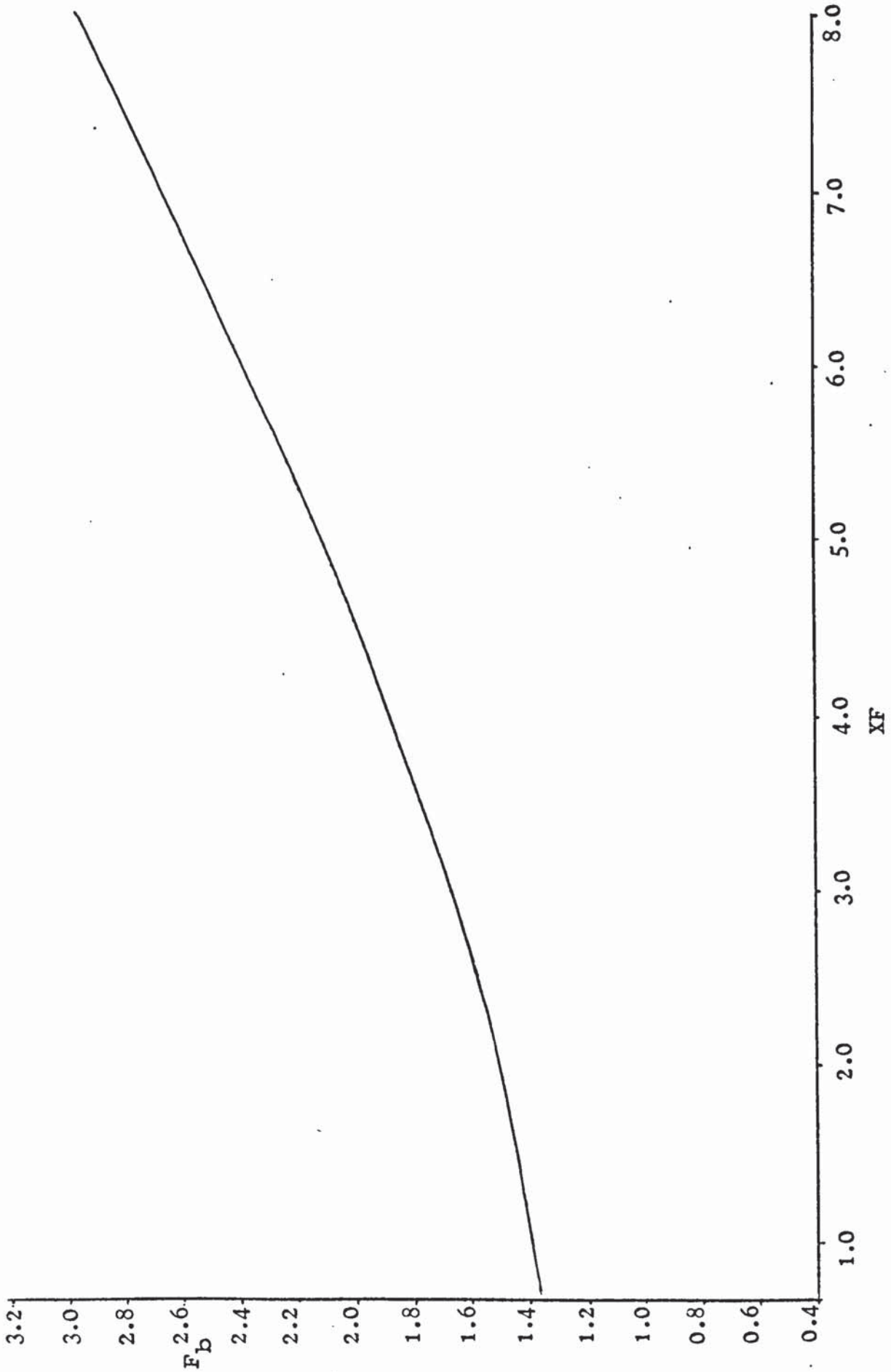

Figure 6.7 Graph of $S_b v/s^R L$ for Correlation based upon Model B (eqn.6.24)

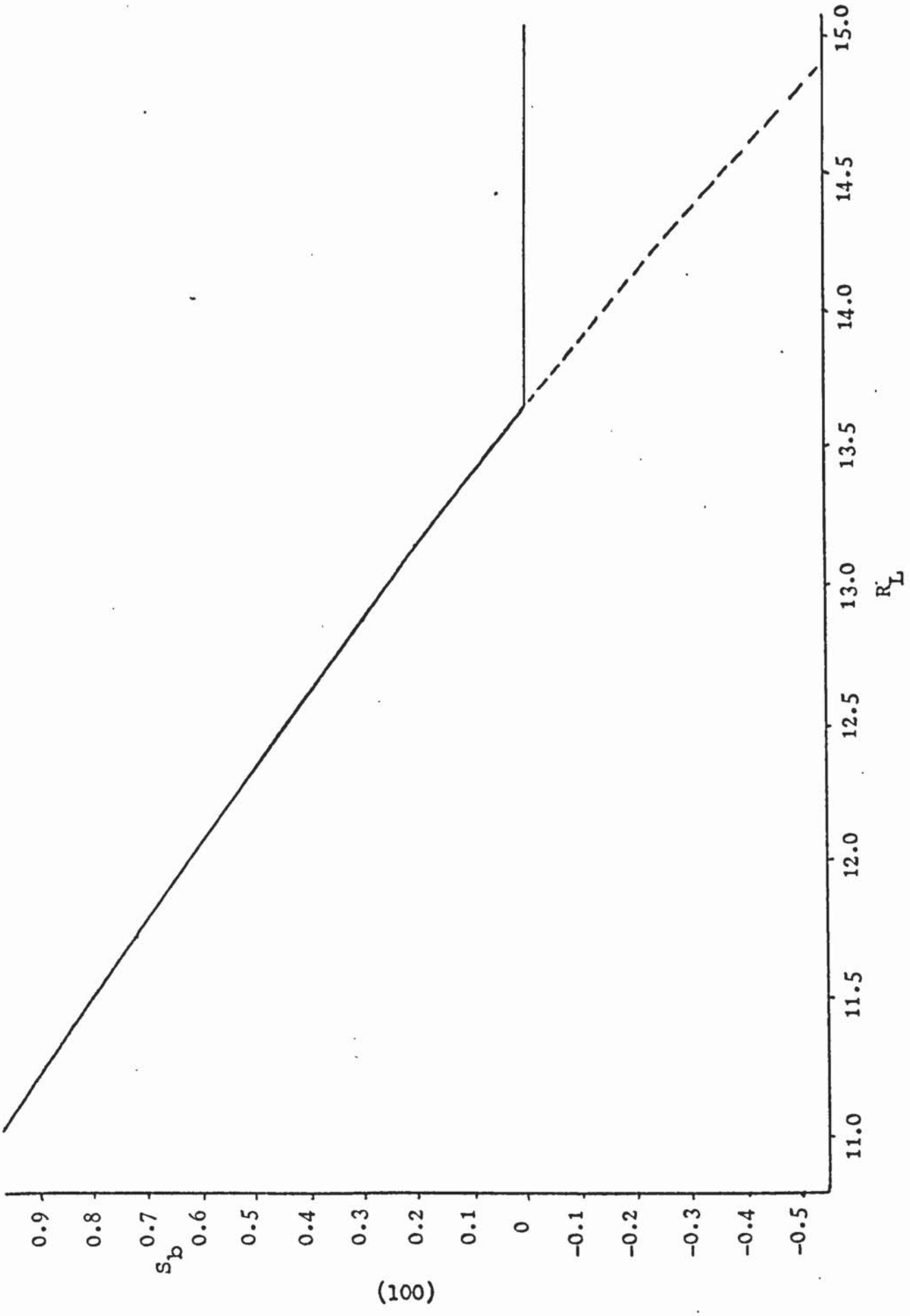

number is the most notable difference between this correlation and those discussed in section 6.33. As the Froude number is defined as $\frac{V_m^2}{G.D}$ and since G and D are constant in this work the variation in the Froude number reflects the variation of the two-phase velocity. The two-phase velocity can be approximately related to the single phase flow velocity by

$$V_m = V_{tp} = \frac{V_L x}{\rho_v} \qquad 6.28$$

If ρ_v is assumed to be constant then

$$V_m \propto V_L x \qquad 6.29$$

The plot of F_b against XF can be very roughly approximated by a straight line of slope 0.3, then,

$$F_b = 0.3 \ln((V_L x)^{1.12}) + 0.3 \ln((\frac{x}{1-x})^{0.9}) + C \qquad 6.30$$

where C is some arbitrary constant. If this equation is combined with equation 6.26 then it can easily be shown that, ignoring the $(1 - x)$ term and the effect of variation in the physical properties, that

$$h_{film} \propto V_L^{0.84} x^{0.6} \qquad 6.31$$

A similar analysis can be performed on the correlation, based on model A, defined by the equations 6.16 to 6.20 giving

$$h_{film} \propto V_L^{0.86} x^{0.61} \qquad 6.32$$

It is remarkable how similar equations 6.31 and 6.32 are considering the great simplifications involved in their derivation. The value of the power on V_L would seem to confirm the applicability of the Dittus Boelter equation (see section 2.2) to two-phase heat transfer since the values of the power on V_L, 0.84 and 0.86 are close to the Dittus Boelter value of 0.8. This would seem to indicate

Figure 6.8 Plot of Wall Temperatures and Bulk Temperature for Run 29

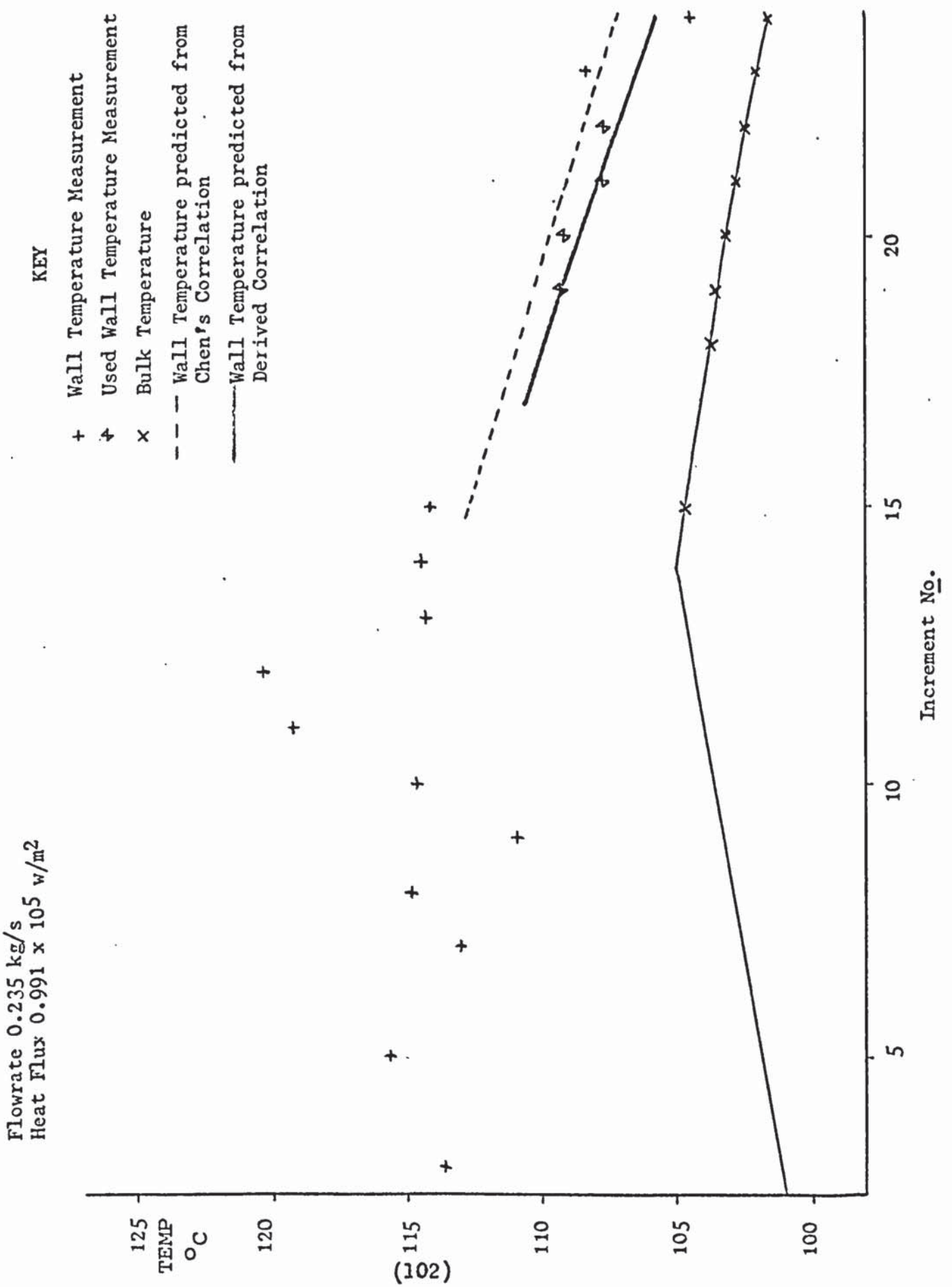

Figure 6.9 Plot of Wall Temperature and Bulk Temperatures for Run 35

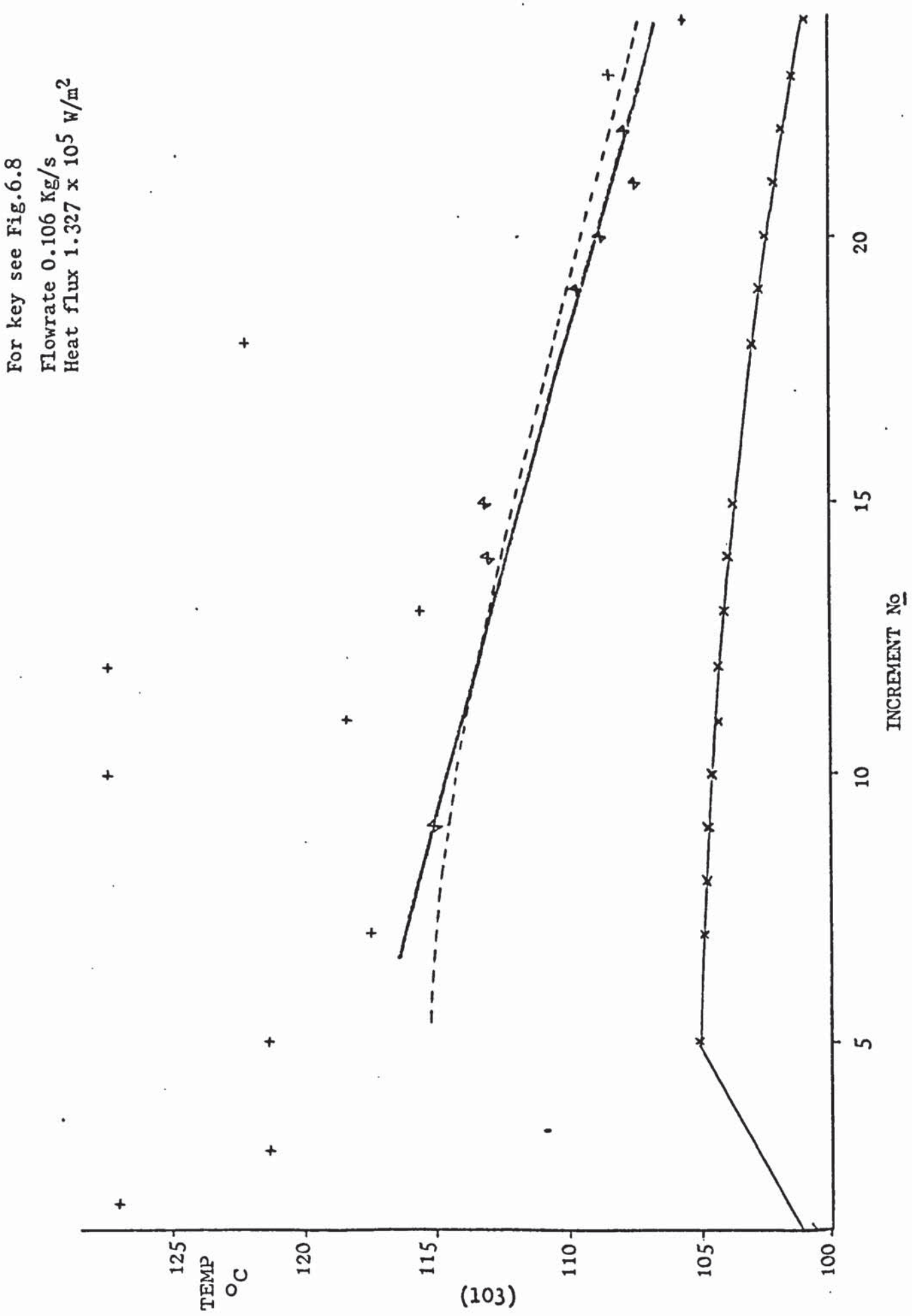

Figure 6.10 Plot of Wall Temperatures and Bulk Temperatures for Run 45

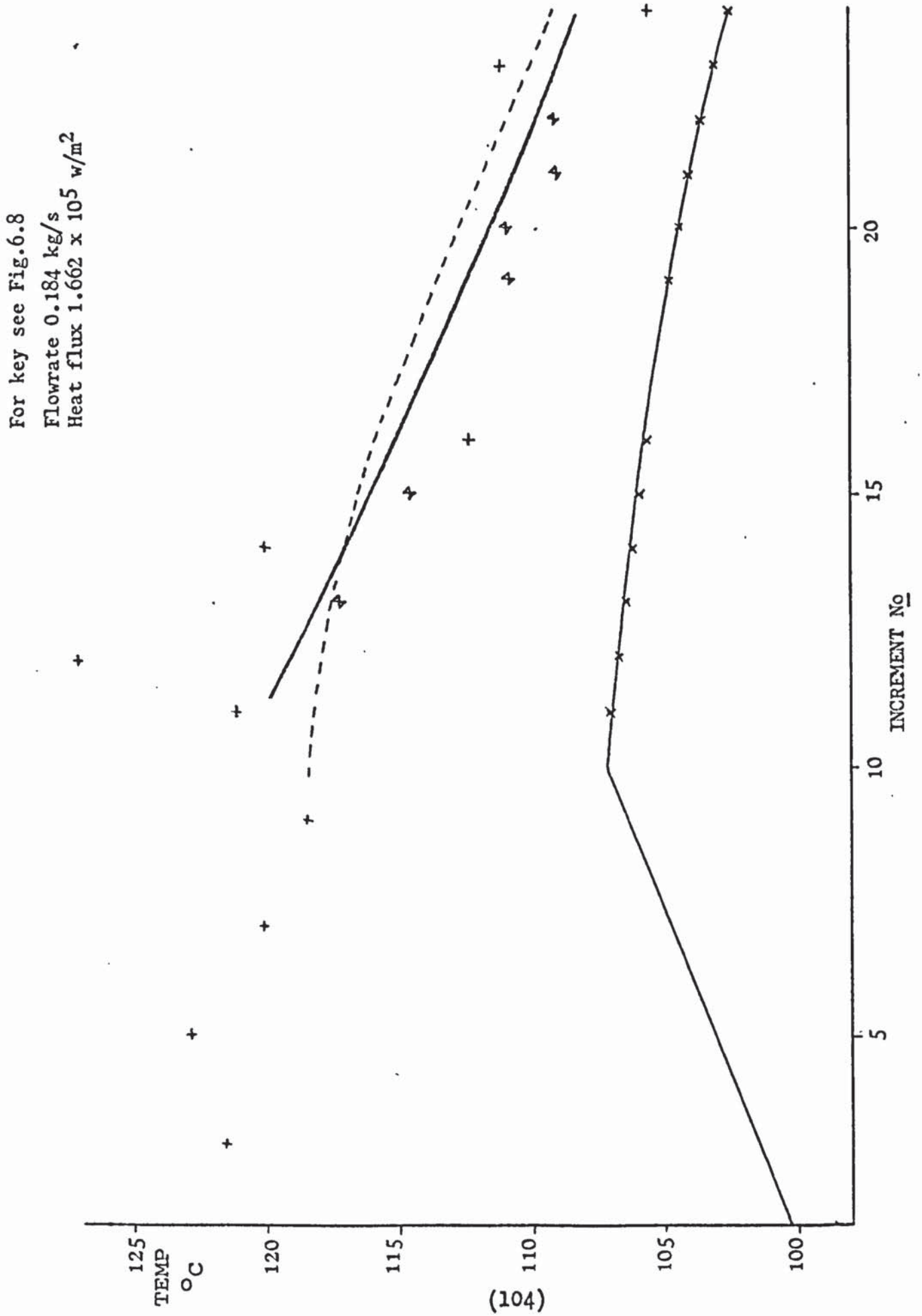

Figure 6.11 Plot of Wall Temperatures and Bulk Temperatures for Run 53

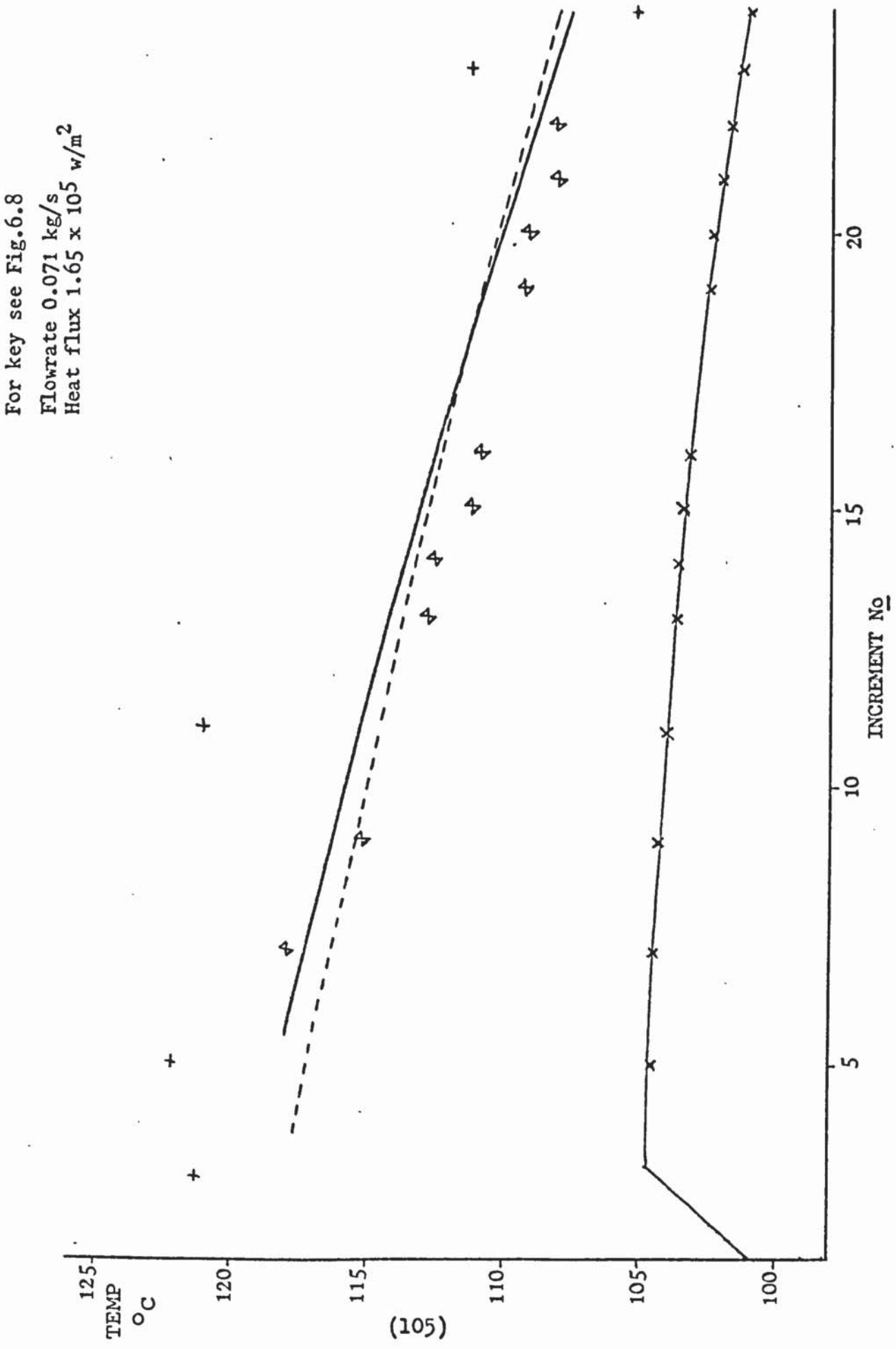

Figure 6.12 Plot of Wall Temperatures and Bulk Temperatures for Run 73

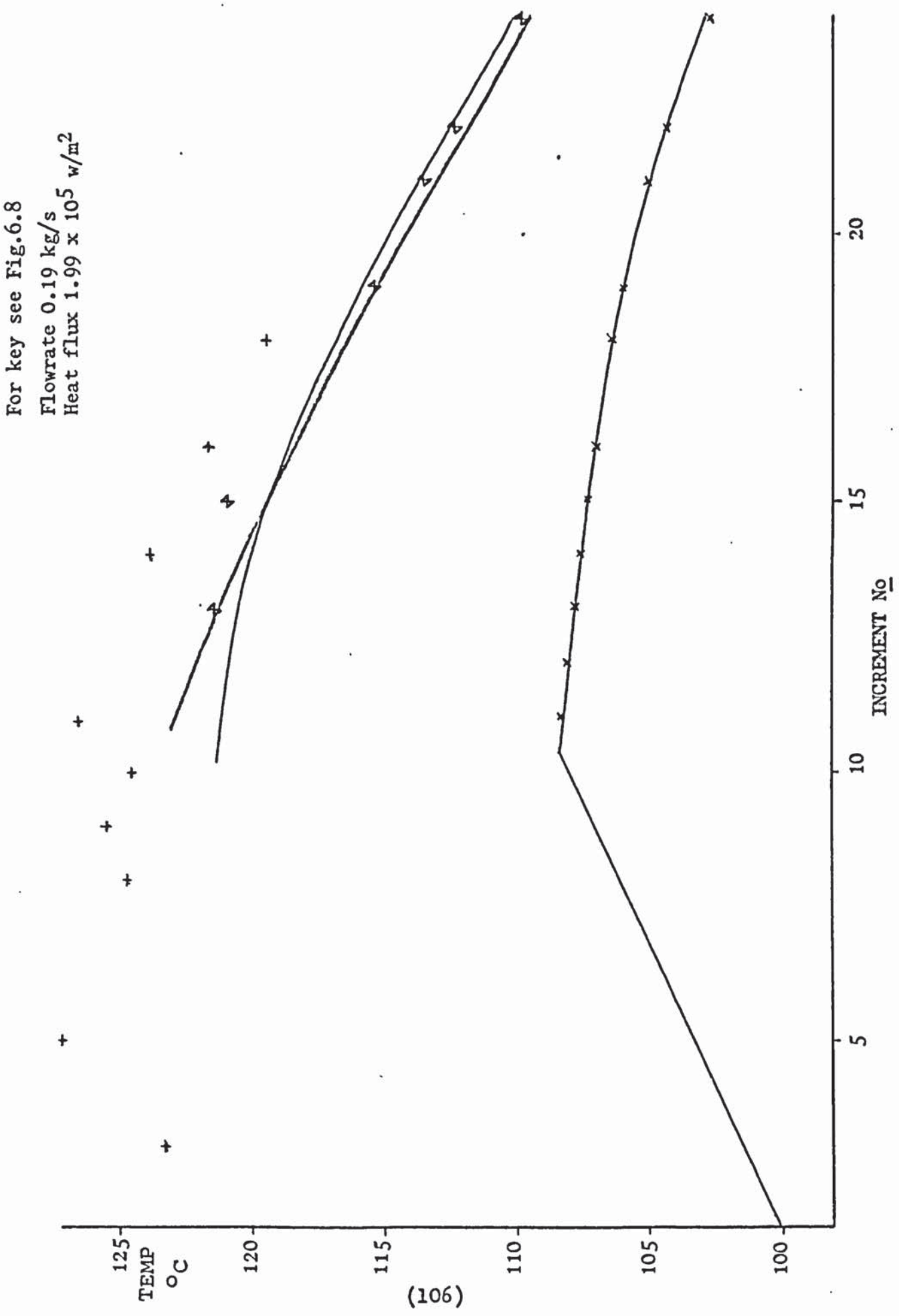

Figure 6.13 Plot of Wall Temperatures and Bulk Temperatures for Run 81

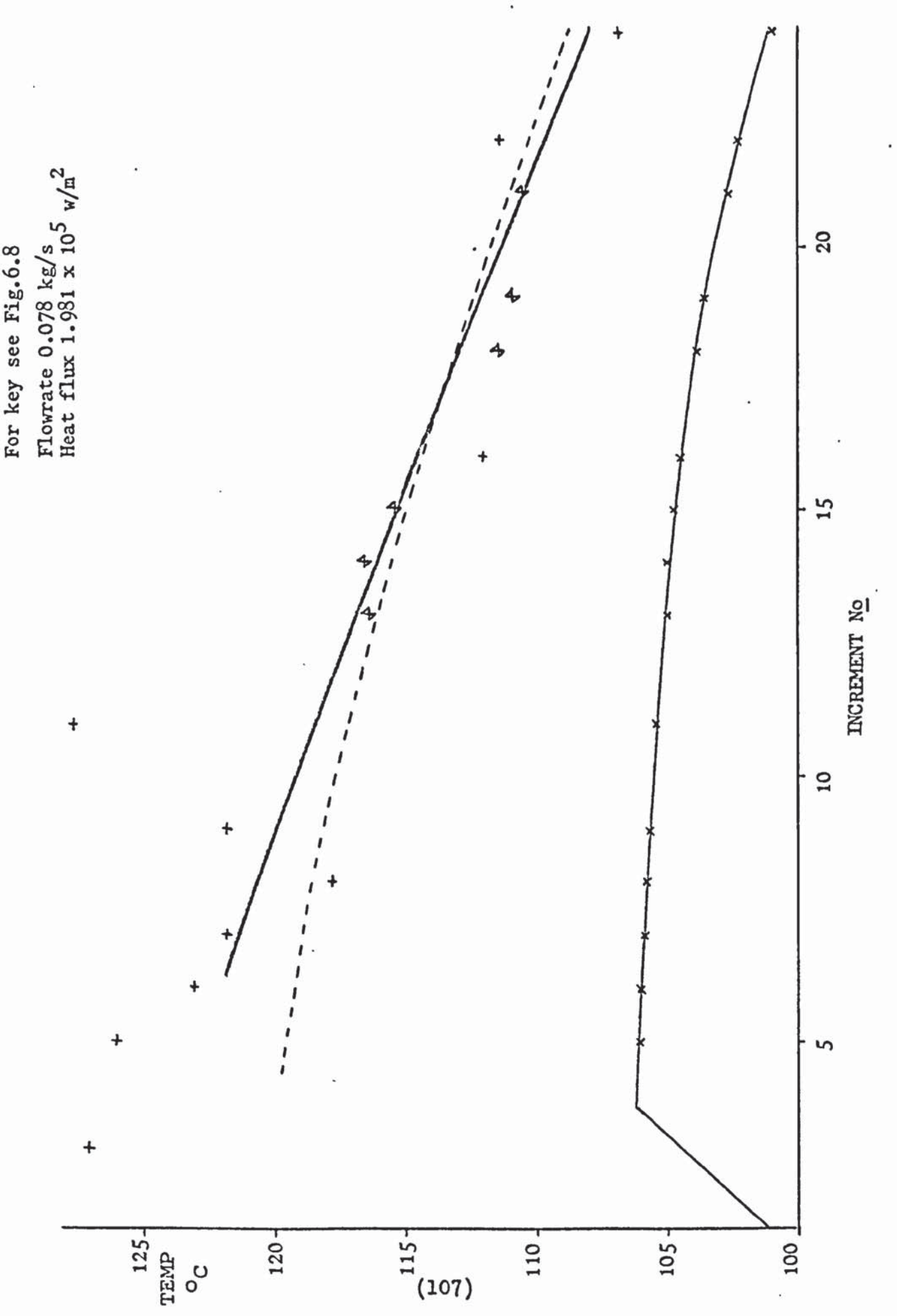

Figure 6.14 Plot of Wall Temperatures and Bulk Temperatures for Run 86

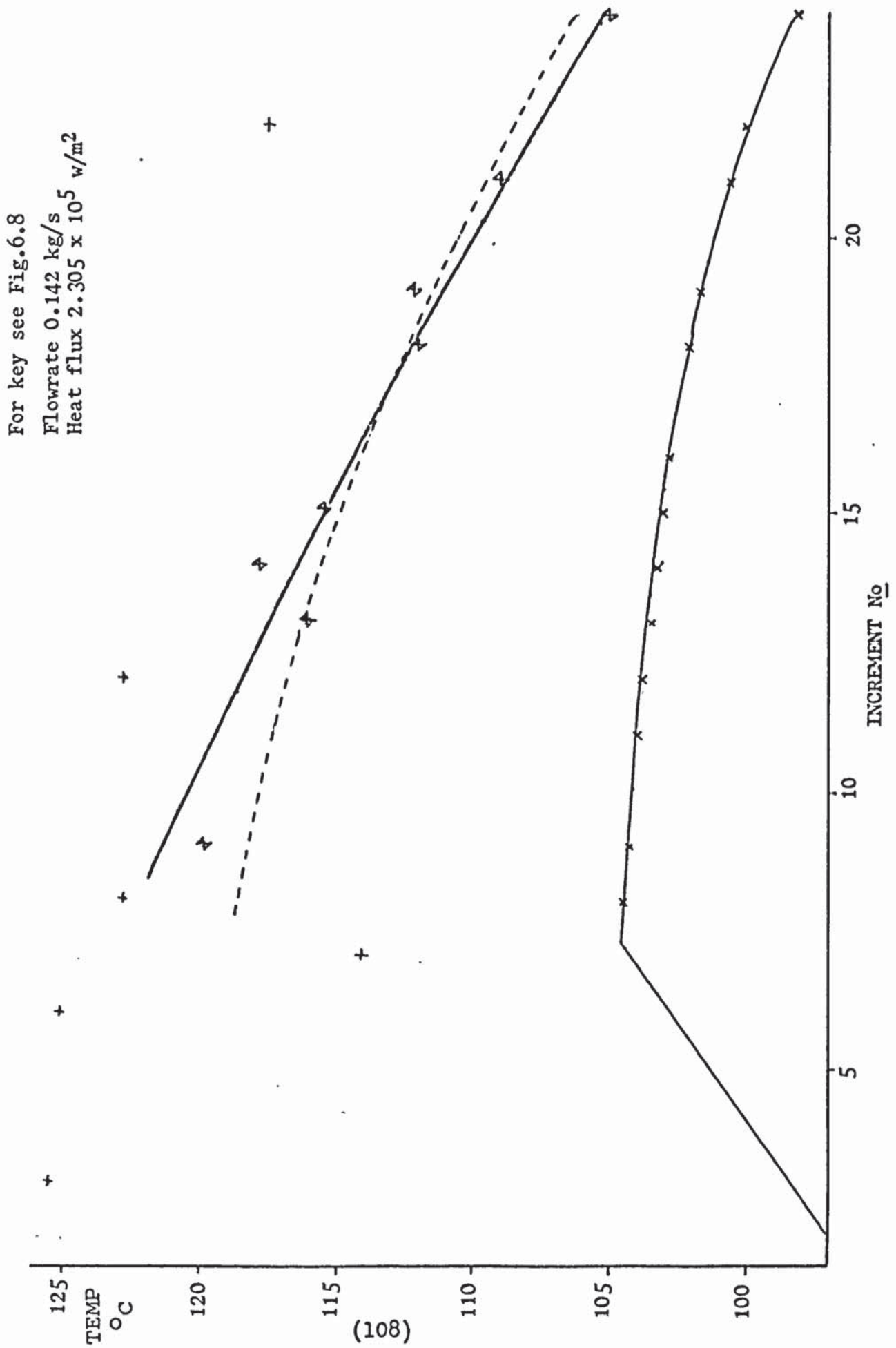

Figure 6.15 Plot of Wall Temperatures and Bulk Temperatures for Run 146

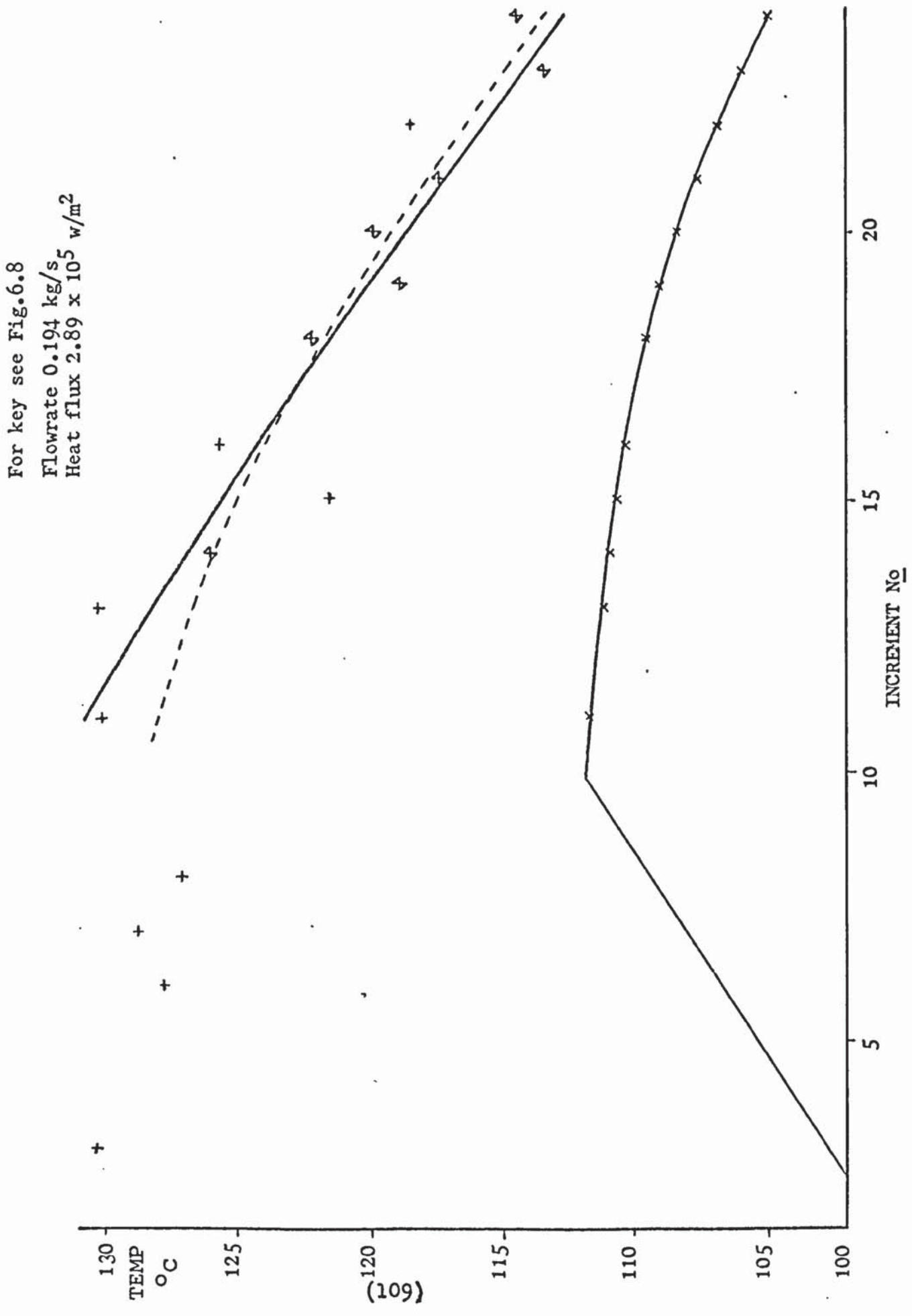

Figure 6.16 Plot of Wall Temperatures and Bulk Temperatures for Run 153

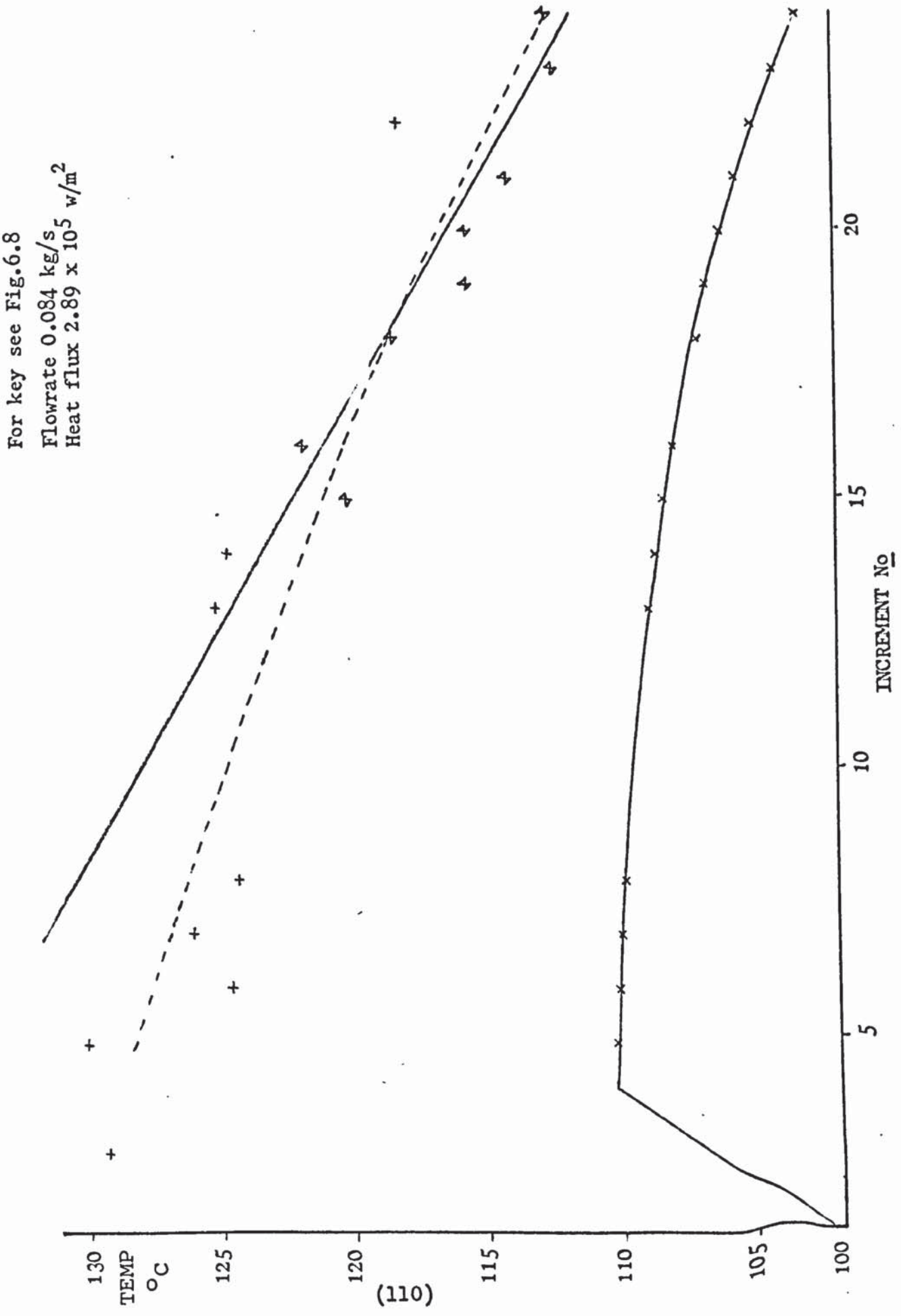

that Model A is a better form of correlation for two phase heat transfer than Model B since the Dittus Boelter equation is an integral part of the model. This conclusion is partially confirmed by the slightly larger error associated with Model B. However it may be that the form of the equation for h_{film} model B is better than that in model A but that the power on the Reynolds number on model B is not the optimum. Unfortunately it was not possible to investigate this possibility using the Davy, Swann and Campey method discussed earlier (see 5.32) due to lack of available computer time.

In equations 6.31 and 6.32 the power on v_L represents very roughly the relationship between v_L and the convective heat transfer coefficient. One should remember, however, the very great simplifications involved in the derivation of these equations, especially the assumption that the term $(1-x)$ can be ignored. These simplifications will have greatly modified the original more complicated form of relationship given by equations 6.16 to 6.20 and equations 6.21 to 6.27.

VI.4 Ethylene Diacetate-Water Data

The ethylene diacetate data used in fitting the correlation consisted in 322 selected points covering the following range of conditions:

Flowrate 0.076 - 0.253 kg/s (382 - 1271 kg/m^2s)

Heat flux 1.31 - 2.89 x 10^5 w/m^2

Quality 0.5 - 13.5%

As previously mentioned the azeotrope heat transfer coefficients were found to be far higher than expected. This anomaly was explained when the ethylene diacetate was found to have partially hydrolysed. This was first suggested by the strong acetic acid smell of the azeotrope which had been used for the experimental runs. That a chemical reaction had occurred was confirmed by surface tension measurements which were taken.

Figure 6.17 shows a plot of the surface tension measurements taken; the triangles show measurements taken from freshly made up azeotrope while the crosses show measurements taken of azeotrope which had been used for the experimental runs. The used azeotrope had been kept for approximately a week at room temperature before these measurements were taken. The lower group of crosses are from measurements taken first; while the upper group of crosses are from measurements taken after the azeotrope had been kept at 80°C for about two hours. It is clear from this plot that the surface tension of the used azeotrope was greatly affected by being kept at 80°C for a couple of hours. The most likely explanation for the results found is that at high temperature the ethylene diacetate is subject to reversible hydrolysis with the equilibrium amount of hydrolysis increasing with the temperature. It is likely that the hydrolysis was catalysed by the copper ions present in the liquid due to the acetic acid formed slightly corroding the copper

Figure 6.17 Plot of Surface Tension Measurement of EDA-Water Mixture

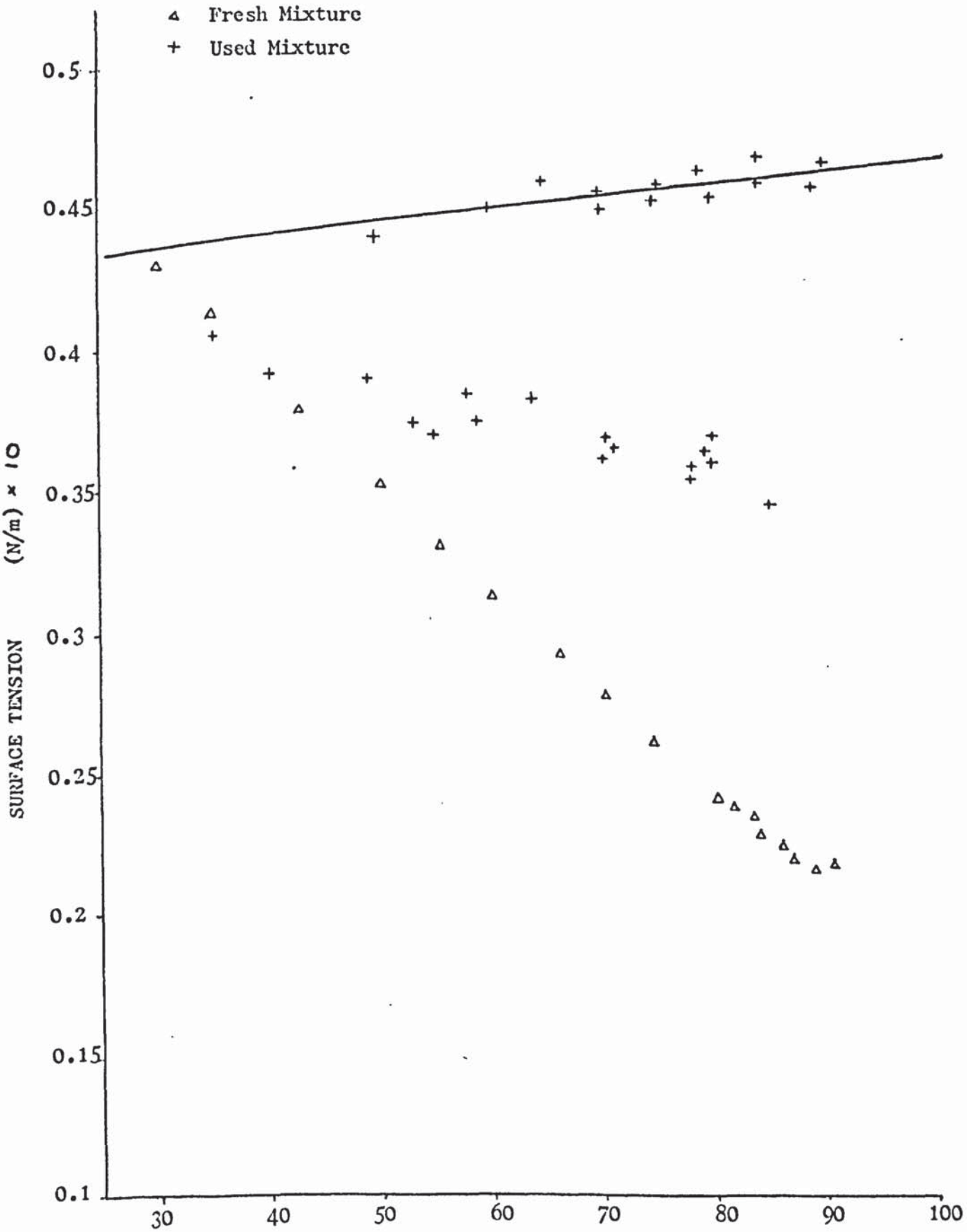

tube. The presence of copper ions in the liquid was confirmed by the slight green colouration of the liquid residue left when the azeotrope was later distilled before storage. This green colour gradually turned deep blue over a period of about a week. This probably represented cuprous ions being oxidised to cupric ions. The presence of cupric ions was later confirmed by chemical tests.

Surface tension measurements were required for the analysis of the data and thus it was necessary to decide upon which group of surface tension measurements were the most applicable for use with the heat transfer results. It was eventually decided that the upper group of crosses in Fig. 6.17 were the most applicable as it was assumed that these best represented conditions in the experimental rig. The optimum line drawn through these points is shown in Fig. 6.17. Further details are given in appendix III

The partial hydrolysis does not only affect the surface tension, it will also affect all of the other physical properties, but however the effect of a slight amount of hydrolysis on any other physical property except surface tension is likely to be small.

Another effect of the hydrolysis reaction is that once any hydrolysis has taken place the experimental liquid no longer acts as an azeotrope and thus the results cannot be analysed solely in terms of heat transfer since mass transfer effects due to concentration differences between the phases must be taken into account.

However the main effect upon the results caused by the hydrolysis was probably due to the heat of reaction of the hydrolysis reaction. As no heat of reaction

could be found in the literature an attempt was made to calculate the heat of reaction using the methods given by Reid and Sherwood (R2). It was assumed that the reaction that occurred was

$$(CH_3\ CO_2\ CH_2)_2 + H_2O \rightleftharpoons CH_3CO_2CH_2CH_2OH + CH_2COOH$$

A value for the heat of reaction of -10.6 kcal/gmole was found, showing the reaction to be endothermic as would be expected. However this calculated value is subject to a large amount of error and thus can only be considered an approximate value.

That the reaction is endothermic is important since the reaction can act as an additional heat transfer mechanism for, as the equilibrium amount of hydrolysis increases with temperature, it is probable that the hydrolysis reaction occurs mainly at the hottest part of the experimental section, the tube wall. This results in heat being absorbed by the reaction causing a lower tube wall temperature and thus a higher heat transfer coefficient. The reverse reaction would probably mainly occur in cooler core, thus the reaction acts as a heat transfer mechanism moving heat from the tube wall to the core.

It is theoretically possible, although difficult, to calculate the equilibrium amount of hydrolysis at various temperatures using the estimated value for the heat of reaction. However this was not attempted since it was felt that the estimated values would be subject to so much error as to be meaningless.

Because of this additional heat transfer mechanism,

as well as the other effects of the hydrolysis reaction mentioned above, it would seem that none of the previously discussed models would be applicable to the data. However for the sake of completeness the data was fitted to Model A (see section 3.1). The optimum fit found was:

$$XF = \ln\left(\frac{1}{XTT}\right) - 0.0851 \ln(Fr) \quad 6.33$$

$$F_L = 2.3664 + 0.7132\ XF - 0.0351\ XF^2 - 0.001967\ XF^3 \quad 6.34$$

$$R_L = \ln(Re_{tp}) = \ln(Re) + 2.1065\ F_L \quad 6.35$$

$$S = -8.258 + 1.151\ R_L + 0.0012\ R_L^2 - 0.003078\ R_L^3 \quad 6.36$$

These equations are used in conjunction with equations 6.3, 6.4 and 6.5.

This fit had a root mean square percentage error of 10.637%. Fig. 6.18 shows the plot of F_L v/s XF and Fig. 6.19 shows the plot of S v/s R_L. The most obvious difference between the F_L plot for the ethylene diacetate-water date and the equivalent F_L plot for the water data (Fig. 6.3) is the much higher F_L values found for the ethylene diacetate-water data. This partly reflects the higher heat transfer coefficients found in the ethylene diacetate-water data but is also due to the comparatively large negative value of the exponent on the Froude Number which reduces the XF values for the ethylene diacetate-water data.

The S v/s R_L plot, Fig. 6.19, shows a highly unusual shape. This would seem to reflect the inappropriateness of the model when used for heat transfer with chemical reaction. However, considering the lack of applicability of the model it is surprising that the root mean square

Figure 6.18 Graph of F_L v/s XF for EDA-Water Data (Eqn 6.34.)

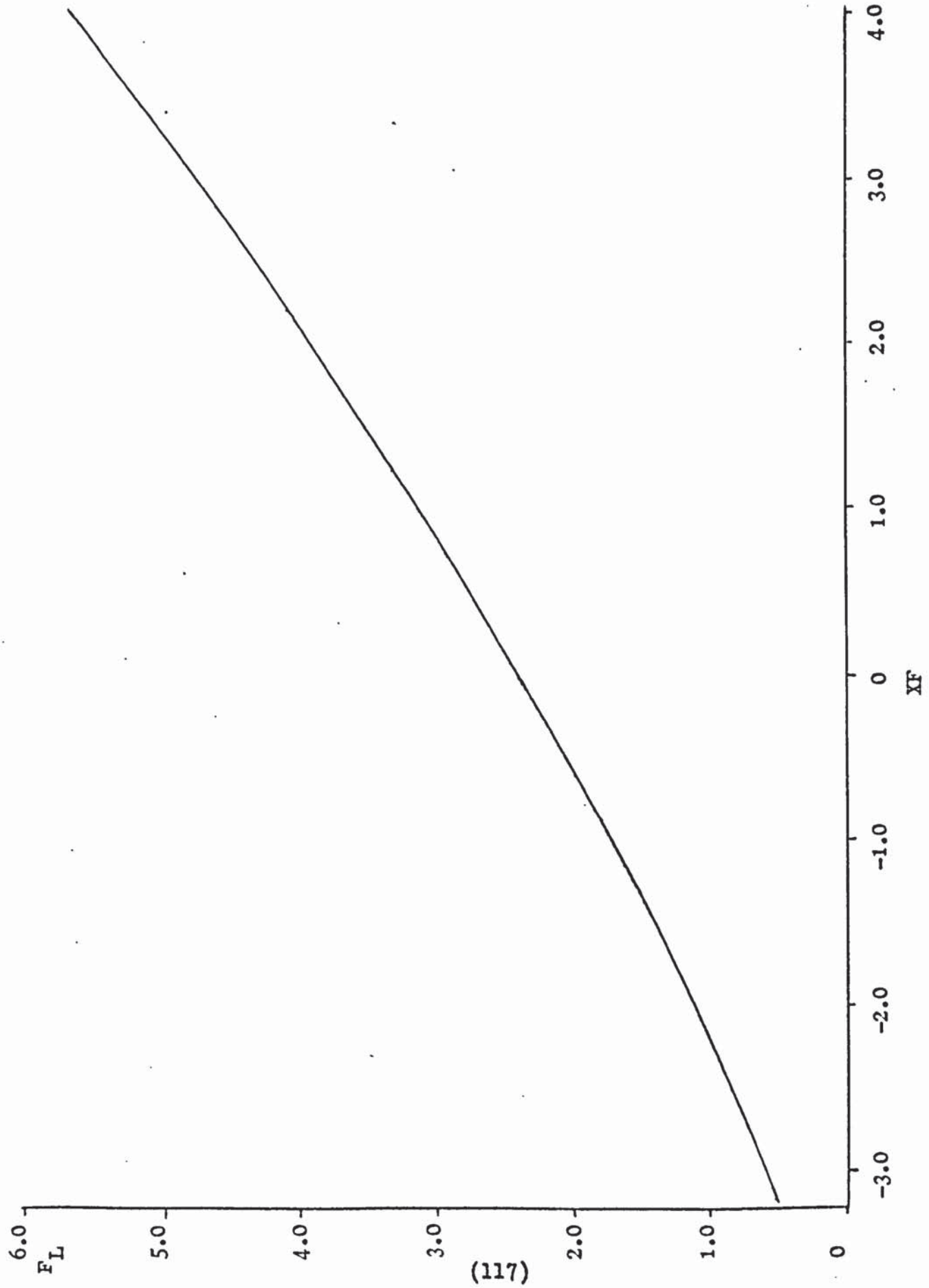

Figure 6.19 Graph of S v/s R_L for EDA-Water Data (Eqn 6.36.)

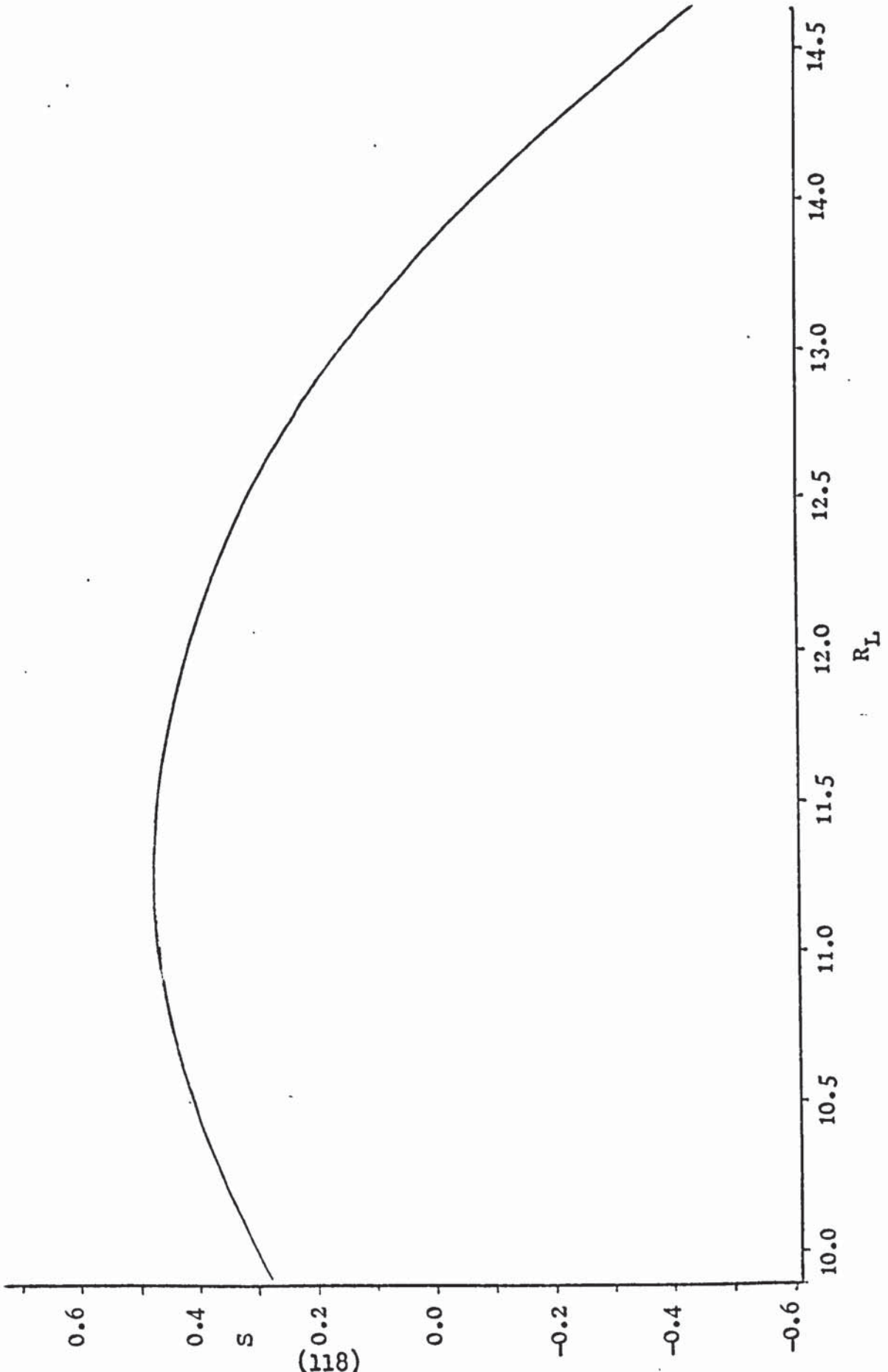

percentage error is lower than that for the water data. It is probable that this is partly due to the complexity of the model. The large number of fitted parameters allows the model to fit, fairly accurately, data for which the model is not really applicable. Also the ethylene diacetate-water data probably had a lower experimental error associated with it.

Although the hydrolysis reaction has been disadvantageous in the present work it is possible that such a reacting system could be used to advantage in a situation where the highest possible heat transfer coefficients were desirable, however, the long term chemical stability of such a system could be a problem.

VII Conclusions and Recommendations for Further Work

1) Single component flow boiling heat transfer data can be adequately correlated using models based upon Chen's correlation.

2) Non-linear optimisation methods, particularly that of Davis, Swann and Campey are suitable for fitting flow boiling heat transfer data and the various models used in this work. However such optimisation procedures can require a large amount of computer time to reach the optimum parameter values.

3) The ethylene diacetate water azeotrope is unsuitable for use as an experimental fluid for flow boiling heat transfer experiments due to hydrolysis. However this reversible reaction appeared to greatly improve the boiling heat transfer coefficient and the ethylene diacetate water mixture, and the others like it, deserve further study as by using them it might be possible to greatly increase heat transfer rates in boilers.

4) An experimental rig allowing higher accuracy in the data should be used for further experiments. This could be achieved by using a thin walled tube heated by passing an electric current through it. This would allow much higher accuracy in the wall temperature measurements.

5) A much wider range of experimental conditions should be covered and with a range of experimental fluids in order to derive a more general correlation.

VIII

BIBLIOGRAPHY

A1 Allen, W.F.
Trans. A.S.M.E., 73, 257,(1951).

B1 Baker, O.
Oil and Gas Journal, 26 July,(1954).

B2 Baroczy, C.J.
A.I.Ch.E. reprint No. 37, paper presented at 8th Nat. Heat Transfer Conf., Los Angeles,(Aug. 1965).

B3 Bennett, J.A.R., Collier, J.G., Pratt, H.R.C. and Thornton, J.D.
Trans. Inst. Chem. Engrs., 39(2), 113-126,(1961).

C1 Calus, W.F., Denning, R.K., di Montegnacco, A. and Gadston, J.
Chem. Eng. Journal, 6, 223-250,(1973).

C2 Chawla, J.M.
Paper B.5.7., 4th Int. Heat Transfer Conf., Versailles,(1970).

C3 Chen, J.C.
I. and E.C. Proc. Des. and Dev., 5(3), 322,(1966).

C4 Chisholm, D. and Sutherland, L.A.
Paper 4 presented at Symposium of Fluid Mechanics and Measurements in Two-Phase Flow Systems, University of Leeds,(Sept. 1969).

C5 Chisholm, D.

Paper 35 presented at 1968 Thermodynamics and Fluid Mechanics Convention I. Mech.Engrs., Bristol,(March 1968).

C6 Chou, C.

Ind. Eng. Chem., 50, 799,(1959).

C7 Coleby, J.

M.Sc. Project, University of Aston,(1972).

C8 Collier, J.G.

'Convective Boiling and Condensation', McGraw-Hill,(1972).

C9 Collier, J.G., Lacey, P.M.C. and Pulling, D.J.

Trans.Inst. Chem. Engrs., 42, T127-T139,(1964).

C10 Coulson, J.M. and Richardson, J.F.

'Chemical Engineering', Volume One, 2nd Ed.,(1966).

D1 Davis, E.J. (New York State University)

Personal Communication, Aston University,(1974).

D2 Swann, W.H.,

I.C.I. Central Instrument Laboratory Research Report No. 64/3, (1964).

D3 Davis, W.J.

Brit. Chem. Eng., 8(7), 462,(1963).

D4 Dengler, C.E. and Addoms, J.N.

Chem. Eng. Prog. Symp. Ser., 52(18), 95-103,(1956).

D5 Dukler, A.E.

M.S. Thesis, University of Delaware,(1949).

E1 Engineering Sciences Data Unit,

Report No. 67016, (April 1967).

F1 Fried, L.

Chem. Eng. Prog. Symp. Ser., 50(9), 47-51,(1954).

F2 Forster, H.K. and Zuber, N.

A.I.Ch.E. Journal, 1, 532,(1955).

G1 Gibson-Robinson, M.

Personal Communication, University of Aston,(1974).

G2 Golan, L.P. and Stenning, A.H.

Paper No. 14 presented at Symposium on Fluid Mechanics and Measurements in Two-Phase Flow Systems, Leeds University,(Sept.1969).

G3 Govier, G.W., Radford, B.A. and Dunn, J.S.

Can. J. Chem. Eng., 35, 55,(1957).

G4 Govier, G.W. and Short, W.L.

Can. J. Chem. Eng., 36, 195,(1958).

G5 Griffith, P.

A.N.L. 6796,(1963).

G6 Guerrieri, S.A. and Talty, R.D.

Chem. Eng. Prog. Symp. Ser., 52(18), 69-77,(1956).

H1 Haberstron, R.E. and Griffith, P.

A.S.M.E., Paper No. 65-HT-52,(1965).

H2 Hewitt, G.F. and Roberts, D.N.

Report A.E.R.E. - M 2159, H.M.S.O.,(1969).

H3 Honeywell Series 16 Software. Model 316 and 516 Basic Language, May 1971, Document No. 7013 007 2543; M449.

H4 Hsu, Y.Y.
Paper 61-WA-177 presented at A.S.M.E. Winter Annual Meeting, New York,(Dec. 1961).

H5 Hughmark, G.A.
Chem. Eng. Prog., 65(7), 67, (July, 1969).

I1 Isbin, H.S., Sher, N.C. and Eddy, K.C.
A.I.Ch.E. Journal, 3(1), 136, (1957).

J1 Johnson, H.A. and Abou-Sabe, A.H.
Trans. A.S.M.E., 74, 977-987,(1952).

J2 Jones, A.
Computer Journal, 13(3), 301-308, (1970).

K1 Kegel, P.K.
B.Ch.E. Thesis, University of Delaware,(1948).

L1 Lapidus, L.
'Digital Computation for Chemical Engineers',
McGraw-Hill,(1962).

L2 Lockhart, R.W. and Martinelli, R.C.
Chem. Eng. Prog., 45, 39,(1949).

M1 Martinelli, R.C. and Nelson, D.B.
Trans. A.S.M.E., 70, 695,(1948).

M2 Moissis, N.
J. Heat Transfer, P.366, Nov.(1963).

N1 Nagaragan, R. and Adelman, M.
Can. J. Chem. Eng., 48, 39,(1970).

P1 Penman, T.G. and Tait, R.W.
Ind. and Eng. Chem. Fund., 4(4), 404-416,(1965).

P2 Porteous, A.
Brit. Chem. Eng.,14(9), 117-119,(1969).

P3 Pujol, L. and Stenning, A.H.
Proc. Int. Symp. Co-current. Gas-Liquid Flow,
University of Waterloo, Canada, P.401-453, Sept.(1968).

R1 Radovich, N.A. and Moissis, R.
Report No. 7-7673-22, Dept. of Mech. Eng., M.I.T.(1962).

R2 Reid, R.C. and Sherwood, T.K.
'Properties of Liquids and Gases', 4th Ed., McGraw-Hill,
(1968).

R3 Richard, J.M.
J. Phys. D (Appl.Phys.), 4, L15-L18,(1971).

R4 Rohsenow, W.M.
Trans. A.S.M.E., 74, 969-975,(1952).

R5 Rosenbrock, H.H.
Computer Journal, 3, 175-184,(1960).

R6 Rosson, H.F. and Myers, J.A.
Chem. Eng. Prog. Symp. Ser., 61(59), 190-199,(1965).

S1 Sato, T., Minamiyama, T., Yanai, M., Tokura, T. and Ito, Y.
Heat Transfer: Japanese Research, 1(4), 1-30,(1972).

S2 Schrock, V.E. and Grossman, L.M.
Nucl. Sci. Eng., 6, 245-250,(1959).

S3 Schrock, V.E. and Grossman, L.M.
Final report, Institute of Engineering Research, University of California, Berkeley,(1959).

S4 Schrock, V.E. and Grossman, L.M.
Nucl. Sci. Eng., 12, 474-481,(1962)

S5 Simpson, H.C. and Wallis, A.S.
Paper 18, Symposium on Boiling Heat Transfer in Steam Generating Units and Heat Exchangers, Manchester, (Sept.1965).

S6 Somerville, G.F.
Report UC RL-10527, Lawrence Radiation Laboratory, University of California,(Oct. 1962).

S7 Sze-Foo, C. and Ibele, W.
Paper 62-WA-170, presented at Winter Annual Meeting in New York of A.S.M.E., (Nov. 1962).

T1 Tong, L.S.
'Boiling Heat Transfer and Two-Phase Flow',
Wiley,(1966).

T2 Tong, L.S.
Nucl. Eng. Des., 21, 1-25,(1972).

W1 Weast, R.C.
Handbook of Chemistry and Physics, 53rd Ed.,
CRC Press,(1972).

W2 Wright, R.M.
Ph.D. Thesis, U.C.R.L. - 9744, University of California,
(1964).

W3 Wright, R.M., Somerville, G.F., San, R.L. and
Bromley, L.A.
Chem. Eng. Prog. Symp. Ser., 61(57), 220-229,(1965).

Z1 Zuber, N. and Fried, E.
A.R.S. Journal, 1332-1341, (Sept. 1962).

Z2 Zuber, N., Staub, F.W., Bywaard, G. and Kroeger, P.G.
G.E.A.P. - 5417,(1 67).

APPENDIX I

THERMOCOUPLE CALIBRATION

I.1 THERMOELECTRIC POTENTIAL APPROXIMATION ERRORS

I.1.1 Chromel-Alumel

The thermoelectric power of Chromel-Alumel thermocouples between 0°C and 200°C is approximately 40 uV/°C and thus with an amplification of 250 a 1 volt reading on the D.V.M. was equivalent to approximately 100°C. Assuming 1 volt on the D.V.M. to be exactly equivalent to 100°C gave a varying error over the temperature range 0°C to 240°C which is shown in Fig. (I.1). This error plot was represented by three straight lines with a maximum error of 0.1°C.

The equations of the three lines are:-

For 0°C to 41°C

$$E = 0.0037 \times T_a \qquad \text{I.1}$$

for 41°C to 125°C

$$E = 0.0359 \times T_a - 1.31 \qquad \text{I.2}$$

and for 125°C to 235°C

$$E = 0.0027 \times T_a + 2.86 \qquad \text{I.3}$$

where E is the error (°C) and T_a is the apparent temperature in °C.

The true temperature T is given by

$$T = T_a - E \qquad \text{I.4}$$

I.1.2 Copper-Constantan

A similar error plot as for Chromel-Alumel can be drawn for copper-constantan thermocouples and is given in Fig. (I.2). This error plot was best represented by a

Figure I.1 Plot of Error v/s Apparent Temperature for Chromel/Alumel Thermocouples and Fitted Straight Lines

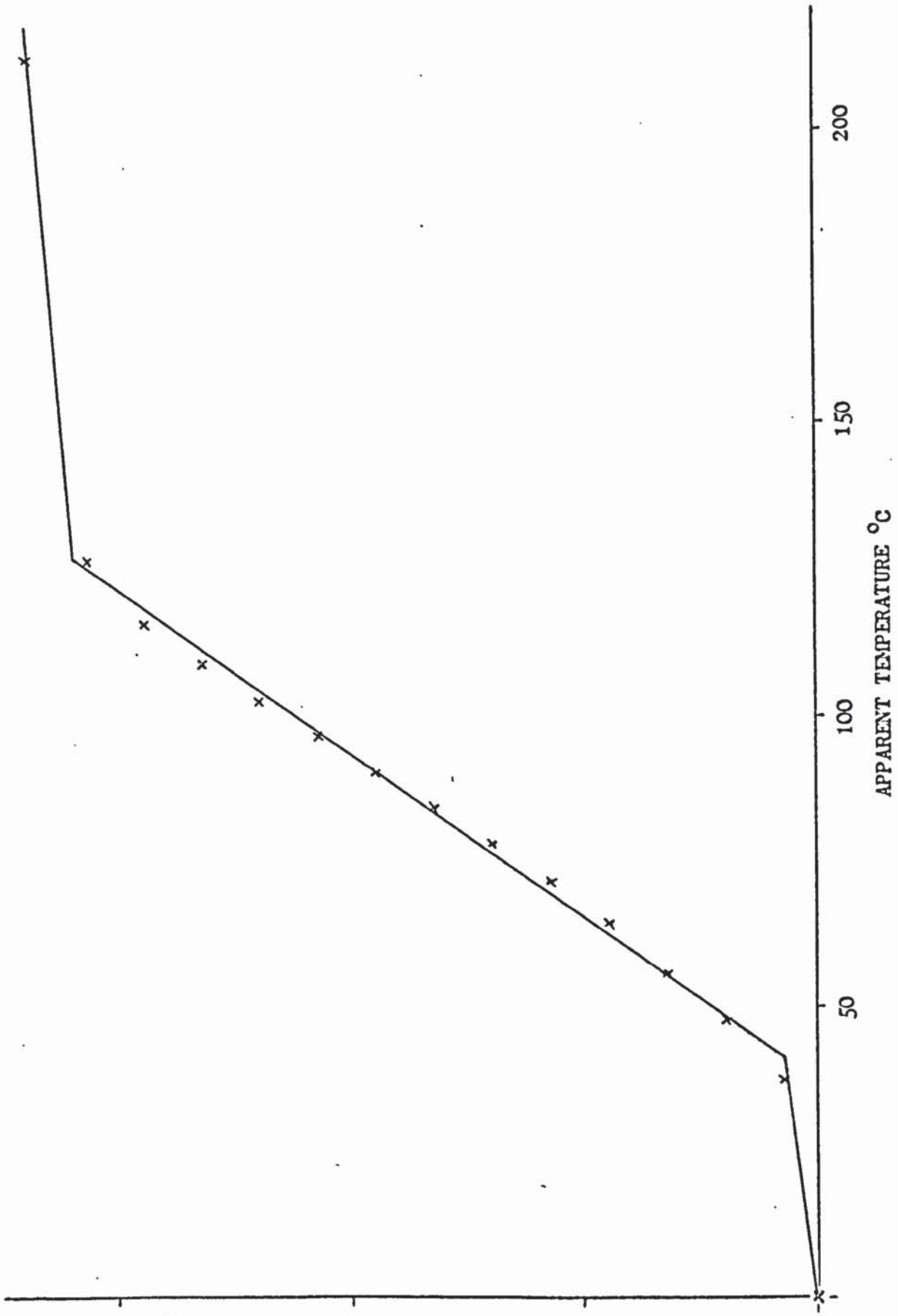

Figure I.2 Plot of Error v/s Apparent Temperature for Copper/Constantan Thermocouples and Fitted Polynomial

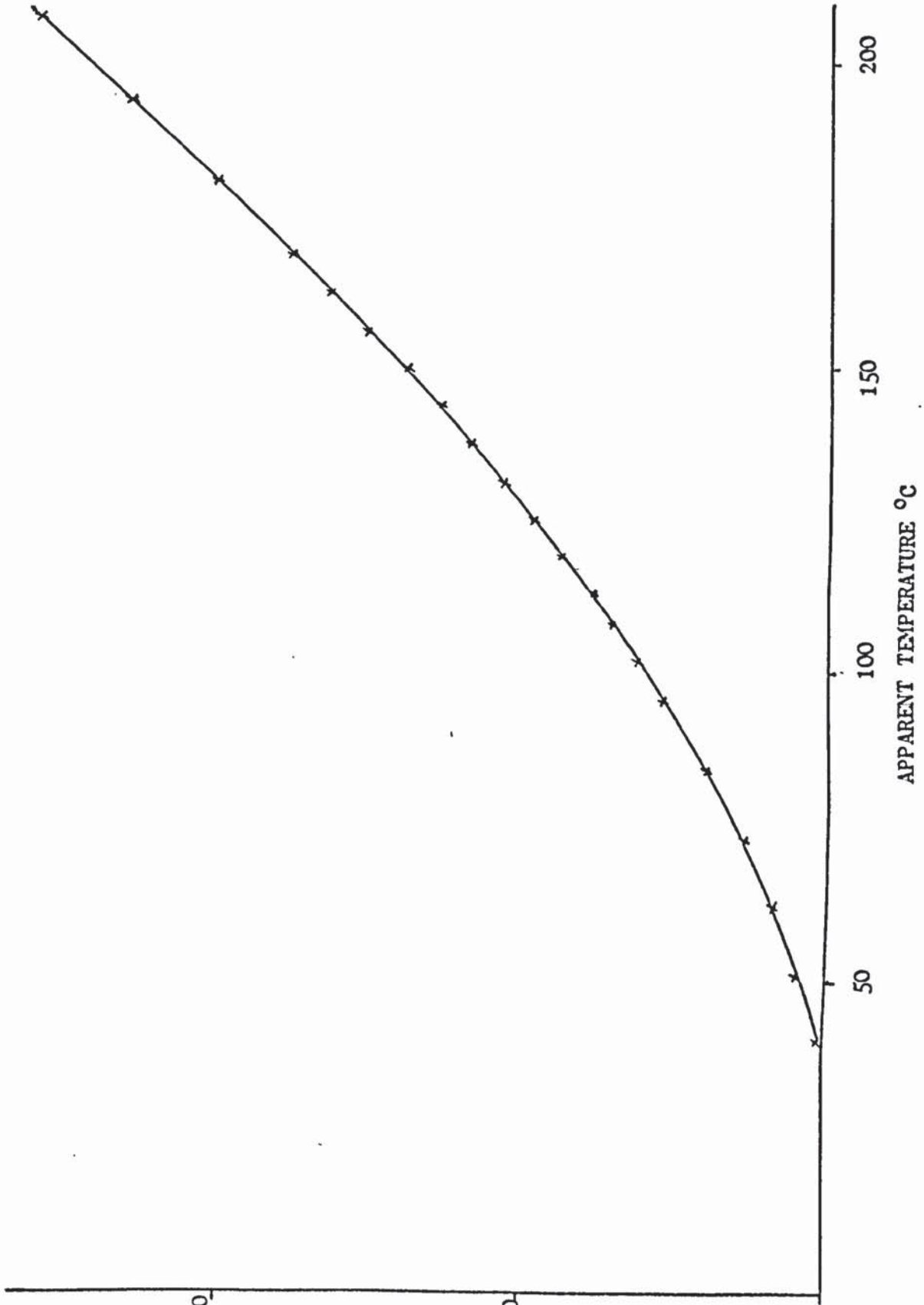

polynomial approximation for the range 15°C to 240°C. The best four parameter equation was:-

$$E = 1.307 + 6.0 \times 10^{-3}T_a - 7.3326 \times 10^{-4}T_a^2 - 6.0454 \times 10^{7}T_a^3 \quad \text{I.5}$$

and as with the Chromel-Alumel thermocouples equation (I.4) applies.

The same Chromel-Alumel reference junction was used for all of the thermocouples. This resulted in an error in the copper-constantan thermocouple readings due to the different thermoelectric potentials of the two types of thermocouples. However, in the range 14°C to 29°C the thermoelectric power of both types of thermocouple is identical. Thus providing the temperature of the junction between the two types of thermocouple was in this range the error had a constant value of approximately 0.2°C. This error was not specifically allowed for, but was incorporated in the thermocouple calibrations.

I.2 THERMOCOUPLE CALIBRATIONS

When the thermocouples were calibrated between 15°C and 100°C using a potentiometer, the measured errors in the thermocouple readings were all in the range $\pm$ 1°C. However when the D.V.M. was used the errors were found to be much greater; +2.5°C to +8.0°C for the chromal-alumel thermocouples, and -1.2°C to +1.5°C for the copper-constantan thermocouples. For the chromel-alumel thermocouples the value of the error increased with temperature while for the copper-constantan thermocouples the value of the error decreased. These differences between the two types of thermocouple could be explained if it was assumed that most

of the error was due to some effect of the impedance of the thermocouples, since the measured resistances of the chromel-alumel thermocouples were in the range 200 Ω to 300 Ω while those of the copper-constantan thermocouples were in the range 20Ω to 25 Ω. Also the resistance of the chromal-alumel thermocouples increased with temperature while the resistance of the copper-constantan thermocouples decreased with temperature.

From experimental work performed to investigate this effect it was found that the variation in error for each thermocouple appeared to be approximately linear with respect to temperature. This being assumed, the correction required at any temperature could be determined if the error at any two temperatures were known. The two temperatures chosen were that of cold mains water ($\sim 16^{o}C$) and hot water from the reboiler ($\sim 98^{o}C$) (see IV.2)

Since this correction was applied before the thermo-electric potential approximation correction, the two calibration temperatures had to be expressed as apparent temperatures, T_a, as defined previously. These of course were different for the two types of thermocouple.

However the corrections had to be based upon the temperature readings as given by the D.V.M. If T_{a_1} and T_{a_2} are the apparent temperatures of the cold and hot liquids used for calibration, then:

$$T_{r_1} = T_{a_1} + E_{r_1} \qquad \text{I.6}$$

and $$T_{r_2} = T_{a_2} + E_{r_2} \qquad \text{I.7}$$

where E_{r_1} and E_{r_2} are the thermocouple errors at T_{a_1} and T_{a_2} and T_{r_1} and T_{r_2} are the D.V.M. readings.

Assuming an equation of the form

$$E_r = C_1 + C_2 T_r \qquad \text{I.8}$$

then it can be shown that

$$C_2 = \frac{(E_{r2} - E_{r1})}{(T_{r2} - T_{r1})} \qquad \text{I.9}$$

and

$$C_1 = E_{r1} - \frac{(E_{r2} - E_{r1})}{(T_{r2} - T_{r1})} T_{r1} \qquad \text{I.10}$$

In this way, for each day's runs C_1 and C_2 were determined for each of the thermocouples. To eliminate the hand calculation of up to 24 values of C_1 and C_2 these were calculated in the computer programme used to process the raw data.

APPENDIX II

II ROTAMETER CALIBRATION

The Rotameter used was a standard 24S with stainless steel float as supplied by Rotameter Co. Ltd.

The rotameter was calibrated at room temperature ($14^{\circ}C$ - $18^{\circ}C$) for water using the bucket and stopwatch method. The calibrations were all performed with the rotameter in situ and great care was taken, both when calibrating and when experimental runs were being performed to ensure that the rotameter was exactly vertical. When the values were plotted it was found that the experimental plot was almost indistinguishable from the standard calibration for cold water at $15^{\circ}C$ as supplied with the instrument.

The rotameter was then calibrated with hot water ($95^{\circ}C$ - $98.5^{\circ}C$). The two calibrations are shown in Fig. (II.1)

Figure II.1 Calibration Chart for Rotameter

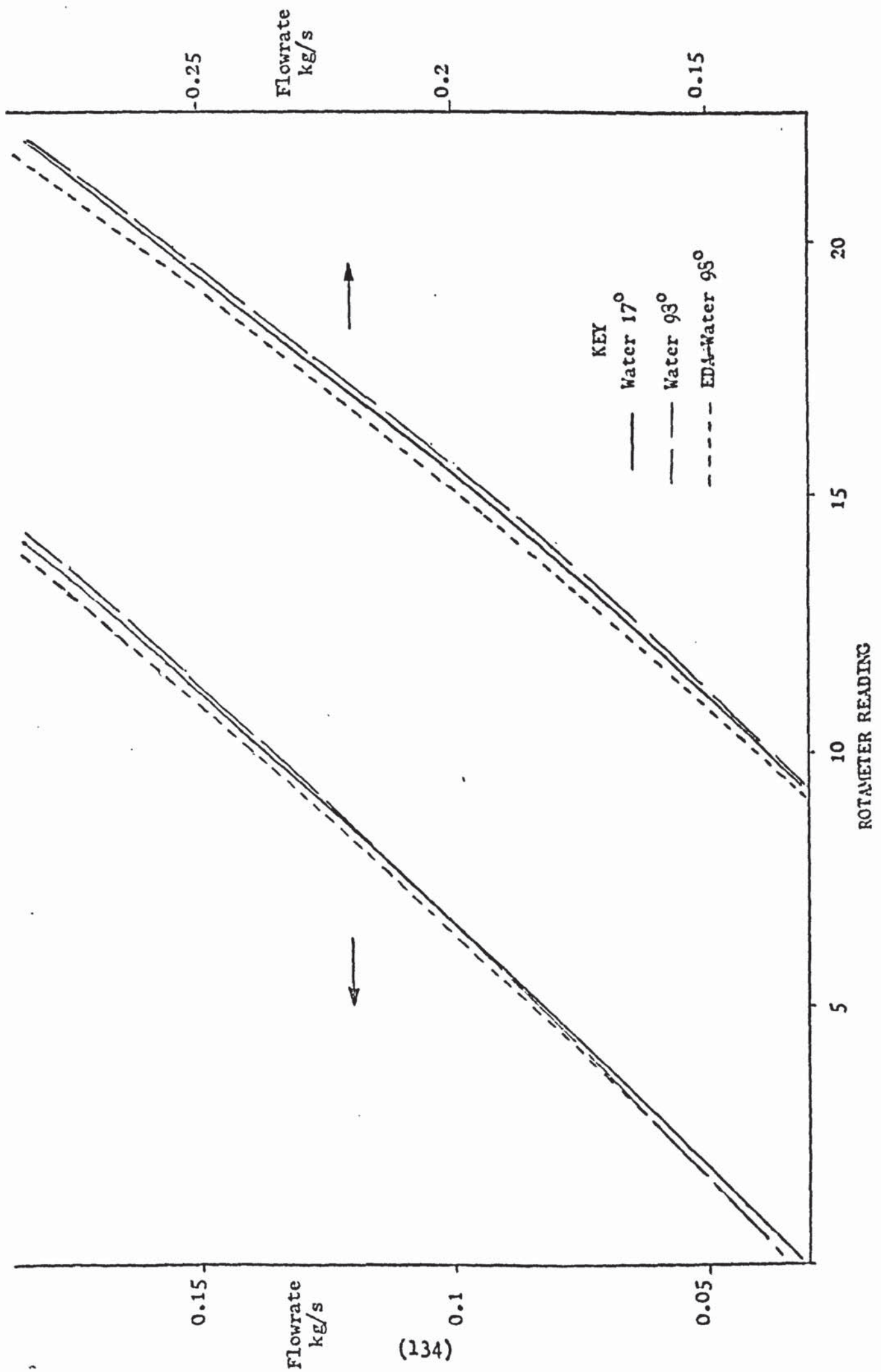

and as can be seen, the hot water and cold water plots are quite close, apart from at very low flow rates.

The calibration of the rotameter for the EDA-water azeotrope was carried out using the calibration booklet supplied with the instrument. However, instead of using the standard calibration curves for the instrument, as given in the booklet, the curves were derived from the hot water plot, in order to obtain a higher accuracy. The EDA-water azeotrope calibration is shown in Fig. (II.2) together with the hot water plot.

APPENDIX III

III PHYSICAL PROPERTIES

The physical properties of both of the experimental fluids used were required, as functions of temperature, in the programmes used in the analysis of the experimental data. Polynomials of the first or second order were generally found to be quite adequate to represent the data over the range of interest.

III.1 Water Physical Properties

The water physical property data was taken from Ref. W1. Apart from liquid viscosity, vapour pressure and vapour density, which require special treatment, all the physical properties were fitted to first or second order polynomials.

III.1.1 Liquid Viscosity

Ref. C10 gave the following equation for the viscosity of water between $0^{o}C$ and $100^{o}C$

$$\mu_f = 0.1/(2.1482 \times (T - 8.435 + \sqrt{8078.4 + (T - 8.435)^2} - 120.4) \quad \text{III.1}$$

where T is ^{o}C and μ_f is in Poiseuilles.

When tested this equation was found to be accurate to $\pm$ 1.0% between 0°C and 120°C.

Table III.1 Viscosity in Micropoiseilles

°C	10.0	20.0	30.0	40.0	50.0	60.0	70.0	80.0	90.0	100.0	110.0	120.0
A	1304	1002	798.3	653.9	547.8	467.3	404.8	355.4	315.6	283.1	254.8	231.0
B	1314	1008	803.3	657.0	550.6	469.5	406.9	356.9	316.9	284.1	256.9	234.1

A : Ref(W1). B : Equation III.1

III.1.2 Vapour Density (Saturated)

An equation of the form

$$\rho_g = \frac{K\,p}{(T + 273.15)} \qquad \text{III.2}$$

was used to predict vapour density. It was found sufficiently accurate to assume K as a constant over the range 80°C to 130°C. The optimum value for K was 2.202×10^{-3} with T in °C and p in N/m^2 giving

$$\rho_g = 2.202 \times 10^{-3}\ p\ /(T + 273.15) \qquad \text{III.3}$$

with ρ_g in kg/m^3. This equation was accurate to $\pm$ 1%.
If water vapour was ideal K would be 2.167×10^{-3}.

Table III.2 ρ_g in kg/m^3

T °C	80	90	100	110	120	130
Ref. W1	.2934	.4236	.5998	.8264	1.121	1.496
Equation III.3	.2929	.4250	.5979	.8241	1.116	1.483

III.1.3 Vapour Pressure

The most suitable algorithm found for incorporating in the computer programmes was that by Richards (R3)
The equation for vapour pressure is

$$\ln(p) = t(13.3185 - t(1.976 + t(0.6445 + 0.1799\ t))) \qquad \text{III.4}$$

where $t = 1 - \frac{373.15}{T}$ III.5

and T is in °K and p in atms.

To find the temperature from the vapour pressure the following procedure was used.

A first approximation is given by

$$t_1 = \ln(p)/13.3185 \qquad \text{III.6}$$

then the iteration

$$t_{n+1} = t_1 + ((0.1299\ t_n + 0.6445)\ t_n + 1.976)t_n^2/13.3185 \qquad \text{III.7}$$

is performed until $|t_{n+1} - t_n| < 10^{-5}$

then $$T = \frac{373.15}{1 - t_n} - 273.15 \qquad \text{III.8}$$

where T is in ^{o}C.

This algorithm was found to be accurate to $0.02^{o}C$ over the range $10^{o}C$ - $135^{o}C$ when finding the temperature and accurate to 0.04% when finding the vapour pressure.

III.1.4 Liquid Density

The data in Ref. C8 was given as specific volume v . This was fitted to a second order polynomial

$$v = 1/\rho_f = 1012.1 + 0.40775(T-50) + 3.285 \times 10^{-3}\ (T-50)^2 \qquad \text{III.9}$$

$$\text{then } \rho_f = {}^{1000}/(1.0121 + 4.0775 \times 10^{-4}(T-50)+3.285\times10^{-6}(T-50)^2) \qquad \text{III.10}$$

where ρ_f is in kg/m^3 and T is in ^{o}C.

This equation is accurate to 0.25% over the range $15^{o}C$ to $150^{o}C$.

Table III.4 ρ_f in Kg/m^3 T in ^oC

^oC	10	20	30	40	50	60	70	80	90	100	110	120
A	999.8	999.6	998.2	992.2	988.0	983.2	977.7	971.8	965.3	958.3	951.0	943.1
B	999.1	998.2	994.8	991.7	988.0	983.8	978.9	972.4	967.5	960.8	953.5	945.2

A : Ref. C8 B : Equation III.10

III.1.5 Liquid Thermal Conductivity

The thermal conductivity data was fitted to a second order polynomial.

$$k_f = 0.643 + 1.06 \times 10^{-3}(T-50) - 6.0 \times 10^{-6}(T-50)^2 \qquad \text{III.11}$$

where k_f is in joules/metre^oC and T in ^oC.

This equation fitted the data to within 0.5% over the range 10^oC to 130^oC.

Table III.5 k_f in joules/metre sec °k T in ^oC

^oC	20	30	40	50	60	70	80	90	100	110	120
A	0.603	0.618	0.631	0.643	0.653	0.662	0.670	0.676	0.681	0.684	0.687
B	0.605	0.619	0.632	0.643	0.653	0.662	0.669	0.676	0.681	0.685	0.687

A : Ref. C8 B : Equation III.11

III.1.6 Liquid Specific Heat

The liquid specific heat was fitted to a second order polynomial.

$$C_{pf} = 4179 + 0.1\ (T-40) + 0.01\ (T-40)^2 \qquad \text{III.12}$$

where C_{pf} is in joules/kg^oC and T in ^oC. This equation fitted the data to within 0.4% in the range 10^oC to 130^oC.

Table III.6 C_{pf} in joules/kg^oC T in ^oC

^oC	10	20	30	40	50	60	70	80	90	100	110	120	130
A	4194	4182	4179	4179	4181	4185	4191	4198	4207	4218	4230	4244	4262
B	4185	4181	4129	4179	4181	4185	4191	4199	4209	4221	4235	4251	4279

A : Ref. C8 B : Equation III.12

III.1.7 Surface Tension

The surface tension data was fitted to a second order polynomial.

$$\sigma = 0.06784 - 1.7225 \times 10^{-4}(T-50) - 1.745 \times 10^{-7}(T-50)^2 \qquad \text{III.13}$$

where σ is in N/m and T in ^{o}C. This equation fitted the data to within 0.3% in the range 50°C to 130°C.

Table III.7 σ x 100 N/m T in ^{o}C

^{o}C	50	60	70	80	90	100	110	120	130
Ref. C8	6.793	6.619	6.44	6.257	6.069	5.878	5.683	5.485	5.283
Eqn III.13	6.784	6.612	6.437	6.248	6.066	5.881	5.691	5.495	5.287

III.1.8 Heat of Vapourisation

The heat of vaporisation data was fitted to a first order polynomial.

$$Lv = 2.255 \times 10^{6} - 2600\ (T-100) \qquad \text{III.14}$$

where Lv is in joules/kg and T in ^{o}C. This equation is accurate to 0.15% in the range 50° to 130°C.

Table III.8 Lv in joules/kg x 10^{-3}

^{o}C	50	60	70	80	90	100	110	120	130
Ref. C8	2383	2358	2333	2308	2283	2257	2230	2202	2174
Eqn. III.14	2385	2359	2333	2307	2281	2255	2229	2203	7177

III.1.9 Vapour Specific Heat

The vapour specific heat data was fitted to a second order polynomial.

$$Cp_g = 2034 + 4.15\ (T-100) + 0.031\ (T-100)^2 \qquad \text{III.15}$$

where Cp_g is in joules/kg^{o}C. This equation fitted the data to within 0.4% in the range 50° to 130°C.

Table III.9 Cp_g in joules/kg°C

°C	50	60	70	80	90	100	110	120	130
Ref. C8	1912	1924	1946	1970	1999	2034	2076	2125	2180
Eqn. III.15	1904	1918	1938	1963	1996	2034	2079	2129	2187

III.1.10 Vapour Viscosity

The vapour viscosity data was fitted first order polynomial.

$$\mu_g = 1.206 \times 10^{-5} + 3.8 \times 10^{-8} \text{ (T-100)} \qquad \text{III.16}$$

where μ_g is in poiseiulles. This equation fitted the data to within 1% over the range 50°C to 130°C.

Table III.10 μ_g in micropoiseiulles

°C	50	60	70	80	90	100	110	120	130
Ref. C8	10.10	10.50	10.89	11.29	11.67	12.06	12.45	12.83	13.20
Eqn. III.16	10.22	10.60	10.98	11.34	11.74	12.06	12.42	12.78	13.14

III.2 WATER-EDA AZEOTROPE PHYSICAL PROPERTIES

The only physical properties of the water-EDA azeotrope that were found in the literature (W1) were

1) Boiling point 99.7°C at 760 mm Hg
2) Composition 15.4% EDA by weight
3) Density 1.012 gm/cm^3 at boiling point

However, from previous experience it had been found that tabulated data on azeotropes was not always reliable. Hence these values were checked and found to be accurate. Other physical property data had to be either predicted or measured. The azeotrope physical property values which were measured were: surface tension, viscosity and density. To predict

the physical properties of the azeotrope it was necessary first to determine the physical properties of pure EDA. The liquid specific heat was the only physical property of EDA which was measured. The methods given by Reid and Sherwood (R2) were used to predict the physical properties of EDA which were not measured or found in the literature. For more details of the methods used see Ref.R2.

III.2.1 Physical Properties of Pure EDA

(1) Liquid Specific Heat

The specific heat of EDA was measured by dropping an iron weight of known temperature and mass into a flask containing a measured weight of EDA and measuring the temperature rise with an accurate thermometer. The heat capacity of the flask had previously been determined by using the same procedure with water.

The value of the specific heat of EDA obtained in this way was 0.483 cals/gas^{o}C. This value was assumed to be applicable over the range 15^{o}C to 130^{o}C.

(2) Specific Heat of Vapour

Using Reid and Sherwood's equation 5.7 and Table 5.7 the value of vapour specific heat of EDA was estimated as

$$Cp_g = 170.3 + 0.447\ (T-100) \qquad \text{III.17}$$

where Cp_g is in joules/gm mole^{o}C and T in ^{o}C.

(3) Heat of Vapourisation

Ref. W1 gave the heat of vapourisation as 52259 joules/gm mole. However this value was given as part of a list of vapour pressure constants over the range 30^{o}C to 190^{o}C. Hence it was necessary to assume that this value could be used over the complete range.

(4) Thermal Conductivity of Liquid

Using equation 10.55 in Reid and Sherwood calculated as 1.451×10^{-5} joules/m ^{o}K at 100°C. It was assumed that variation in k_f over the range 90° to 130°C would be small and that this value could be used over the whole range.

(5) Viscosity of Gas

Using equation 9.9 in Reid and Sherwood calculated to be 97.6 micropoises at 100°C. Since gas viscosity is relatively insensitive to temperature it was assumed that this value could be used over the range 90° to 130°C.

III.2.2 Azeotrope Physical Properties

(1) Latent Heat of Vaporisation

It was assumed that the heat of vaporisation was a weighted mean of the heats of vaporisation of the two pure components then

at 100°C H_2O: $L_v = 2.2415 \times 10^6$ joules/kg

EDA: $L_v = 0.3626 \times 10^5$ joules/kg

then $$L_v = 2.2415 \times 10^6 \times 0.846 + 0.3626 \times 10^6 \times .154 \quad \text{III.18}$$

$$= 1.955 \times 10^6 \text{ joules/kg}$$

(2) Vapour Pressure

It was decided to use the Clausius-Clapeyron Equation to predict the vapour pressure variation with respect to temperature. The form of the equation used is:-

$$\ln(p) = -\frac{L_v}{RT} + C \quad \text{III.19}$$

the heat of vaporisation is already known (see above) thus only one experimental value is needed to determine the

only unknown, C. Using the known value of the boiling point of the azeotrope at atmospheric pressure the value of C was found to be 13.14. Inserting the known values of R and C, equation I.19 becomes

$$\ln(p) = -\frac{4895.3}{T} + 13.14 \qquad \text{III.20}$$

where T is in ^{o}K and p in atms.

(3) Vapour Density

Assuming ideal gas behaviour, the vapour density of the mixture can be determined assuming the mixture to be a single gas of suitable molecular weight.

Mole wt of mixture = 18 x 0.978 + 146 x 0.02195

= 20.82

then at N.T.P.

$$\rho_g = \frac{20.84}{2.24} \times 10^4 \text{ gm/cm}^3$$

$$= 9.29 \times 10^{-1} \text{ kg/m}^3$$

$$\text{then } \rho_g = 9.29 \times 10^{-1} \times \frac{273.15}{T + 273.15} \times \frac{p}{101325} \qquad \text{III.21}$$

$$= 2.545\ p/(T + 273.15) \qquad \text{III.22}$$

where ρ_g is given in kg/m^3 with p in N/m^2 and T in ^{o}C.

(4) Vapour Viscosity

Using equation 9.37 in Reid and Sherwood the vapour viscosity of the vapour mixture was determined as

$$\mu_g = 126.7 \text{ micropoises}$$

Vapour viscosity is comparatively insensitive to temperature and this value can be assumed over the range $90^{o}C$ to $130^{o}C$ without any appreciable error. Indeed, since the molecular concentration of EDA is so low (2.195%), this mixture viscosity value is within 0.8% of the pure water value, hence the effect of even a fairly large error in the predicted EDA value would be very small on the mixture value.

(5) Liquid Thermal Conductivity

Using equation 10.61 in Reid and Sherwood the liquid thermal conductivity of the vapour mixture was determined as

k_f = 0.549 watts/m^{o}K

at 100^{o}C. This value was assumed over the range 90^{o}C to 130^{o}C.

(6) Liquid Density

The density of the water-EDA azeotrope was measured over the temperature range 80^{o}C to 98.5^{o}C at approximately 5^{o}C intervals using a specific gravity bottle calibrated at each temperature using water. The data was fitted to a straight line equation

$$\rho_f = 1012.0 - 0.98 \ (T - 100) \qquad \text{III.23}$$

where ρ_f is in kg/m^3 and T in ^{o}C.

(7) Liquid Viscosity

The viscosity of the water-EDA azeotrope was measured, by the analytical group in the department, using a U-tube viscometer. The viscometer was used for both the azeotrope and for water over the range 83^{o}C to 98^{o}C at 3^{o}C intervals. When the discharge times were plotted against temperature both liquids gave straight line plots.

It was assumed that the viscosity of water was given by equation I.1 as described previously. The viscosity of the azeotrope was determined using the equation

$$\frac{\eta_1}{\eta_2} = \frac{t_1 \rho_1}{t_1 \rho_2} \qquad \text{III.24}$$

where η_1, η_2 are the kinematic viscosities, t_1 and t_2 the discharge times, and ρ_1 and ρ_2 the densities of the two

liquids. Assuming the discharge time plots could be extrapolated, the viscosity of the azeotrope was determined from 90°C to 130°C at intervals of 1°C. These viscosity values were correlated with respect to temperature using a suitable fitting procedure. The equation derived was

$$\mu_f = 0.001777 - 1.9496 \times 10^{-5}T - 5.274 \times 10^{-8}T^2 \qquad \text{III.25}$$

where μ_f is in poiseiulles and T in °C.

The computed R.M.S. error for the derived fit was 4.66×10^{-7} poiseiulles. This corresponds to about 0.1%.

(7) Surface Tension

The surface tension data shown in Fig. 6.17 was fitted to a straight line. The best line found was:

$$\sigma = 0.0468 - 0.000052\ (T - 100) \qquad \text{III.26}$$

where σ is in N/M and T in °C.

APPENDIX IV

COMPUTER PROGRAMS

IV.1 Programs for the Honeywell 316

IV.1.1 Program I

The purpose of this program was to process the raw experimental data and to output the derived values of the required variables at each increment in a tabular form. The data input could be either on paper tape or could be typed in using a teletype at run time. The program was written in Basic 16 and was run on the departmental Honeywell 316.

The listing given below is that of the program for the water runs with both types of thermocouple being used; runs 16-61. Minor modifications to the program were necessary for the water runs 61 on, when only one type of thermocouple was used. For the EDA-water azeotrope runs (runs 101-145) the statement functions and the subroutines for physical properties had to be altered.

A list of the variables, arrays and statement functions is given after the program listing, together with output from a typical run.

```
1  REM    PROGRAM TO PREPARE AND PRESENT THERMOSYPHON DATA
2  REM    PROGRAM FOR RUNS 16-60. WATER ONLY. TABULAR OUTPUT.
3  REM    D.MOORE   20/6/74
4  REM
5  DIM A(24),B(24),C(2,24),I(24),E(24),F(24),G(24),H(24),K(2,24)
6  DIM L(24),M(24),N(24),P(24),T(24),S(24),T(24),V(24),Y(24)
7  DIM X(24),Y(24),Z(24)
15 REM
16 REM    FUNCTIONS FOR WATER PHYSICAL PROPERTIES
17 REM
19 DEF FNS(V)=.6784E-01-.17225E-03*(V-50)-.1745E-06*(V-50)↑2
20 DEF FNI(V)=V+1.307-.1E-04*(6064*V+73.526*V*V-.68454E-01*V*V*V)
21 DEF FNC(V)=4179+.1*(V-40)+.1E-01*(V-40)*(V-40)
22 DEF FNH(V)=.2255E-7-2E-10*(V-100)
23 DEF FNP(V)=2034+4.15*(V-100)+.31E-01*(V-100)*(V-100)
24 DEF FNL(V)=1000/(1.0121+.40775E-03*(V-50)+.3225E-05*(V-50)↑2)
25 DEF FNE(V)=.2202E-02/(V+273.15)
26 DEF FNV(V)=.1/(9.1452*(V-8.435+SQR(8178.4+(V-8.435)↑2))-120.4)
27 DEF FNS(V)=.1206E-04+.38E-07*(V-100)
28 DEF FNK(V)=.643+.106E-02*(V-50)-.6E-05*(V-50)*(V-50)
29 DEF FNL(V)=.249E-01+.1E-03*(V-100)
30 REM
31 REM      RIG CONSTANTS
32 REM
33 D1=.159E-01:A=3.14159*D1*D1/4:H2=.762E-01
34 A1=3.14159*D1*H2:N1=24: GOTO 40
35 REM
36 REM    INPUT OF T/C CALIBRATION DATA
37 REM
38 INPUT C1,C2,C3,C4
39 FOR I=1,N1: INPUT C(1,I),C(2,I): NEXT I: GOSUB 600
40 FOR I=1,5: PRINT : NEXT I
42 REM
43 REM     INPUT OF RUN DATA
44 REM
45 INPUT H1,F,H,T1,P3,P1,P0
46 IF H1<1 GOTO 38
56 H=H/2
57 P3=P3*133.322
58 P1=P3+1333.22*P1
61 N9=0
67 REM
68 REM      INPUT OF INCREMENT DATA; T(WALL) AND P(BULK)
69 REM
70 FOR I=1,N1
71 Y(I)=1
75 INPUT T(I),P(I)
77 IF T(I)<10 THEN Y(I)=0
78 P(I)=P3+1333.22*P(I)
79 NEXT I
80 GOSUB 620
85 PC=P3+97.92*PG-.525*(P(N1)-P(N1-1))
92 REM
```

```
 93  REM     CALCULATION OF T(BLCK) AT FIRST INCREMENT
 94  REM
 95  B(1)=T1+H/(2*F*FNC(T1))
 97  HA=H/A1
 98  G=F/A
100  REM
101  REM  CALCULATION OF B(I),S(I),B(I),T(I),N9,X(I),H(I)
102  REM
104  FOR I=1,N1
105  X(I)=0
106  N(I)=0
107  V(I)=0
109  IF I>18.5 GOTO 115
110  IF (I/2-INT(I/2))<.3 THEN B(I)=FNI(B(I)): GOTO 122
115  Z=P(I)
116  IF Z<41 THEN  GOTO 122
117  E=.359E-01*Z-1.31
118  IF Z>125 THEN E=.27E-02*Z+2.86
121  P(I)=Z-E
122  IF Y(I)<.5 THEN B(I)=B(I-1)
130  P9=P(I)
131  GOSUB 810
132  S(I)=T9
150  IF I<1.5 GOTO 160
152  IF N(I-1)>.5 GOTO 170
153  B(I)=B(I-1)+H/(F*FNC(T(I-1)))
160  IF S(I)>B(I) THEN T(I)=B(I): GOTO 190
170  T(I)=S(I)
171  IF N9<.1 THEN N9=I
175  N(I)=1
180  HS=H+F*(T(I-1)-T(I))*((1-X(I-1))*FNC(T(I))+X(I-1)*FNG(T(I)))
185  X(I)=X(I-1)+HS/(FNH(T(I))*F)
190  H(I)=HA/(B(I)-T(I))
200  NEXT I
207  REM
208  REM      CALCULATION OF M(I),G(I),N(I),V(I)
209  REM
210  FOR I=N9,N1
220  V1=F*((1-X(I))/FNE(T(I))+X(I)/(FNE(T(I))*P(I)))
222  V0=X(I)*F/(V1*FNE(T(I))*P(I))
224  M(I)=(FNV(T(I))/FNH(T(I)))^.1*SQR(FNE(T(I))*P(I)/FNC(T(I)))
226  M(I)=M(I)*((1-X(I))/X(I))^.9
228  G(I)=V1*V1/(9.81*D1*A*A)
229  G(I)=.19*M(I)*G(I)^.185
230  V3=V1/A
232  IF N(I-1)>3.5 GOTO 265
233  IF N(I-1)>1.5 GOTO 245
234  IF N(I-1)>3.5 GOTO 265
236  N(I)=1
238  V(I)=V0/(1.2+.22/V3)
240  IF V(I)>.3 THEN N(I)=2
242  IF N(I)=1 GOTO 300
245  N(I)=2
248  S1=G*(1-X(I))/(FNE(T(I))*SQR(9.81*E1))
250  S2=G*X(I)/SQR(9.81*D1*FNC(T(I))*FNE(T(I))*P(I))
252  IF S2>(.139+.11E-01*S1) THEN N(I)=3
254  IF S1<1.5 GOTO 256
255  IF S2<.9 GOTO 258
256  IF S2>(.9+.6*S1) GOTO 265
258  V(I)=V0/(1.2+.56*SQR(9.8*D1)/V3)
260  GOTO 300
```

```
265  N(I)=4
266  IF S1<3 GOTO 268
267  IF S2>1 THEN N(I)=5
268  Y=.21E-01*FND(T(I))*G↑.686/(FNE(T(I))*P(I))
270  IF Y<2.5 GOTO 274
271  IF Y>300 GOTO 274
272  IF G>950 GOTO 274
273  GOTO 277
274  T8=SQR(1+20/M(I)+1/(M(I)*M(I)))
275  V(I)=(T8-1)/T8
276  GOTO 300
277  Y1=Y↑.333
278  X2=Y-1
280  Y3=1+(Y-Y1)*X(I)
282  V(I)=(SQR(Y3*Y3*4*Y2*X(I)*Y)-Y3)/(2*Y2)
300  NEXT I
307  REM
308  REM     CALCULATION OF R(I),L(I),K(1,I),K(2,I),A(I),Z(I)
309  REM
310  FOR I=N9,N1
312  R(I)=G*(1-X(I))*D1/FNV(T(I))
314  GOSUB 630
315  T7=W(I): GOSUB 660
316  GOSUB 675
317  L(I)=A(I)*F(I)+D(I)*(Z(I)*T8↑.24*P8↑.75)
318  K(2,I)=L(I)
320  FOR J=1,3
321  T7=T(I)+H6/K(2,I): GOSUB 660
322  K(2,I)=A(I)*F(I)+D(I)*(Z(I)*T8↑.24*P8↑.75)
324  NEXT J
325  K(1,I)=T7
326  Z(I)=Z(I)*T8↑.24*P8↑.75
330  NEXT I
397  REM
398  REM       STATEMENTS FOR TABULAR OUTPUT
399  REM
400  PRINT TAB(15),"RUN NUMBER",R1: PRINT
410  PRINT TAB(17),"FLOWRATE",F;: PRINT "KGS/S"
420  PRINT TAB(17),"HEAT FLUX",H6;: PRINT "W/M.M"
430  PRINT TAB(17),"TEMP IN",T1
439  PRINT TAB(17),"PRESSURE IN",P1;: PRINT "N/M.M"
450  PRINT
460  PRINT TAB(11),"I",TAB(19),"N(I)",TAB(32),"V(I)",TAB(46);
461  PRINT "T(I)",TAB(59),"H(I)"
465  FOR I=1,N1
466  IF Y(I)<.5 GOTO 475
471  PRINT TAB(7);I;TAB(16);N(I),V(I),T(I),H(I)
475  NEXT I
479  PRINT
480  PRINT TAB(11),"I",TAB(19),"X(I)",TAB(32),"H.CALC.";
481  PRINT TAB(46),"H.EST.",TAB(60),"W.EST"
488  FOR I=N9,N1
489  IF Y(I)<.5 GOTO 492
491  PRINT TAB(7);I,X(I),L(I),K(2,I),K(1,I)
492  NEXT I
493  PRINT
494  PRINT TAB(11);"I",TAB(18),"REF",TAB(33),"XTT",TAB(47);
495  PRINT "F(I)",TAB(61),"S(I)"
496  FOR I=N9,N1
497  IF Y(I)<.5 GOTO 499
```

```
498  PRINT TAB(7);I,P(I),M(I),F(I),D(I)
499  NEXT I: PRINT
520  GOTO 40
530  REM  ************************************************************
531  REM
532  REM              SUBROUTINES
533  REM             *************
534  REM
598  REM     SUBROUTINE TO CALCULATE T/C CALIBRATION PARAMETERS
599  REM
600  FOR I=1,N1
601  IF I>18.5 GOTO 604
602  IF (I/2-INT(I/2))<.3 GOTO 606
604  C5=C1+C(1,I):C6=C2+C(2,I): GOTO 608
606  C5=C3+C(1,I):C6=C4+C(2,I)
608  C(1,I)=C(1,I)-C5*(C(2,I)-C(1,I))/(C6-C5)
610  C(2,I)=(C(2,I)-C(1,I))/C6
612  NEXT I
614  RETURN
617  REM
618  REM    SUBROUTINE TO CORRECT T/C VALUES
619  REM
620  FOR I=1,N1
622  P(I)=P(I)-C(1,I)-C(2,I)*R(I)
623  NEXT I
624  RETURN
627  REM
628  REM     SUBROUTINE TO CALCULATE F AND S VALUES
629  REM
630  IF (1/M(I))>.6 THEN F(I)=EXP(1.04-.695*LOG(M(I)))
632  IF (1/M(I))<.6 THEN F(I)=EXP(.772-.372*LOG(M(I)))
634  IF F(I)<1 THEN F(I)=1
640  E(I)=F(I)+1.25*R(I)
641  IF F(I)<.1E05 GOTO 645
642  IF E(I)>.3E06 GOTO 646
643  D(I)=.99-.602*(LOG(E(I))/2.303-4)
644  GOTO 650
645  D(I)=1: GOTO 650
646  D(I)=.1
650  RETURN
657  REM
658  REM    SUBROUTINE TO CALCULATE DELTA.P AND DELTA.T
659  REM
660  T9=1-373.15/(273.15+T7)
662  P8=EXP(T9*(13.3185-T9*(1.967+T9*(.6445+.1299*T9))))
664  PR=ABS(.101325E06*P8-P(I))
666  TR=ABS(T7-T(I))
668  RETURN
672  REM
673  REM     SUBROUTINE TO CALCULATE  H(MIC) AND H(MAC)
674  REM
675  Z(I)=.122E-02*FNK(T(I))+.79*FNC(T(I))+.45*FNL(T(I))+.49
676  Z(I)=Z(I)/(FNH(T(I))+.24*(FNE(T(I))*F(I))+.24)
677  Z(I)=Z(I)/(FNS(T(I))+.5*FNV(T(I))+.29)
680  A(I)=.23E-01*R(I)+.8*(FNV(T(I))*FNC(T(I))/FNK(T(I)))+.4
681  A(I)=A(I)*FNK(T(I))/D1
685  RETURN
806  REM
```

```
807  REM  SUBROUTINE TO CALCULATE T.SAT FROM P.SAT
808  REM
810  T2=LOG(P9/.101325E06)/13.3185
812  T3=T2
814  FOR J=1,4
816  T4=T2+((.1299*T3+.6445)*T3+1.976)*T3*T3/13.3185
818  IF ABS(T4-T3)<.1E-04 GOTO 824
820  T3=T4
822  NEXT J
824  T9=373.15/(1-T4)-273.15
826  RETURN
999  END
```

****

RUN NUMBER 45

FLOWRATE .184 KGS/S
HEAT FLUX .162232E 06 W/M.M
TEMP IN 99.5
PRESSURE IN .136655E 06 N/M.M

I	N(I)	W(I)	T(I)	H(I)
1	0	120.134	99.8976	8016.71
2	0	130.638	100.693	5417.58
3	0	121.578	101.488	8075.04
5	0	122.945	103.077	8165.31
6	0	133.283	103.871	5515.93
7	0	120.123	104.665	.104953E 05
9	0	118.425	106.253	.133283E 05
10	0	134.178	107.046	5979.32
11	2	123.459	106.983	9846.28
12	3	127.547	106.771	7308.72
13	3	117.645	106.497	.145524E 05
14	3	120.176	106.252	.116512E 05
15	3	114.408	105.943	.191649E 05
16	3	112.32	105.631	.242514E 05
19	3	110.803	104.807	.270559E 05
20	3	110.817	104.453	.254907E 05
21	3	108.992	103.898	.318461E 05
22	3	109.099	103.367	.283043E 05
23	4	111.266	102.998	.196216E 05
24	4	105.472	102.658	.576629E 05

I	X(I)	H.CALC.	H.EST.	W.EST
11	.162057E-02	.166695E 05	.134542E 05	118.223
12	.35204E-02	.195852E 05	.136403E 05	117.618
13	.553663E-02	.146039E 05	.145891E 05	117.615
14	.749768E-02	.165563E 05	.150343E 05	116.909
15	.95776E-02	.147447E 05	.15573E 05	116.418
16	.116611E-01	.146786E 05	.160157E 05	115.83
19	.176949E-01	.182672E 05	.189653E 05	113.367
20	.198525E-01	.195029E 05	.199422E 05	112.59
21	.223816E-01	.205364E 05	.211028E 05	111.587
22	.248622E-01	.219356E 05	.222428E 05	110.661
23	.270414E-01	.234694E 05	.232337E 05	109.98
24	.291631E-01	.235739E 05	.241917E 05	109.365

I	REF	XIT	F(I)	S(I)
11	.555799E 05	12.327	1	.542074
12	.553581E 05	6.10263	1.10424	.510721
13	.550963E 05	4.03612	1.28782	.461706
14	.548538E 05	3.05556	1.42831	.429099
15	.545706E 05	2.4354	1.55407	.402890
16	.542866E 05	2.02668	1.66399	.381842
19	.535114E 05	1.3678	2.27578	.253296
20	.532036E 05	1.22425	2.45808	.259696
21	.527694E 05	1.0873	2.66933	.234899
22	.523526E 05	.979	2.87126	.213074
23	.520393E 05	.900799	3.04228	.195738
24	.51746E 05	.835613	3.20533	.180157

VARIABLES

A cross-sectional area of tube (m^2)

A1 wall area in each increment (m^2)

C1 cold water temp. for chromel/alumel thermocouple calibration (^oC)

C2 hot water temp. for chromel/alumel thermocouple calibration (^oC)

C3 cold water temp. for cu/con thermocouple calibration (^oC)

C4 hot water temp. for cu/con thermocouple calibration (^oC)

C5 used in determination of thermocouple calibration parameters

C6 used in determination of thermocouple calibration parameters

D1 inside diameter of experimental tube (m)

E calculated error in thermocouple calibration (^oC)

F mass flowrate (kg/s)

G mass flowrate per unit area (kg/m^2s)

H heat flux per increment (W)

H2 length of increment (m)

H5 heat available for vapourisation in increment (W)

H6 heat flux at wall in each increment (W/m^2)

I increment number. Step parameter

J step parameter

N1 number of increments

N9 increment where boiling commences

PO pressure at outlet of tube (N/m^2) (input as

P1 pressure at inlet of tube (N/m^2) (input as cm Hg gauge)

P3 atmospheric pressure (N/m^2) (input as mm Hg)

P8 $p_{SAT} - p_b$ (N/m^2)

P9 used in subroutine to find T_{SAT} from p_{SAT}

R1 run number

S1 Jf' } see 1.111 and 1.112

S2 Jg' }

T1 inlet temperature (^oC)

T2 }

T3 } used in subroutine to find T_{SAT} from p_{SAT}

T4 }

T7 wall temperature used in subroutine to find P8 and T8 (^oC)

T8 1) $T_w - T_b$ (^oC)

2) ϕ_f , Lockhart Martinelli two-phase multiplier

T9 used in subroutine to find T8 and P8

VO voidage assuming no slip

V1 volumetric two-phase flowrate (m^3/s)

V3 two-phase flow velocity assuming no slip (m/s)

X2 }

Y } used to estimate voidage in annular flow

Y1 }

Y3 }

Z experimental wall temperature (^oC)

ARRAYS

A(24) value of h_{con}

B(24) bulk temperature assuming no boiling in increment (^{o}C)

C(2,24) thermocouple calibration constants

D(24) value of S calculated from Chen's correlation

E(24) value of Re_{tp} calculated from Chen's correlation

F(24) value of F calculated from Chen's correlation

G(24) value of XTF

H(24) experimental value of heat transfer coefficient ($W/m^{2o}C$)

K(2,24) K(1,I) is estimated wall temperature using Chen's correlation (^{o}C)

K(2,I) is the corresponding heat transfer coefficient ($W/m^{2o}C$)

L(24) the calculated value of the heat transfer coefficient using Chen's correlation and the experimental wall temperature ($W/m^{2o}C$)

M(24) value of XTT

N(24) shows assumed flow pattern

N(I) = 1 bubbly flow

N(I) = 2 slug flow

N(I) = 3 churn flow

N(I) = 4 annular flow

P(24) pressure at increment (N/m^2)

R(24) value of Re in increment

S(24) value of saturation temperature T_{SAT} (^{o}C)

T(24) bulk temperature in increment (^{o}C)

V(24) estimated value of voidage in increment

W(24) wall temperature, Tw , in increment (^{o}C)

X(24) value of quality, x, in increment

Y(24) Y(I) = 0 if thermocouple is broken, else Y(I) = 1

Z(24) value of h_{mic} in increment

NOTE. The 24 values in the arrays correspond to the 24 increments in the tube.

STATEMENT FUNCTIONS

FNS(V) value of surface tension, σ, at V°C

FNI(V) value of calibration error for cu/con thermocouple at V°C

FNC(V) value of liquid specific heat, Cp_f, at V°C

FNH(V) value of heat of vapourisation, Lv, at V°C

FNG(V) specific heat of vapour, Cp_g, at V°C

FND(V) liquid density, ρ_f, at V°C

FNE(V) used to find vapour density ρ_g, at V°C

FNV(V) liquid viscosity, μ_f, at V°C

FNW(V) vapour viscosity, μ_g, at V°C

FNK(V) liquid conductivity, k_f, at V°C

FNL(V) vapour conductivity, k_g, at V°C

IV.1.2 Program II

The purpose of this program was to output on paper tape selected data points for further analysis. The data was input on paper tape with selection of data being carried out through the teletype.

SS3 and SS4 referred to in the program are sense switches on the computer console. When sense switch 3 is on, input is on paper tape, while if sense switch 4 is on, output is on paper tape. When sense switches 3 and 4 are are off input and output are through a teletype.

As with Program I the listing shown below is of the program for runs 16-61. Similar modifications as to Program I were required for the different groups of experimental runs.

A list of the variables and arrays used in addition to those used in Program I is given after the program listing and a typical teletype output.

```
1  REM   PROGRAM TO PREPARE AND PRESENT THERMOSYPHON DATA
2  REM    PAPER TAPE OUTPUT.      WATER RUNS ONLY.
3  REM      20/6/74.      D.MOORE.
5  DIM A(24),B(24),C(2,24),D(24),E(24),F(24),G(24),H(24),K(2,24)
6  DIM L(24),M(24),N(24),P(24),R(24),S(24),T(24),V(24),W(24)
7  DIM X(24),Y(24),Z(24)
8  DIM J(24),O(24)
19  DEF FNS(V)=.6784E-01-.17225E-03*(V-50)-.1745E-06*(V-50)↑2
20  DEF FNI(V)=V+1.307-.1E-04*(604*V+73.526*V*V-.60454E-01*V*V*V)
21  DEF FNC(V)=4179+.1*(V-40)+.1E-01*(V-40)*(V-40)
22  DEF FNH(V)=.2255E07-2600*(V-100)
23  DEF FNG(V)=2034+4.15*(V-100)+.31E-01*(V-100)*(V-100)
24  DEF FND(V)=1000/(1.0121+.40775E-03*(V-50)+.3225E-05*(V-50)↑2)
25  DEF FNE(V)=.2202E-02/(V+273.15)
26  DEF FNV(V)=.1/(2.1482*(V-8.435+SQR(8078.4+(V-8.435)↑2))-120.4)
27  DEF FNW(V)=.1206E-04+.38E-07*(V-100)
28  DEF FNK(V)=.643+.106E-02*(V-50)-.6E-05*(V-50)*(V-50)
29  DEF FNL(V)=.249E-01+.1E-03*(V-100)
30  REM
31  REM          RIG CONSTANTS
32  REM
33  D1=.159E-01:H2=.762E-01:A=3.14159*D1*D1/4
34  A1=3.14159*D1*H2:N1=24: GOTO 45
35  REM
36  REM      INPUT OF T/C CALIBRATION DATA
37  REM
38  INPUT C1,C2,C3,C4
39  FOR I=1,N1: INPUT C(1,I),C(2,I): NEXT I
40  GOSUB 600
42  REM
43  REM            INPUT OF RUN PARAMETERS
44  REM
45  INPUT R1,F,H,T1,P3,P1,P0
46  IF R1<1 GOTO 36
56  H=H/2
57  P3=P3*133.322
58  P1=P3+1333.22*P1
59  H6=H/A1
60  G=F/A
61  N9=0
67  REM
68  REM     INPUT OF INCREMENT DATA; T(WALL), P(BULK)
69  REM
70  FOR I=1,N1
71  Y(I)=1
75  INPUT W(I),P(I)
77  IF W(I)<10 THEN Y(I)=0
78  P(I)=P3+1333.22*P(I)
79  NEXT I
80  GOSUB 620
92  REM
93  REM     CALCULATION OF T(BULK) AT FIRST INCREMENT
94  REM
95  B(1)=T1+H/(2*F*FNC(T1))
```

```
100  REM
101  REM     CALCULATION OF  W(I),T(I),X(I),H(I),N9
102  REM
103  FOR I=1,N1
105  X(I)=0
109  IF I>18.5 GOTO 115
110  IF (I/2-INT(I/2))<.3 THEN W(I)=FNI(W(I)): GOTO 122
115  Z=W(I)
116  IF Z<41 THEN  GOTO 122
117  E=.359E-01*Z-1.31
118  IF Z>125 THEN E=.27E-02*Z+2.86
121  W(I)=Z-E
122  IF Y(I)<.5 THEN W(I)=W(I-1)
130  P9=P(I)
131  GOSUB 810
132  S(I)=T9
150  IF I<1.5 GOTO 160
152  IF N9>.5 GOTO 170
153  B(I)=B(I-1)+H/(F*FNC(T(I-1)))
160  IF S(I)>B(I) THEN T(I)=B(I): GOTO 190
170  T(I)=S(I)
171  IF N9<.1 THEN N9=I
180  H5=H+F*(T(I-1)-T(I))*((1-X(I-1))*FNC(T(I))+X(I-1)*FNG(T(I)))
185  X(I)=X(I-1)+H5/(FNH(T(I))*F)
190  H(I)=H6/(W(I)-T(I))
200  NEXT I
202  REM
203  REM       OPERATOR   MESSAGE
204  REM
205  PRINT "SWITCH OFF S.S3"
206  REM
207  REM      CALCULATION OF  M(I),J(I),G(I)
208  REM
210  FOR I=N9,N1
220  V1=F*((1-X(I))/FND(T(I))+X(I)/(FNE(T(I))*P(I)))
222  V0=X(I)*F/(V1*FNE(T(I))*P(I))
224  M(I)=(FNV(T(I))/FNW(T(I)))↑.1*SQR(FNE(T(I))*P(I)/FND(T(I)))
226  M(I)=M(I)*((1-X(I))/X(I))↑.9
228  J(I)=V1*V1/(9.81*D1*A*A)
229  G(I)=.19*M(I)*J(I)↑.185
300  NEXT I
307  REM
308  REM    CALCULATION OF R(I),Z(I),A(I). (A(I) IN SUBROUTINE)
309  REM
310  FOR I=N9,N1
312  R(I)=G*(1-X(I))*D1/FNV(T(I))
316  GOSUB 675
326  T7=W(I): GOSUB 660
327  Z(I)=Z(I)*T8↑.24*P8↑.75
330  NEXT I
332  REM
333  REM          OPERATOR MESSAGE
334  REM
335  PRINT "RUN NUMBER",R1
336  D8=0
337  REM      INTERACTIVE LOOP FOR SELECTION OF DATA POINTS TO
338  REM      BE DISCARDED.  DATA FROM INCREMENT (I) IS DISCARDED
339  REM      IF D9 IS INPUT AS 0 FOR INCREMENT (I).
341  REM
```

```
342  FOR I=N9,N1
344  IF Y(I)<.1 THEN O(I)=0: GOTO 352
346  O(I)=1
348  PRINT I;: INPUT D9
350  IF D9<.5 THEN O(I)=0
351  D8=D8+O(I)
352  NEXT I
353  REM
354  REM            OPERATOR  MESSAGE
355  REM
356  PRINT "PUT ON S.S.3 AND 4 NOW, THEN S.S.4 OFF AFTER TAPE O/P"
357  REM
358  REM      PAPER TAPE OUTPUT OF RUN PARAMETERS
359  REM
360  PRINT INT(R1)
361  PRINT INT(D8)
362  Z=H6: GOSUB 750
363  Z=F: GOSUB 750
366  REM
367  REM     PAPER TAPE OUTPUT OF DATA FROM SELECTED INCREMENTS
368  REM
369  FOR I=N9,N1
370  IF O(I)<.5 GOTO 380
372  Z=H(I): GOSUB 750
373  Z=A(I): GOSUB 750
374  Z=Z(I): GOSUB 750
375  Z=LOG(1/M(I)): GOSUB 750
376  Z=J(I): GOSUB 750
377  Z=LOG(R(I)): GOSUB 750
380  NEXT I
390  GOTO 45
392  REM   ***************************************************
393  REM
590  REM                        SUBROUTINES
591  REM                       *************
597  REM
598  REM     SUBROUTINE TO CALCULATE T/C CALIBRATION PARAMETERS
599  REM
600  FOR I=1,N1
601  IF I>18.5 GOTO 604
602  IF (I/2-INT(I/2))<.3 GOTO 606
604  C5=C1+C(1,I):C6=C2+C(2,I): GOTO 608
606  C5=C3+C(1,I):C6=C4+C(2,I)
608  C(1,I)=C(1,I)-C5*(C(2,I)-C(1,I))/(C6-C5)
610  C(2,I)=(C(2,I)-C(1,I))/C6
612  NEXT I
614  RETURN
617  REM
618  REM         SUBROUTINE TO CORRECT T/C VALUES
619  REM
620  FOR I=1,N1
622  W(I)=W(I)-C(1,I)-C(2,I)*W(I)
623  NEXT I
624  RETURN
657  REM
658  REM     SUBROUTINE TO CALCULATE  DELTA.P AND DELTA.T
659  REM
660  T9=1-373.15/(273.15+T7)
662  PR=EXP(T9*(13.3185-T9*(1.967+T9*(.6445+.1299*T9))))
```

```
664  P8=ABS(.101325E06*P8-P(I))
666  T8=ABS(T7-T(I))
668  RETURN
672  REM
673  REM    SUBROUTINE TO CALCULATE  H(MIC) AND H(MAC)
674  REM
675  Z(I)=.122E-02*FNK(T(I))↑.79*FNC(T(I))↑.45*FND(T(I))↑.49
676  Z(I)=Z(I)/(FNH(T(I))↑.24*(FNE(T(I))*P(I))↑.24)
677  Z(I)=Z(I)/(FNS(T(I))↑.5*FNV(T(I))↑.29)
680  A(I)=.23E-01*R(I)↑.8*(FNV(T(I))*FNC(T(I))/FNK(T(I)))↑.4
681  A(I)=A(I)*FNK(T(I))/D1
685  RETURN
747  REM
748  REM     SUBROUTINE TO OUTPUT DATA IN EXPONENTIAL FORM
749  REM
750  N=0
753  IF Z=0 THEN Z=.1E-10
755  Z1=SGN(Z)
760  Z=ABS(Z)
765  IF Z<10 GOTO 785
770  Z=Z/10
771  N=N+1
775  GOTO 765
780  Z=Z*10
781  N=N-1
785  IF Z<1 GOTO 780
790  Z=INT(Z*.1E06+.5)/.1E06
795  IF Z=10 THEN Z=1:N=N+1
800  IF Z=INT(Z) THEN Z=Z+.1E-04
803  PRINT Z1*Z
804  PRINT INT(N)
805  RETURN
807  REM
808  REM     SUBROUTINE TO CALCULATE T.SAT FROM P.SAT
809  REM
810  T2=LOG(P9/.101325E06)/13.3185
812  T3=T2
814  FOR J=1,4
816  T4=T2+((.1299*T3+.6445)*T3+1.976)*T3*T3/13.3185
818  IF ABS(T4-T3)<.1E-04 GOTO 824
820  T3=T4
822  NEXT J
824  T9=373.15/(1-T4)-273.15
826  RETURN
999  END
```

****

```
PUT ON S.S.3 AND S.S.4, THEN S.S.4 OFF AFTER O/P
SWITCH OFF S.S.3
RUN NUMBER      142
     7   11
     8   10
    11   11
    13   11
    14   11
    15   10
    16   11
    18   10
    19   10
    20   11
    21   11
    22   11
    23   11
    24   11
O.K?
!!
PUT ON S.S.3 AND S.S.4, THEN S.S.4 OFF AFTER O/P
SWITCH OFF S.S.3
RUN NUMBER      143
     6   10
     7   11
     8   10
    11   11
    13   11
    14   11
    15   10
    16   11
    18   10
    19   10
    20   11
    21   11
    22   11
    23   11
    24   11
O.K?
!!
PUT ON S.S.3 AND S.S.4, THEN S.S.4 OFF AFTER O/P
SWITCH OFF S.S.3
RUN NUMBER      144
     5   10
     6   11
     7   11
     8   10
    11   11
    13   11
    14   11
    15   10
    16   11
    18   10
    19   10
    20   11
    21   11
    22   11
    23   11
    24   11
O.K?
!!
```

VARIABLES

D8 number of points output from run

D9 logical variable for data selection

N value of exponent of variable to be output

Z absolute value of variable to be output

Z1 variable representing sign of output variable

ARRAYS

J(24) value of Froude Number at increment I.

O(24) selection variable. If O(I) = 0 data point is discarded

IV.1.3 Program III

When it was decided to use model II (see Chapter III) to correlate the experimental data the Prandl Number, Pr, was required in addition to the variables output by Program II. Thus Program II had to be altered so as to output the Prandl number in a similar way as the variables output by Program II. Since this meant that all of the data had to be processed again it was decided to output four other variables which might be useful for future work. Thus the values of the pressure, bulk temperature, wall temperature and quality were output as well.

A listing of this program has not been given since this program is very similar to Program II.

IV.2 Fortran Programs

IV.2.1 Iterative Linear Method

A listing of the Fortran program implementing the iterative linear method described in Chapter V is given below. This program was run on the University's ICL 1905E digital computer.

The program uses the subroutine F4CFORPL which is called from the Scientific Subroutine Library available on the ICL 1905E. The subroutine uses Chekyshev orthogonal polynomials to find the best polynomial fit upon the data for the F_L and S functions.

ITERATIVE LINEAR PROGRAM

```
      MASTER ANALDAT
      REAL LXT(520),LRE(520),S(520),H(520),HC(520),LSX(520),HM(520)
     1,LF(520),FC(6),SC(6),W(520),R(520),P(1100),FRMS(6),SRMS(6)
      INTEGER RI
      DO 19 I=1,6
      FC(I)=0.0
   19 SC(I)=0.0
      P(3)=0.0
      P(4)=1.0
      P(5)=0.0
      NP=0
  119 READ(3,101) RI
  101 FORMAT(I4,2E13.6)
      IF(RI.EQ.0) GOTO 121
      READ(3,101) NPR,FL,FF
      DO 120 I=NP+1,NP+NPR
  120 READ(3,102) H(I),HC(I),HM(I),LXT(I),FR,LRE(I)
  102 FORMAT(6E13.6)
      NP=NP+NPR
      GOTO 119
  121 NO=5
      NL=10
      FC(1)=1.24234
      FC(2)=0.55903
      FC(3)=0.065231
      FC(4)=0.0050257
```

```
      FC(5)=0.0
      FRMS(5)=0.0
      MN=5*NC+2*NP+3
      NM=MN-5
      WRITE(2,103) NP
  103 FORMAT(23H NUMBER OF DATA POINTS  ,15)
      WRITE(2,104)
      DO 100 K=1,NL
      DO 50 I=1,NP
      Z=LXT(I)
      LF(I)=FC(1)+7*(FC(2)+Z*(FC(3)+Z2(FC(4))))
      S(I)=(H(I)-HC(I)*EXP(LF(I)))/HM(I)
      LSX(I)=LRE(I)+1.25*LF(I)
   50 CONTINUE
      P(1)=-1.0
      DO 51 I=1,NC
      CALL F4CFORPL(NP,NC,MN,LSX,S,R,W,SC,P)
      SRMS(I)= P(2)
   51 CONTINUE
      DO 60 I=1,NP
      Z=LSX(I)
      S(I)=SC(1)+Z*(SC(2)+Z*(SC(3)+Z*(SC(4)+Z*(SC(5)))))
      F=(H(I)-HM(1)*S(I))/HC(I)
      IF (F.LE. 1.0) F=1.0
      LF(I)=ALOG(F)
   60 CONTINUE
      P(1)=1.0
      DO 61 I=1,NC-1
      CALL F4CFORPL(NP,NC,NM,LXT,LF,R,W,FC,P)
      FRMS(I)= P(2)
```

```
 61 CONTINUE
    DO 65 I=1,NC
 65 WRITE(2,14) I,FC(I), SC(I),FRMS(I),SRMS(I)
 14 FORMAT(15,3X,F15.8,3X,F15.8,2F15.8)
    WRITE(2,104)
104 FORMAT(1H ,//)
100 CONTINUE
    STOP
    END
```

Variables

F	F_L
FF	Heat Flux
FL	Flowrate
FR	Froude number
I	Step variable
K	Step variable
MN	Variable used in subroutine F4CFORPL
NC	Number of coefficients for the F_L and S polynominals
NL	Number of iterative loops
NM	Variable used in subroutine F4CFORPL
NP	Number of data points
NPR	Number of data points in run
RI	Run number
Z	Dummy variable

Arrays

FC	Array of F_L coefficients
FRMS	Array of RMS errors for each F_L coefficient.
H	Array of experimental heat transfer coefficients
HC	Array of convective heat transfer coefficients
HM	Array of nucleat heat transfer coefficients
LF	Array of F_L values
LRE	Array of $\ln(Re)$ values
LSX	Array of $\ln(Re_{tp})$ values
LXT	Array of $\ln(\frac{1}{XTT})$ values
P	Array of values used to control the F4CFORPL subroutine
R	Array of calculated errors of data points
S	Array of S values
SRMS	Array of RMS values for each S coefficient
W	Array of weights for each data point (not used)

IV.2.2 Davis, Swann and Campey Program

A listing of the Fortran programme used, using Davis, Swann and Campey's method described in Chapter V, is given below. This program was run mainly on the UMRCC CDC 760 computer. A list of the variables, arrays and subroutines is given after the program listing. Only those variables and arrays used in the main segment of the program and some used in the subroutine SUMSSQ are given.

As mentioned in section V.2.6 the program had to be altered slightly for each of the models. The program given here is that used for the correlation of the water data to model B.

```
      PROGRAM ROSE(INPUT,OUTPUT,DATA,NDAT,TAPE1=INPUT,TAPE2=OUTPUT,
     1TAPE3=DATA,TAPE4=NDAT)
      COMMON NP,FR(850),XT(850),RE(850),H1(850),H2(850),HF(850),
     1V(12,12),FAH(850)
      DIMENSION X(12),Z(12),E(12),D(12)
      NFUNC=0
      ERROR=0.00001
      ALPHA=2
      BETA=-.5
      READ(1,98) N,ISTOP
      READ(1,99) (X(I), I=1,N)
   98 FORMAT(14,16)
   99 FORMAT(8F10.6)
      CALL IMPDATA
      N1=N-1
   39 CALL SUMSSQ(X,N,YSTAR)
      YNSTAR=SQRT(YSTAR/NP)
      WRITE(2,97) YNSTAR
   97 FORMAT(32H INITIAL VALUE OF RMS ERROR IS ,F9.4 //)
      IFUNC=1
      DO 40 I=1,N
      F(I)=X(I)/100
      DO 41 J=1,N
      IF(J.EQ.I) GO TO 41
      V(I,J)=0.0
   41 CONTINUE
   40 V(I,I)=1.0
   44 YNSTAR=SQRT(YSTAR/NP)
      WRITE(2,650) IFUNC,YNSTAR
      WRITE(2,651) (X(I), I=1,N)
  650 FORMAT( 16,E15.6)
  651 FORMAT(12F10.6 //)
      IFUNC=0
      DO 56 I=1,N
      A=-1.0
      E(I)=E(I)/2.0
      D(I)=0.0
      F1=YSTAR
   43 DO 1 K=1,N
    1 X(K)=X(K)+(E(I)*V(K,I))
      CALL SUMSSQ(X,N,FUNC)
      IFUNC=IFUNC+1
      IF(FUNC.LE.YSTAR) GO TO 47
      NS=0
      DO 2 K=1,N
      STEP=E(I)*V(K,I)
      IF(ABS(STEP) .LT. 2.E-07)  NS=NS+1
    2 X(K)=X(K)-(E(I)*V(K,I))
      IF(ABS(A) .LE.1.E-20) GO TO 110
      IF(NS .GT. N1) GO TO 56
      E(I)=BETA*E(I)
      GO TO 43
   47 YSTAR=FUNC
  734 D(I)=D(I)+E(I)
      E(I)=ALPHA*E(I)
      IF(ABS(A) .LE.1.E-20) F1=F2
      F2=YSTAR
      A=0.0
      GO TO 43
```

```
110 F4=FUNC
    DO 111 K=1,N
111 Z(K)=X(K)+E(I)*V(K,I)/2.0
    CALL SUMSSQ(Z,N,F3)
    IFUNC=IFUNC+1
    S=E(I)/2.0
    IF(F3.GT.F2) GO TO 113
    F1=F2
    F2=F3
    F3=F4
    YSTAR=F2
    DO 112 K=1,N
112 X(K)=Z(K)
    D(I)=D(I)+S
113 S1=2.0*(F1-2.0*F2+F3)
    IF(S1.LE.0.1E-08) GO TO 56
    S=S*(F1-F3)/S1
    DO 114 K=1,N
114 Z(K)=X)K)+S*V(K,I)
    CALL SUMSSQ(Z,N,FUNC)
    IFUNC=IFUNC+1
    IF(FUNC.GE.F2) GO TO 56
    YSTAR=FUNC
    D(I)=D(I)+S
    DO 115 K=1,N
115 X(K)=Z(K)
 56 CONTINUE
    DO 57 I=1,N
    IF(ABS(E(I)).GT. ERROR) GO TO 75
 57 CONTINUE
    GO TO 647
 75 CALL VECTOR(N,D)
    NFUNC=NFUNC+IFUNC
    IF(NFUNC.GT.ISTOP) GO TO 652
    GO TO 44
647 WRITE(2,649)
649 FORMAT(12H OPTIMISED)
652 YNSTAR=SQRT(YSTAR/NP)
    WRITE(2,650) IFUNC,YNSTAR
    WRITE(2,651)(X(I), I=1,N)
    GO TO 39
    END

    SUBROUTINE VECTOR(N,D)
    DIMENSION D(N),ALPH(12,12),AMSQ(12),AMOD(12)
    COMMON NP,FR(850),XT(850),RE(850),H1(850),H2(850),HF(850)
   1,ARRAY(12,12),FAH(850)
    SMA=1.0E-14
    SUM1=0.0
    DO 90 I=1,N
 90 SUM1=SUM1*(D(I)**2)
    BMOD=SQRT(SUM1)
    DO 92 I=1,N
    SUM=0.0
    DO 91 J=1,N
 91 SUM=SUM*(D(J)*ARRAY(I,J))
```

```
 92 ALPH(I,1)=SUM
    DO 30 M=2,N
    D(M-1)=0.0
    SUM2=0.0
    DO 50 I=1,N
    SUM=0.0
    DO 49 J=1,N
 49 SUM=SUM+(D(J)*ARRAY(I,J))
    ALPH(I,M)=SUM
 50 SUM2=SUM2+(ALPH(I,M)**2)
 30 AMOD(M)=SQRT(SUM2)
    AMOD(1)=RMOD
    DO 88 I=1,N
 88 AMSQ(I)=AMOD(I)**2
    DO 96 I=1,N
    IF(AMOD(1).LT.SMA) GO TO 96
    ARRAY(I,1)=ALPH(I,1)/AMOD(1)
 96 CONTINUE
    DO 93 K=2,N
    DO 93 I=1,N
    IF(AMOD(K).LT.SMA) GO TO 93
    IF((AMSQ(K-1)-AMSQ(K)).LT.SMA) GO TO 93
    ARRAY(I,K)=((ALPH(I,K)*AMSQ(K-1))-(ALPH(I,K-1)*AMSQ(K)))/
   1((AMOD(K-1)*AMOD(K))*SQRT(AMSQ(K-1)-AMSQ(K)))
 93 CONTINUE
    RETURN
    END

    SUBROUTINE SUMSSQ(Z,N,SSQ)
    COMMON NP,FR(850),XT(850),RE(850),H1(850),H2(850),HF(850),
   1V(12,12),FAH(850)
    DIMENSION X(12),Z(12)
    DO 180 I=1,N
180 X(I)=Z(I)
    X(3)=X(3)/10.0
    X(4)=Z(4)/100.0
    X(5)=Z(5)*10.0
    X(9)=X(9)/100.0
    X(10)=X(10)/100.0
    SSQ=0.0
    DO 190 I=1,NP
    XF=XT(I)+X(4)*FR(I)
    F=X(1)+XF*(X(2)+XF*(X(3)+XF*X(9)))
    P1=RE(I)+X(8)*F
    S=X(5)+P1*(X(6)+P1*(X(7)+P1*X(10)))
    S=0.5*(ABS(S)+S)
    H3=FAH(I)/(1.0+X(11)*ALOG(1.0+5.0*H1(I)/X(11))/H1(I))
    DIFF=H3*EXP(F)+H2(I)*S-HF(I)
    ERR=DIFF*100.0/HF(I)
190 SSQ=SSQ+ERR*ERR
    RETURN
    END
```

```
      SUBROUTINE IMPDATA
      DIMENSION IERR(2,100), INUM(5,100)
      COMMON NP,FR(850),XT(850),RE(850),H1(850),H2(850),HF(850),
     1V(12,12),FAH(850)
      INTEGER RI
  110 FORMAT(514)
  111 FORMAT(14,2E13.6)
  112 FORMAT(6E13.6)
      RP=0.5
      DO 35 I=1,100
      IERR(1,I)=0
      IERR(2,I)=0
      DO35 J=1,5
   35 INUM(J,I)=0
      READ(1,110) N
      DO 36 I=1,N
      READ(1,110) IERR(1,I), IERR(2,I)
      IE=IERR(2,I)
   36 READ(1,110) INUM(J,I),J=1,IE)
      J=1
      NP=1
   40 K=100
      READ(3,110) RI
      READ(4,110) IR
      IF(Ri.EQ.0) GOTO 105
      READ(3,111) NPR,HFLUX,FLOWR
      READ(4,111) N,H,F
      IF(RI.NE.IERR(1,J)) GOTO 100
      K=J
      J=J+1
  100 DO 102 I=1,NPR
      READ(3,112) HF(NP),H1(NP),H2(NP),XT(NP),FR(NP),RE(NP)
      READ(4,112) X,W,T,P,H1(NP)
      FAH(NP)=43.02*SQRT(0.32*EXP(RE(NP)))
      FR(NP)=ALOG(FR(NP))
      IF(K.FQ.100) GOTO 104
      IE=IERR(2,K)
      DO 101 L=1,IF
      IF(I.EQ.INUM(L,K)) GOTO 102
  101 CONTINUE
  104 NP=NP+1
  102 CONTINUE
      GOTO 40
  105 NP=NP-1
      RETURN
      END
```

IV.2.21 Subroutines

Vector (N,D)

This subroutine re-othogonalizes the search vectors after each iteration as explained in V.25 and V.26. This subroutine was taken from a program written by Gibson-Robinson (G1) and was based upon one originally given in Davis, Swann and Campey's paper (D2).

IMPDATA

This subroutine reads in the data to be optimised allowing, if required, any data points to be ignored as specified by the input into the arrays IERR and INUM. When the program was used to optimise model B this subroutine also calculated the values of hf (FAH( )).

SUMSSQ (Z,N,SSQ)

This subroutine calculates the sum of squares percentage error on the data for values of the correlation parameters supplied in the array X ( ). The sum of squares percentage error is returned to the main segment as SSQ. This subroutine had to be altered for each different form of correlation investigated.

IV.2.22 Variables

A		Program control parameter
ALPHA	α	(2.0)
BETA	β	(-0.5)
ERROR		used to terminate program when apparent convergence achieved.
F1,F2,F3,F4		values of root mean square error used for quatratic interpolation.
FUNC		value of root mean square error returned from SUMSSQ

I	Step variable
IFUNC	Number of sum of square evaluations in iteration.
ISTOP	Maximum number of sum of square evaluations to be allowed.
J	Step variable
N	Number of parameters to be optimised.
N1	N - 1
NP	Number of data points.
NFUNC	Total number of sum of squares evaluations performed.
NS	Number of parameter step lengths of negligible size.
S	Vector step length found from quadratic interpolation.
S1	Parameter used in determining value of S.
STEP	Step length.
YNSTAR	Lowest root mean sum of squares error found.
YSTAR	Sum of squares percentage error.

Arrays

D	Array of progress achieved along each vector in iteration.
E	Array of vectorial step lengths.
FR	Array of ln(Fr) values.
FAH	Array of values of hf.
H1	Array of convective heat transfer coefficients.
H2	Array of nucleate heat transfer coefficients.
HF	Array of experimental heat transfer coefficients.
RE	Array of ln(Re) values.
V	Array of othogonal search vectors.
X	Array of best parameters found.
XT	Array of $\ln(\frac{1}{XTT})$ values.
Z	Array of parameter values whose error is to be found by subroutine SUMSSQ.